
Non-Equilibrium Scaling Analysis of Quantum Dots in the Kondo Regime

Peter Fritsch



München 2009

Non-Equilibrium Scaling Analysis of Quantum Dots in the Kondo Regime

Peter Fritsch

Dissertation
an der Fakultät für Physik
der Ludwig–Maximilians–Universität
München

vorgelegt von
Peter Fritsch
aus Augsburg

München, den 19. März 2009

Erstgutachter: Prof. Dr. S. Kehrein

Zweitgutachter: Prof. Dr. U. Gerland

Tag der mündlichen Prüfung: 10. Juni 2009

Reality is wrong. Dreams are for real.
Tupac Shakur

Contents

Deutsche Zusammenfassung	1
Motivation	3
1 Introduction	5
1.1 The Kondo Problem	5
1.1.1 Historic Remarks	5
1.1.2 Equilibrium Model	6
1.1.3 Scaling Approaches	8
1.2 The Non-Equilibrium Kondo Model	10
1.2.1 Experimental Realization	10
1.2.2 The Coulomb Blockade Regime	11
1.2.3 Model and Hamiltonian	12
1.2.4 Previous Approaches	14
1.2.5 Decoherence Effects	15
1.3 General Non-Equilibrium Theory	16
1.3.1 Linear Response Theory	16
1.3.2 The Keldysh Formalism	18
1.3.3 Scattering State Approaches	20
1.4 The Flow Equation Method	21
1.4.1 General Setup	22
1.4.2 Infinitesimal Unitary Transformations	23
1.4.3 Tunneling in a Double Well	25
1.4.4 Perturbative Truncation of the Unitary Transformation	29
1.4.5 Normal-Ordering	31
1.4.5.1 Formalism	31
1.4.5.2 Basic Examples	32
1.5 Summary	35
2 Flow Equation Treatment of the Kondo Hamiltonian	37
2.1 1-loop Flow Equations	37
2.1.1 Basic Commutation Relations	37
2.1.2 Generator	38

2.1.3	Flow Equations	39
2.1.4	Scaling Analysis (1-loop)	40
2.1.5	Newly Generated Terms	42
2.2	2-loop Flow Equations	44
2.2.1	Basic Commutation Relations	44
2.2.2	Ansatz Hamiltonian and Generator	44
2.2.3	Flow Equations	46
2.2.4	Diagonal Parametrization	48
2.2.5	Scaling Analysis (2-loop), Isotropic Model	52
2.2.5.1	Magnetic field only	52
2.2.5.2	Voltage Bias, Temperature, and Combinations with Magnetic Field	56
2.2.5.3	Decoherence Effects and Higher Orders	60
2.2.6	Scaling Analysis, Anisotropic Model	60
2.2.6.1	General 1-loop scaling	61
2.2.6.2	2-loop Scaling, Magnetic Field Only	63
2.2.6.3	2-loop Scaling Voltage Bias Temperature and Combinations with Magnetic Field	64
2.3	Summary	65
3	Observables	67
3.1	Introduction	67
3.2	The Flow Equation Way	68
3.2.1	Zero Temperature	68
3.2.2	Nonzero Temperature	69
3.2.3	Non-Equilibrium	70
3.2.4	Time Evolution	70
3.2.5	Zero Temperature Correlation Functions	71
3.2.6	Nonzero Temperature Correlation Functions	72
3.3	Spin Operator	73
3.3.1	Transformation of S^z	73
3.3.2	Magnetization	76
3.3.3	Spin-Spin Correlation Function	78
3.3.4	Transformation of $S^{x/y}$	80
3.4	T-Matrix	82
3.4.1	Construction	82
3.4.2	Flow Equations	84
3.4.2.1	Lowest Order	84
3.4.2.2	Higher Orders	85
3.4.3	Results	87
3.5	Temperature vs. Voltage Bias	88
3.5.1	Spin-Spin Correlation Function	89
3.5.1.1	Zero Magnetic Field	89

3.5.1.2	Nonzero Magnetic Field	90
3.5.2	T-Matrix	93
3.5.3	Magnetization	95
3.5.4	Static Spin Susceptibility	97
3.6	Summary	99
4	Thermal Non-Equilibrium	101
4.1	Flow Equation Analysis	102
4.1.1	Basic Relations	102
4.1.2	1-loop Scaling Analysis	102
4.1.3	2-loop Scaling Analysis	103
4.2	Numerical Results	105
4.2.1	Effective Temperature	105
4.2.2	Static Spin Susceptibility	106
4.3	Summary	107
5	Conclusion	109
A	Numerics Trivia	111
A.1	Solution of the Flow Equations	111
A.2	Additional Approximations	112
A.2.1	Correlation and Response Function	112
A.2.2	Magnetization	112
A.2.3	Static Spin Susceptibility	113
B	Math	115
B.1	Momentum Summation, 2-loop	115
B.2	Rewriting the 2-loop Scaling Equations	117
C	Commutators	119
C.1	Hamiltonian, 1-loop	119
C.2	Hamiltonian, 2-loop	120
C.3	Trafo S^z	122
C.4	Trafo S^x	123
C.5	T-Matrix, Lowest Order	124
C.6	T-Matrix, Higher Order Terms	125
	List of Figures	127
	Bibliography	131
	List of Publications	141
	Acknowledgments	143

Curriculum Vitae

145

Deutsche Zusammenfassung

Das Kondo Problem beschreibt die faszinierende Physik einer magnetischen Störstelle eingebettet in ein nicht magnetisches Metall. Die schwache Hybridisierung des einfach besetzten magnetischen Niveaus des Störstellenatoms, der so genannte Kondo Spin, mit den Leitungsbandelektronen des Wirtsmetalls führt zu einer starken Korrelation des gesamten Elektronensystems. Wird eine Spannung an ein makroskopisches Kondo System angelegt, so fällt nur ein kleiner Bruchteil der Spannung auf der Längenskala eines Atoms ab und die Störstelle befindet sich in einem Quasi-Gleichgewicht. Transport durch solche Systeme kann durch die so genannte Linear Response Theorie beschrieben werden.

Experimenteller Fortschritt in der Miniaturisierung von Halbleiterstrukturen öffnete einen neuen Bereich in der Festkörperphysik: Nanostrukturen. Durch Verwendung von Halbleiter Heteroübergängen wurde es möglich künstliche Atome mit einer typischen Größe von einhundert Nanometern zu formen. An diesen so genannten Quantenpunkten können vergleichsweise große Spannungsdifferenzen direkt angelegt werden. Genau genommen legt nicht die Spannungsdifferenz sondern die Stromstärke, die auch von der Stärke der Hybridisierung des Kondo Spins mit den Leitungsbandelektronen abhängt, fest ob sich das System im Gleichgewicht befindet oder nicht. Ein Quantenpunktsystem kann jedoch vergleichsweise leicht aus dem Gleichgewicht gebracht werden. In solchen Situationen kann die Physik des Systems nicht mehr mit Linear Response Theorie beschrieben werden, statt dessen müssen bessere Methoden entwickelt und natürlich auch angewandt werden. Speziell in stark korrelierten Elektronensystemen ist dies nicht trivial.

Diese Arbeit beschäftigt sich mit der Entwicklung einer perturbativen Renormierungsgruppenbeschreibung des Kondo Problems sowohl in Gleichgewichts- als auch in Nichtgleichgewichtssituationen mit Hilfe der Flußgleichungsmethode. Der Schwerpunkt dieser Arbeit liegt in der Bestimmung der statischen und dynamischen Eigenschaften des Kondo Spins, da diese wertvolle Einblicke in die Physik des Systems ermöglichen. Im Detail bestimmen wir die Magnetisierung und die statische Spinsuszeptibilität inklusive der führenden logarithmischen Korrekturen. Im thermodynamischen Gleichgewicht reproduzieren wir dabei die asymptotischen Bethe Ansatz Ergebnisse, im Nichtgleichgewicht konnten diese Größen bisher nur in führender Ordnung (ohne logarithmische Korrekturen) bestimmt werden. Des Weiteren berechnen wir die Spin-Spin Korrelationsfunktion und die T-Matrix. Beide Größen wurden bereits intensiv untersucht. Wir erweitern die bisher bekannten Ergebnisse auf das gesamte mit unserer Methode zugängliche Parameterregime.

Typischerweise sind Vielteilchenmethoden in der theoretischen Festkörperphysik auf das Linear Response Regime fokussiert. Hier müssen nur wenige niederenergetische Freiheitsgrade berücksichtigt werden. In stark angeregten System wie zum Beispiel im Nichtgleichgewicht tragen jedoch Prozesse auf vielen Energieskalen zu den physikalischen Eigenschaften des Systems bei. In der Flußgleichungsmethode werden deshalb Wechselwirkungsmatrixelemente ausintegriert anstelle von Zuständen wie in konventionellen Renormierungsgruppenverfahren. Durch das Beibehalten aller Zustände im Hilbertraum können Systeme auf allen Energieskalen untersucht werden, auch im Nichtgleichgewicht.

Motivation

The Kondo problem describes the fascinating physics of a magnetic impurity embedded in a nonmagnetic metal. The weak hybridization of the singly occupied magnetic level of the impurity atom with the conduction band electrons in the metallic host leads to strong correlations of the system's electrons. If a voltage bias is applied to a macroscopic Kondo system, only a tiny fraction of the voltage bias drops on the length scale of an atom and the impurity is in quasi-equilibrium. Transport through such systems is described by linear response theory.

Recent experimental progress on the miniaturization of semiconductor structures pioneered a new field in condensed matter physics: nanostructures. Using semiconductor heterojunctions it became possible to construct artificial atoms with typical sizes of about one hundred nanometer. At these so-called quantum dots strong voltage biases of up to several hundred millivolt can be directly applied. As a comparison, applying five hundred millivolt to a structure with the size of five Ångström corresponds to a field strength of 10^9 V/m. The dielectric strength of air is only about 3×10^6 V/m.

Though not the strength of the electric field but the strength of the current through the system, which also depends on the hybridization of the impurity (dot) level with the conduction band electrons, determines whether the system is in equilibrium or not, in a quantum dot setup it is rather simple to drive the system far out of equilibrium. In such a situation linear response theory fails to explain the physics of the system and more sophisticated methods have to be developed and applied. Especially for strongly correlated electron systems far out of equilibrium this turns out to be highly nontrivial. In this thesis we develop a perturbative scaling picture of the Kondo problem for both equilibrium and non-equilibrium situations using the flow equation method. We focus on the static and the dynamic properties of the impurity (dot) spin, since these give valuable insight into the physics of the system.

The equilibrium Kondo problem has been formally solved by the Bethe Ansatz, however dynamical quantities cannot be easily accessed within this approach. In non-equilibrium so far results have only been derived in leading order using non-equilibrium perturbation theory and the perturbative renormalization group. In this thesis we rederive in leading logarithmic order the previously known equilibrium results for the magnetization and the static spin susceptibility of the Kondo spin and present results for the non-equilibrium magnetization and the non-equilibrium static spin susceptibility including the leading logarithmic corrections. The equilibrium spin-spin correlation function is well understood,

also in the context of the spin boson model. We extend the previously known results to non-equilibrium. In addition we work out the T-matrix which describes the scattering of conduction band electrons at the impurity (dot). The T-matrix is well studied in both equilibrium and non-equilibrium situations. We extend the previously known results to the full parameter regime accessible within our approach.

Typical many-particle methods in condensed matter theory focus on the quasi-equilibrium linear response regime. Here only few low energy degrees of freedom have to be taken into account. In highly excited systems, e.g. in far out of equilibrium situations, many energy scales contribute to the physical properties of the system. In the flow equation approach therefore interaction matrix elements are integrated out instead of integrating out states as in conventional scaling approaches. By retaining all states in the Hilbert space also systems prepared in highly excited far out of equilibrium situations can be studied on all energy scales.

This thesis is outlined as follows. In Chap. 1 we give a general introduction to the Kondo problem, non-equilibrium physics, and the flow equation method. The scaling equations for the Kondo model are worked out and analyzed in Chap. 2. In Chap. 3 we give an introduction to the evaluation of observables within the flow equation approach and present results for various observables in the equilibrium and the non-equilibrium Kondo model. This chapter contains the key results of this thesis. In Chap. 4 we study a quantum dot in the Kondo regime coupled to two leads at different temperature. We give a short summary of the key results in Chap. 5.

Chapter 1

Introduction

1.1 The Kondo Problem

1.1.1 Historic Remarks

The Kondo effect was first observed by de Haas *et al.* in the 1930's while measuring the resistivity of "pure" metals [1–4]. Upon lowering the temperature one finds a minimum in the resistivity of nonmagnetic metals containing a small concentration of magnetic impurities, a plot of the original data is shown in Fig. 1.1. When lowering the temperature even further the resistance increases and saturates at a finite value at zero temperature. Systematic experimental and theoretical analysis showed that this effect is due to a screening of the impurity spin by resonant scattering of conduction band electrons leading to an enhanced electron density around the impurities. Bypassing electrons scatter off these so called spin compensation clouds leading to an enhancement of the resistivity. The Kondo model has become a paradigm model for strong-coupling impurity physics in condensed matter theory, for a review see Refs. [5, 6].

The Kondo model has been formally solved exactly using Bethe Ansatz [7, 8], however dynamical quantities like the impurity spectral function are not easily accessible within this framework. Several additional numerical and analytical methods have been developed that get around this limitation [6, 9–17].

Experiments on quantum dots in the Coulomb blockade regime revived the interest in Kondo physics [18–20], a scanning electron microscope image of such a device is shown in Fig. 1.2. If the quantum dot is tuned in such a way that it carries a net spin, resonant tunneling leads to an increase of the conductance up to the unitary limit [21–23]. For small dc-voltage bias $V \ll T_K$ the system can be described using linear response theory and the equilibrium ground state. The situation is quite different for $V \gtrsim T_K$ since the ground state no longer describes the physical properties of the system. Instead one has to use the highly excited and unknown steady state to describe the system. Most theoretical methods developed to study the equilibrium Kondo model however focus on its low-energy properties. The intermediate voltage bias regime $V \approx T_K$ recently became accessible by newly developed methods like the scattering state numerical renormalization group [24],

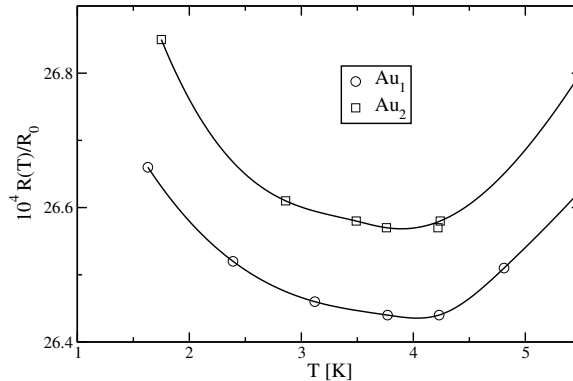


Figure 1.1: Minimum in the resistance of two gold wires (Au₁ and Au₂) at low temperature [2]. The resistance $R(T)$ is plotted in units of R_0 as function of the temperature T , where R_0 denotes the resistance at 273 K. The Au₁- and the Au₂-wire were made from the same source material. The Au₂-wire has been additionally deformed to estimate effects by mechanical deformations of the wire on the residual resistance, the experimental setup is discussed in Ref. [1]. Note that the aim of the experiments [1–4] was to extract the so-called ideal resistance, the resistance due to scattering by thermal lattice vibrations.

the time-dependent density renormalization group [25], and the scattering state Bethe Ansatz [26, 27].

1.1.2 Equilibrium Model

In the simplest case an impurity atom embedded in a host metal leads to a local shift in the potential for the conduction band electrons. A nonzero concentration of impurity atoms then yields a disordered random potential for the host’s conduction band electrons leading to the physics of disordered systems [28].

To describe the Kondo effect a more sophisticated model is needed. As already discussed above, the Kondo effect arises from scattering of conduction band electrons at a localized magnetic impurity. Additional to a shift in the potential such an impurity adds a localized level at its site. This level hybridizes with the conduction band electrons of the host metal leading to fascinating physics, also beyond the Kondo limit of a singly occupied “magnetic” level [5].

The Anderson impurity model describes a localized impurity d-level hybridized with the host’s conduction band electrons:

$$H = \sum_{k,\sigma} \epsilon_k c_{k\sigma}^\dagger c_{k\sigma} + \sum_{\sigma} \epsilon_d d_{\sigma}^\dagger d_{\sigma} + \sum_{k,\sigma} V_k \left(c_{k\sigma}^\dagger d_{\sigma} + c_{k\sigma} d_{\sigma}^\dagger \right) + U d_{\uparrow}^\dagger d_{\uparrow} d_{\downarrow}^\dagger d_{\downarrow}. \quad (1.1)$$

Here $c_{k\sigma}^\dagger, c_{k\sigma}$ are the usual creation and annihilation operators for conduction band electrons with momentum k and spin σ , the corresponding operators for the d-level are given by

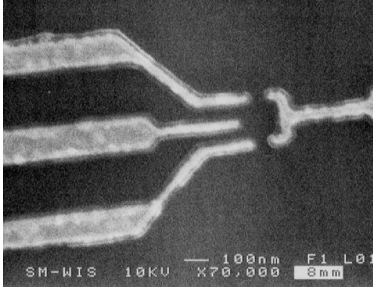


Figure 1.2: Scanning electron microscope image of a quantum dot [18]. The middle electrode on the left controls the energy of the dot relative to the conduction band electrons, the other three control the tunnel barriers between the dot and the leads. The contacts for source and drain at the top and bottom are not shown.

$d_\sigma^\dagger, d_\sigma$. V_k describes the hybridization of the localized d-levels with the conduction electron states and U is the Coulomb repulsion in the d-level. To model a singly occupied (magnetic) impurity a strong Coulomb repulsion $U \gg \Delta$ is required, where $\Delta = \pi V^2 \rho_0(\epsilon_d)$ is the broadening of the impurity level, $\rho_0(\epsilon_d)$ the conduction electron density of states at the impurity level and V is an appropriate average of $|V_k|$. For a comprehensive review on the Anderson impurity model (and also the Kondo model) see Ref. [5].

Since we intend to study effects by magnetic impurities, it is convenient to map the Hamiltonian (1.1) to an effective low-energy analog one where the d-level is always singly occupied. Using the so-called Schrieffer-Wolff transformation [29]

$$H_{\text{Kondo}} = e^S H e^{-S},$$

$$S = \sum_{k,\sigma} V_k \left(\frac{U}{(\epsilon_d - \epsilon_k)(\epsilon_d + U - \epsilon_k)} d_{-\sigma}^\dagger d_{-\sigma} c_{k\sigma}^\dagger d_\sigma + \frac{1}{\epsilon_k - \epsilon_d} c_{k\sigma}^\dagger d_\sigma \right) - \text{h.c.} \quad (1.2)$$

for $n_d = 1$ and neglecting terms of $\mathcal{O}(V^3)$ one finds the so-called Kondo Hamiltonian:

$$H_{\text{Kondo}} = \sum_{k,\sigma} \epsilon_k c_{k\sigma}^\dagger c_{k\sigma} + \sum_{p,q,\alpha,\beta} \frac{J(p,q)}{2} c_{p\alpha}^\dagger \vec{\sigma}_{\alpha\beta} c_{q\beta} \cdot \vec{S}. \quad (1.3)$$

Here $\vec{\sigma}$ is the vector of Pauli matrices, the Kondo coupling J is given by

$$J(p,q) = V_p V_q U \left(\frac{1}{(\epsilon_d - \epsilon_p)(\epsilon_d + U - \epsilon_p)} + \frac{1}{(\epsilon_d - \epsilon_q)(\epsilon_d + U - \epsilon_q)} \right). \quad (1.4)$$

The impurity spin operators are defined as $S^- = d_\uparrow^\dagger d_\uparrow$, $S^+ = d_\downarrow^\dagger d_\downarrow$, $S^z = (d_\uparrow^\dagger d_\uparrow - d_\downarrow^\dagger d_\downarrow)/2$. The momentum dependency of J is usually neglected if the density of states is constant around the Fermi level.

The Kondo Hamiltonian (1.3) was first introduced under the name s-d model by Kasuya [30] based on earlier works by Zener [31]. For a rigorous derivation of the Kondo Hamiltonian using flow equations see Ref. [32].

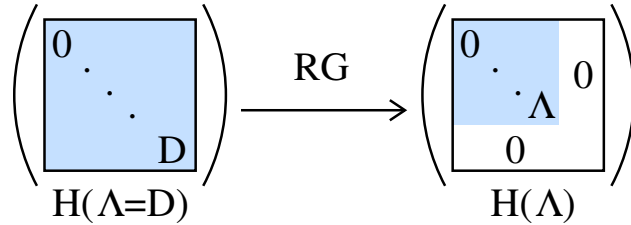


Figure 1.3: In conventional scaling approaches states at high energies are successively integrated out. The scaling parameter Λ describes the progress: while states at energies larger than Λ are already integrated out, states at smaller energies are still retained in the Hamiltonian.

As shown by Kondo [33] in 1964, in second order perturbation theory logarithmic corrections proportional to $-J^3 \ln(k_B T/D)$ arise in the resistance, where $2D$ is the bandwidth. For very small temperature the logarithmic terms dominate over the other contributions to the resistance:

$$R(T) = R_0 + aT^2 + bT^5 - c \ln(k_B T/D) , \quad (1.5)$$

where R_0 is the residual resistance, aT^2 is the electron contribution and bT^5 is the phonon contribution.

1.1.3 Scaling Approaches

It turns out that the physical properties of the Kondo Hamiltonian (1.3) are governed by the energy scale

$$k_B T_K = D \sqrt{\rho J} \exp\left(-\frac{1}{\rho J}\right) , \quad (1.6)$$

where T_K is the so-called Kondo temperature and ρ is the constant density of states. The density of states ρ is easily defined into the coupling J (see e.g. Ref. [34] and references therein), we therefore set $\rho = 1$ in the following. Since T_K is non-analytic in $J = 0$, perturbation theory for small coupling parameter J is futile.¹ At this point renormalization group (RG) approaches come in. The key idea behind (momentum space) RG approaches is to study a system at different energy scales. In condensed matter physics one is typically only interested in the small energy excitations of a model (e.g. scattering process at the Fermi level), but the Hamiltonian contains the full physics at all energy scales. It is therefore convenient to simplify the model in such a way that it only contains the relevant information.² In “conventional” scaling³ approaches the Hamiltonian is simplified by successively integrating out states at high energies.

¹See your favorite textbooks on quantum mechanics and complex analysis.

²To qualify for the name RG this has to be done (or has to be doable) in infinitesimal steps.

³Performing RG transformations is called scaling.

$$\left(\begin{array}{c} \boxed{\begin{array}{c} 0 \\ \cdot \\ \cdot \\ \cdot \\ D \end{array}} \\ H(0) \end{array} \right) \xrightarrow{U(B)} \left(\begin{array}{c} \boxed{\begin{array}{c} 0 \\ \cdot \\ \cdot \\ \cdot \\ 0 \end{array}} \\ H(B) \end{array} \right) \} \Delta\epsilon = B^{-1/2}$$

Figure 1.4: Using infinitesimal unitary transformations a Hamiltonian is brought into a banddiagonal form. The remaining effective bandwidth $\Delta\epsilon$ and the flow parameter B are related via $\Delta\epsilon = B^{-1/2}$. \tilde{D} is a shorthand notation for $D(B)$.

Assume a given problem in the energy range $0..D$ where one is only interested in low energy processes around 0. One then introduces a scaling parameter Λ that describes the progress of the transformation in the following way: at $\Lambda = D$ the system is given containing states at all energies, then the bandwidth Λ is successively reduced until one reaches the desired energy scale, see Fig. 1.3 for an illustration. The reduction of the bandwidth is absorbed in changes of the interaction parameter and possibly also in shifts of the energies. These changes and shifts are called renormalization.

In the context of the Kondo model the most influential scaling method is the “poor man’s scaling approach” by Anderson [35]. Based on this method Rosch *et al.* recently developed a more sophisticated approach based on energy dependent interaction parameters for the Kondo model [11, 36–38]. As in all scaling approaches based on Anderson’s original work renormalizations of energies cannot be included in this RG scheme. Though the shift of the conduction band electron energy levels does not play an important role in single impurity problems, the Zeeman splitting of the impurity (dot) levels due to the magnetic field is important since it e.g. sets the peak positions in the impurity (dot) spectral functions and also in the spin-spin correlation function. In the Kondo model the hybridization of the impurity (dot) levels with the conduction band electron levels leads to a shift of the Zeeman splitting, corresponding to a Knight shift. Note that this shift cannot be included in poor man’s scaling approaches.

Another issue arises in highly excited equilibrium situations, e.g. at high temperature or at high voltage bias. Here also states at high energies give important contributions to the physical properties of the system and conventional scaling approaches have to be stopped at the largest important energy scale, e.g. at $\Lambda = T$ where T is the temperature.

The flow equation method provides a different approach: the Hamiltonian is brought into a banddiagonal form by integrating out interaction matrix elements instead of integrating out states. This is done using infinitesimal unitary transformations. The interaction matrix elements with high energies are eliminated first (by unitary transformations), then successively matrix elements with smaller energies are integrated out, see the illustration in Fig. 1.4. By keeping the states at high energies the systems properties can still be described at all energy scales. Since unitary transformations are used for building up the

RG scheme also shifts of the energy levels are naturally included.

In the Kondo model the poor man's scaling equations are an important limiting case of the RG equations derived with the flow equation method. We therefore do not discuss the poor man's scaling equations here, instead we refer to Chap. 2 where we work out and discuss the scaling equations in their full beauty.

In typical many particle problems RG approaches generate new interactions which appear in higher order of the interaction parameter. One then has to find a suitable truncation scheme, which typically is perturbative in the interaction parameter. The intrinsic energy scale separation of the flow equation method is extremely helpful for deriving a stable expansion, especially in systems with additional dimensionful parameters like the magnetic field (or temperature or voltage bias). We dedicated Sect. 1.4 to a detailed description of the flow equation method.

1.2 The Non-Equilibrium Kondo Model

Recent improvements in the fabrication of semiconductor structures opened a new field in physics. At semiconductor interfaces, so-called semiconductor heterojunctions, artificial systems are formed. Electrons trapped in these systems behave like particles in a box. These localized artificial systems are called quantum dots. Due to their large geometric size (around 100 nanometer) the physical properties of quantum dots can be easier explored than the properties of single atoms on the surface of a bulk material.⁴

The Kondo problem is modeled by a singly occupied level coupled to one or more external leads. If e.g. an electric field is applied to the quantum dot the voltage drops directly at the quantum dot. In contrast, in a bulk material the voltage continuously drops over the full length of the system. It is therefore possible to apply a high voltage bias to the quantum system without bringing the leads out of the ohmic (linear response) regime.

Another way of bringing a quantum dot out of equilibrium is the coupling to external reservoirs at different temperature thereby driving a thermocurrent through the system [39]. This can be achieved by additional cooling (or heating) of one of the reservoirs.

1.2.1 Experimental Realization

The connection of two semiconductor interfaces with different material parameters (e.g. band gap and electron affinity) leads to deformations of the conduction and the valence band. Close to the interface a potential minimum is build up yielding the formation of a two dimensional electron gas. Typically GaAs/AlGaAs heterostructures⁵ are used to build quantum dots in the Kondo regime.

Upon this semiconductor structure metallic gates are brought up to control the parameters of the quantum dot, see Fig. 1.2. By tuning the chemical potentials of the metallic

⁴Exploring the properties of single atoms inside a bulk material is highly nontrivial.

⁵Gallium arsenide / aluminium gallium arsenide heterostructures.

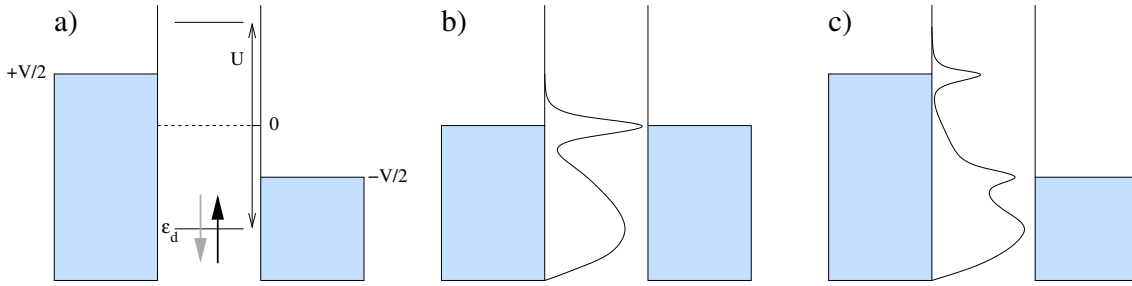


Figure 1.5: Subfig. a) Schematic energy diagram of a quantum dot in the Coulomb blockade regime at zero magnetic field. The lower level at energy ϵ_d is occupied by a single electron (either spin-up or spin-down), the Coulomb repulsion for an additional electron in the upper level is given by U , and V denotes the voltage bias. Subfig. b) In equilibrium the dot's density of states shows a narrow resonance at the Fermi energies of the leads. The lower bump corresponds to the broadened level at ϵ_d . Subfig. c) In non-equilibrium the resonance is split in peaks at the upper and the lower chemical potential.

gates the size and the electron filling of the quantum dot is adjustable. Also the tunneling of electrons between the quantum dot and the external reservoir is controlled by the metallic gates.

1.2.2 The Coulomb Blockade Regime

In the Coulomb blockade regime direct tunneling through the dot is suppressed. To achieve this suppression the quantum dot has to be tuned to a certain parameter regime. We assume that the total number of electrons in the dot is odd, such that the highest energy level is occupied by a single electron and all lower lying levels are double occupied (fully filled). For simplicity we assume zero magnetic field. Then the electron in the highest level is either spin-up or spin-down with equal probabilities. We denote the energy of the singly occupied energy level by ϵ_d , the Coulomb repulsion for adding a second electron in the level is given by U . Note that the strength of the Coulomb repulsion is determined by the size of the quantum dot, the smaller the dot the larger is U .

The dot is coupled to two leads at the chemical potentials $\mu_{l,r} = \pm V/2$ via tunable tunnel barriers. The voltage bias V , the energy ϵ_d , and the Coulomb repulsion U have to be chosen such that $\epsilon_d \ll -V/2$ and $\epsilon_d + U \gg V/2$, see Fig. 1.5 a) for an illustration. The tunneling is then blocked since the lead electrons do not have enough energy to tunnel into the upper level at $\epsilon_d + U$ and the dot electron does not have enough energy to tunnel to lowest the lying empty state in the leads at $-V/2$.

In the Coulomb blockade regime transport through the dot is only possible via the hybridization of the dot level with electron states in the lead, similar to the equilibrium Kondo interaction. In equilibrium the Kondo interaction leads to a narrow resonance in the dot's density of states at the Fermi level, in non-equilibrium this resonance is split in

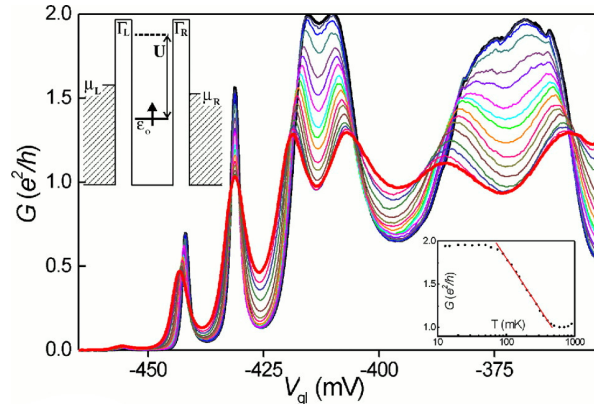


Figure 1.6: So-called Coulomb oscillations in the conductance G for the temperature range 15mK (thick black) to 800mK (thick red) at a magnetic field strength of 0.4 Tesla [23]. The gate voltage V_{gi} is used to alter the occupation of the quantum dot, in the valleys the total number of electrons in the dot is odd, at the peaks the electron number is even. Upon cooling the conductance in the middle valley (and also in the right one) is increased up to the maximal value $G = 2e^2/h$, the so-called unitary limit. Here e is the electronic charge and h is Planck's constant. The left inset shows the same setup as in Fig. 1.5 a), $\Gamma_{L,R}$ is the level broadening Δ (see Sect. 1.1.2) of the dot level by the hybridization with the left and the right lead, the chemical potential is given by $\mu_{L,R} = \pm V/2$, and finally $\epsilon_0 = \epsilon_d$. The inset on the right shows the logarithmic dependence of the center valley's height on the temperature.

resonances at the chemical potentials, see Figs. 1.5 b) and c). The enhancement of the density of states at the chemical potentials yields an increase of the conductance up to the unitary limit [21, 22].

This increase has been experimentally observed by Wiel *et al.* [23], see Fig. 1.6. When changing the total number of electrons in the dot (by the gate voltage) at “high” temperature (where the Kondo effect is suppressed) oscillations in the conductance through the dot are observed. If the total number of electrons in the dot is odd then the system is in the Coulomb blockade regime and tunneling is suppressed yielding a valley in Fig. 1.6. Instead, if the number of electrons is even direct tunneling is possible yielding a peak in Fig. 1.6. When lowering the temperature in the Coulomb blockade regime the Kondo effect sets in leading to an increase of the density of states at the chemical potentials. Thereby the conductance is increased.

1.2.3 Model and Hamiltonian

As main part of this thesis we study a spin-1/2 (Kondo-) coupled to two leads at different chemical potentials, the dot levels are split due to an applied magnetic field. This setup is sketched in Fig. 1.7. In the following we derive a general scaling picture that allows us

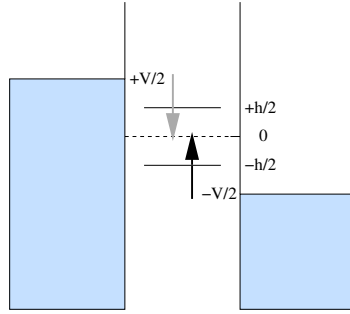


Figure 1.7: Schematic picture of a quantum dot in the Kondo regime coupled to two leads at the chemical potentials $\mu_{l,r} = \pm V/2$. The dot levels are split by an applied magnetic field. Note that in the Kondo model the dot level position ϵ_d enters only indirectly via the coupling J , see Eqs. (1.3) and (1.4). For a sketch it is convenient to set $\epsilon_d = 0$.

to study effects by different decoherence sources within a single framework. Within this framework we are able to study effects by the dc-voltage bias, the temperature, the magnetic field, and combinations of the latter without rederiving the (full) scaling equations.⁶ In addition we study non-equilibrium effects by a thermocurrent driven through the dot. This can be experimentally achieved by preparing the leads at different temperature [39]. The setup in Fig. 1.7 should therefore only be seen as the central motivation for this thesis. This work is a generalization of the previous flow equation analysis of the Kondo model in zero magnetic field [40, 41]. The extension to nonzero magnetic field not only leads to slightly more complicated expressions for the scaling equations. As we show in Chap. 2 the analysis of the flow equations at zero magnetic can be considered as the “trivial special case”. We also discuss scaling for the anisotropic Kondo model where the SU(2) symmetry of the interaction is broken. In addition we derive the impurity (dot) spectral function, the magnetization, the static spin susceptibility, the spin-spin correlation function, and the spin response function in both equilibrium and non-equilibrium situations.

The Hamiltonian of a spin-1/2 Kondo dot in a magnetic field coupled to two leads is given by [42, 43]

$$\begin{aligned}
 H = & \sum_{p,\alpha,\sigma} (\epsilon_p - \mu_\alpha) c_{p\alpha\sigma}^\dagger c_{p\alpha\sigma} - h S^z \\
 & + \sum_{p,q,\alpha,\beta} \frac{J_{\alpha\beta}}{2} \left(\left(c_{p\alpha\uparrow}^\dagger c_{q\beta\uparrow} - c_{p\alpha\downarrow}^\dagger c_{q\beta\downarrow} \right) S^z + \left(c_{p\alpha\uparrow}^\dagger c_{q\beta\downarrow} S^- + \text{h.c.} \right) \right),
 \end{aligned} \tag{1.7}$$

where $\alpha, \beta = l, r$ label the leads, $\sigma = \uparrow, \downarrow$ is the spin index, $\mu_{l,r} = \pm V/2$ is the chemical potential, and h is the magnetic field. Without loss of generality we assume $V \geq 0$. Note that in Refs. [42, 43] a time dependent Schrieffer-Wolff transformation was used to derive the non-equilibrium Hamiltonian (1.7).

⁶Of course the solution of the scaling equations and the evaluation of observables has to be redone for every case.

We split the operator space in even and odd combinations of fermionic operators from left and right lead:

$$\begin{aligned} f_{p\sigma} &= \frac{1}{\sqrt{1+R}}c_{pr\sigma} + \frac{1}{\sqrt{1+1/R}}c_{pl\sigma} \\ g_{p\sigma} &= \frac{1}{\sqrt{1+1/R}}c_{pr\sigma} - \frac{1}{\sqrt{1+R}}c_{pl\sigma} , \end{aligned} \quad (1.8)$$

where $R = J_{ll}/J_{rr}$ is the asymmetry parameter. Note that the f - and g -operators obey fermionic anticommutation relations. If the Hamiltonian (1.7) is derived from an underlying Anderson impurity model [42, 43] the antisymmetric operators $g_{p\sigma}^\dagger, g_{p\sigma}$ completely decouple from the dot and the Hamiltonian (1.7) can be written in terms of the f -operators only:

$$H = \sum_{p,\sigma} \epsilon_p f_{p\sigma}^\dagger f_{p\sigma} - hS^z + \sum_{p,q} \frac{J}{2} \left((f_{p\uparrow}^\dagger f_{q\uparrow} - f_{p\downarrow}^\dagger f_{q\downarrow}) S^z + (f_{p\uparrow}^\dagger f_{q\downarrow} S^- + \text{h.c.}) \right) . \quad (1.9)$$

Here we defined $J = J_{ll} + J_{rr}$ and we used $J_{lr}^2 = J_{rl}^2 = J_{ll}J_{rr}$. The Hamiltonian (1.9) is formally identical to the equilibrium Hamiltonian, only the occupation number

$$n_f(p) = \langle f_{p\sigma}^\dagger f_{p\sigma} \rangle = \begin{cases} 0 & , \epsilon_p > V/2 \\ \frac{1}{1+1/R} & , |\epsilon_p| \leq V/2 \\ 1 & , \epsilon_p < -V/2 \end{cases} \quad (1.10)$$

differs from equilibrium. The equilibrium Kondo temperature is given by Eq. (1.6). By using the Hamiltonian (1.9) we are able to describe the physics of both the equilibrium and the non-equilibrium system in a single scaling picture.

1.2.4 Previous Approaches

In the parameter regime $\max(V, |h|, T) \gg T_K$ the logarithmic divergence in the Kondo problem is cut off by decoherence effects thereby making the situation a weak-coupling problem. This has already been established by previous renormalization group calculations [36–38, 42–46]. This was confirmed by the previous flow equation analysis of the Kondo model with voltage bias [40, 41]. Recently additional scaling approaches to non-equilibrium problems were developed: the real time renormalization group [47–50] and the Coulomb gas representation [51, 52]. The key results of this thesis are the derivation of the spin-spin correlation function, the T-Matrix, the magnetization and the static spin susceptibility in both equilibrium and non-equilibrium situations.

In equilibrium the magnetization and the static spin susceptibility of the dot are well known from Bethe Ansatz [7, 8]. Previous non-equilibrium perturbation theory calculations [46, 53] for the magnetization and the static spin susceptibility derived the correct high voltage / high temperature ($V \rightarrow \infty$ or $T \rightarrow \infty$) results, but the important logarithmic corrections are missing. Using the flow equation approach we are able to calculate the

magnetization and the static spin susceptibility including the leading logarithmic corrections consistently in both equilibrium and non-equilibrium.

The T-Matrix and the closely related impurity spectral function are well studied objects [9, 11–13, 17, 45]. Nevertheless, some parameter regimes as e.g. the crossover from the high voltage regime to the high magnetic field one have not yet been studied. We will rederive the previous results and give additional insights into the crossover regimes. In linear response the conductance is closely related to the spectral function, see Sec. 3.1. Thereby a conductance measurement in the linear response regime indirectly also measures the spectral function. Additionally the spectral function can be measured directly by tunneling experiments [54].

The equilibrium spin-spin correlation function is known in all parameter regimes [14, 15, 45, 55], also in the context of the equilibrium spin boson model. We extend the previous results to the full parameter regime accessible within our method. The corresponding response function can be measured by nuclear magnetic resonance [56, 57] and electron spin resonance [58–60] experiments.

1.2.5 Decoherence Effects

The Kondo effect arises from resonant and coherent spin-flip scattering of low energy conduction band electrons at the impurity (dot) levels, the width of the resonance is proportional to the Kondo temperature T_K . At zero magnetic field these spin-flip scattering processes correspond to low energy excitations of the groundstate. If a high magnetic field $|h| \gg T_K$ is applied, the degeneracy of the levels becomes larger than the width of the Kondo resonance yielding a suppression of resonant spin-flip scattering processes since the overlap of the two levels in energy space becomes negligible.

At high temperature $T \gg T_K$ the broadening of the Fermi edge is much larger than the resonance width and then also incoherent scattering processes with high energy transfer occur in nonnegligible numbers. Their thermal noise leads to relaxation processes of the spin: assume we prepared a spin in a given configuration. Then the relaxation time gives us the time scale on which our initial configuration of the spin decays into another more favorable configuration (e.g. due to the thermal noise). On the other hand the system still performs coherent (low energy) scattering processes. In this context coherence simply means that there exists a phase relation between successive scattering processes. This phase relation affects mainly scattering processes within a certain time scale, the so-called coherence time. Going back to the simple picture of a prepared spin, the conduction band electrons try to prepare the spin in a certain configuration to perform (energetic favorable) scattering processes on this state. If the decoherence time scale is much shorter than the coherence time scale, the latter spin configuration is destroyed by relaxation processes much before the system could finish its coherent scattering processes. Thereby at high temperature coherent scattering processes are suppressed by relaxation processes induced by thermal noise.

The situation is quite different for a Kondo dot with applied high dc-voltage bias $V \gg T_K$ since the resonant scattering processes do not care much about the position of

the chemical potential. Note that in the Kondo model the dot is assumed to be singly occupied at all times. Though conduction band electrons from both chemical potentials scatter in resonance with the dot levels, the coherence is destroyed by the shot noise of the current through the dot. Of course, the current not only depends on the voltage bias, also the strength of the Kondo coupling $J_{\alpha\beta}$ enters. As shown by Kaminski *et al.* [42, 43] the current I through the dot is in leading order given by ($V \gg T_K$)

$$I = \frac{e^2}{\hbar} \frac{3\pi}{4} \frac{1}{(\ln(V/T_K))^2} \frac{V}{(1+R)(1+1/R)}, \quad (1.11)$$

where e is the electronic charge $R = J_{ll}/J_{rr}$ is the asymmetry parameter. Thereby a large enough voltage bias automatically leads to a large enough current.

1.3 General Non-Equilibrium Theory

From hydrodynamics it is well-known that in far out of equilibrium systems dramatic effects may occur. Famous examples are the Rayleigh-Bénard convection and the Taylor-Couette instability, for a review see e.g. Ref. [61]. In quantum mechanical systems such massive non-equilibrium effects have not yet been observed. However, it is an interesting question if such situations can be realized also in quantum systems.

In recent experiments on semiconductor quantum dots [18–20, 39] and on ultracold quantum gases [62, 63] quantum systems with tunable parameters were modeled, also in far out of equilibrium situations. These experiments provide an excellent basis for studying non-equilibrium quantum systems, both for theorists and experimentalists.

In this section we give a short introduction to linear response theory. We briefly discuss why linear response theory typically fails to describe the physics of systems far out of equilibrium. In addition, we briefly review selected methods to describe quantum systems in non-equilibrium, namely the Keldysh formalism and the scattering state approach.

1.3.1 Linear Response Theory

The response of a system to a small perturbing external field or probe potential is typically discussed in linear response theory. The Hamiltonian of the system is given by H_0 , the probe potential is given by $H_p(t)$. For simplicity we assume that H_0 is time independent. For example the probe Hamiltonian for an external electric potential $U(r, t)$ coupling to the electronic charge density $\rho(r)$ is given by

$$H_p(t) = \int dr \rho(r)U(r, t) . \quad (1.12)$$

The time evolution of the state $|\Psi\rangle$ is studied in the interaction picture ($\hbar = 1$):

$$i \frac{\partial}{\partial t} |\Psi(t)\rangle = H |\Psi(t)\rangle = (H_0 + H_p(t)) |\Psi(t)\rangle . \quad (1.13)$$

To simplify this expression we define

$$|\Phi(t)\rangle = \exp(iH_0t) |\Psi(t)\rangle . \quad (1.14)$$

The time evolution of $|\Phi(t)\rangle$ is given by

$$\begin{aligned} i\frac{\partial}{\partial t}|\Phi(t)\rangle &= -H_0|\Phi(t)\rangle + \exp(iH_0t) i\frac{\partial}{\partial t}|\Psi(t)\rangle \\ &= -H_0|\Phi(t)\rangle + \exp(iH_0t) (H_0 + H_p(t))|\Psi(t)\rangle \\ &= \exp(iH_0t) H_p(t) \exp(-iH_0t) |\Phi(t)\rangle . \end{aligned} \quad (1.15)$$

It is convenient to define the shorthand notation

$$H_p^I(t) = \exp(iH_0t) H_p(t) \exp(-iH_0t) . \quad (1.16)$$

Integration of Eq. (1.15) yields

$$|\Phi(t)\rangle = |\Phi(-\infty)\rangle - i \int_{-\infty}^t dt_1 H_p^I(t_1) |\Phi(t_1)\rangle . \quad (1.17)$$

Here $|\Phi(-\infty)\rangle$ is a suitable eigenstate of the unperturbed system describing the initial preparation of the system. The integration range is given by $t_1 = -\infty..t$ since in quantum mechanics all previous processes have to be taken into account. In contrast, for a description in classical mechanics the state of the system at any time $t_1 < t$ is sufficient. Formally Eq. (1.17) can be solved by iteration:

$$\begin{aligned} |\Phi(t)\rangle &= |\Phi(-\infty)\rangle - i \int_{-\infty}^t dt_1 H_p^I(t_1) |\Phi(-\infty)\rangle + \\ &\quad + \int_{-\infty}^t dt_1 \int_{-\infty}^{t_1} dt_2 H_p^I(t_1) H_p^I(t_2) |\Phi(-\infty)\rangle - \dots . \end{aligned} \quad (1.18)$$

If the interaction H_p^I is sufficiently weak only the linear term has to be taken into account. This provides the essence of linear response theory.

In general the iterative solution can only be truncated for probe potentials that change slower than the system's reaction time, so-called adiabatic switching processes. Typically this is the case for infinitesimal slow switching of the probe potential only. Otherwise one has to consider that the iterative solution (1.18) is not an expansion in the interaction parameter but in the interaction parameter integrated over time. At long time scales (much larger than one over interaction parameter) a truncated iterative solution simply yields the time evolution of the highest order terms in the perturbation series and not the time evolution of the expanded state. For example an expansion in fourth order at very long times scales ($t \rightarrow \infty$) is simply proportional to t^4 . The terms dominating the

perturbative truncation of the time evolution at very long times scales are called secular terms.

Transport in the Kondo Model is a nontrivial problem. The voltage drop at magnetic impurities embedded in a metallic host is typically very small since the voltage drops over the full length of the host metal. Here linear response theory is sufficient. In quantum dots the situation is different since here the voltage bias is directly applied to the dot and can be tuned to comparatively large values. If the voltage bias is large enough to drive a strong current through the dot, then the system can no longer relax to an equilibrated state. Instead the system relaxes to the so-called steady state, which cannot be described in linear response theory.

A system is in a steady state if its properties are not changing in time and it is not in thermal equilibrium. During the relaxation process the system is in the so-called transient state. The direct opposite of adiabatic switching is instantaneous switching. Here the probe potential is switched on (or off) by a Θ -step-function. Such situations were only recently realized in experiments on ultracold quantum gases [62, 63]. Here again a more sophisticated approach than linear response is needed.

1.3.2 The Keldysh Formalism

The Keldysh formalism is a well-known approach to time evolution, this short introduction is heavily based on Ref. [64].

In the following we discuss the Keldysh formalism focusing on instantaneous switching. At a given time the probe potential - e.g. a strong electric field - is switched on. For very long waiting time ($t \rightarrow \infty$) an infinitely large system relaxes to the steady state. Note that in the Kondo model the correct physical picture is to switch on the interaction J (the hybridization) and not to switch on the voltage bias. Since the time evolution of the given initial configuration of the system is highly nontrivial, it is desirable to work out the physical properties of the system from the (hopefully) simpler initial preparation state of the system.

We begin with an isolated system in thermal equilibrium that is described by the time independent Hamiltonian H_0 for $t < 0$. At $t = 0$ a probe potential H_p is switched on. The full Hamiltonian of the system is then given by

$$H(t) = \begin{cases} H_0 & , t < 0 \\ H_0 + H_p(t) & , t \geq 0 \end{cases} . \quad (1.19)$$

We are mainly interested in the physical properties of the system. In quantum mechanics these are given by the expectation value of some operator O . Its expectation value at $t \leq 0$ is given by $\text{Tr}(\rho_0 O)$, where ρ_0 is the density matrix describing the Hamiltonian H_0 . Since ρ_0 and H_0 commute the expectation value is constant for $t < 0$. At $t > 0$ the time evolution of the expectation value is given by

$$\langle O(t) \rangle = \text{Tr} (\rho_0 U(0, t) O U(t, 0)) , \quad (1.20)$$

where the time evolution operator $U(t_1, t_2)$ is given by the solution of ($\hbar = 1$)

$$\begin{aligned} i \frac{d}{dt_1} U(t_1, t_2) &= H(t_1) U(t_1, t_2) \\ i \frac{d}{dt_2} U(t_1, t_2) &= -U(t_1, t_2) H(t_2) \end{aligned} \quad (1.21)$$

with the boundary condition $U(t, t) = \mathbf{1}$. Formally the solution is given by

$$U(t_1, t_2) = \begin{cases} T_D \exp \left(-i \int_{t_2}^{t_1} dt_3 H(t_3) \right) & , t_1 > t_2 \\ T_D^\dagger \exp \left(-i \int_{t_2}^{t_1} dt_3 H(t_3) \right) & , t_1 < t_2 \end{cases}, \quad (1.22)$$

where T_D is the usual Dyson time ordering operator.

Since we assumed the initial ($t < 0$) system to be in thermal equilibrium, its density matrix is given by

$$\rho_0 = \frac{e^{-\beta(H_0 - \mu N)}}{\text{Tr}(e^{-\beta(H_0 - \mu N)})}, \quad (1.23)$$

with the inverse temperature $\beta = 1/T$ ($k_B = 1$), the chemical potential μ and the number operator N . Provided that the initial Hamiltonian H_0 and the number operator N commute (or $\mu = 0$), it is convenient to introduce the complex time argument $t = -i\beta$. Then the density matrix is given by

$$\rho_0 = \frac{e^{\beta\mu N} U(-i\beta, 0)}{\text{Tr}(e^{\beta\mu N} U(-i\beta, 0))} \quad (1.24)$$

and Eq. (1.20) yields

$$\langle O(t) \rangle = \frac{\text{Tr}(e^{\beta\mu N} U(-i\beta, 0) U(0, t) O U(t, 0))}{\text{Tr}(e^{\beta\mu N} U(-i\beta, 0))}. \quad (1.25)$$

From the time evolution in the numerator one easily reads of a time contour for the time evolution. We first go forward in time from 0 to t , then backward in time from t to 0, and finally from 0 to $-i\beta$ on the imaginary time axis. The contour C is sketched in Fig. 1.8.

In non-equilibrium physics one is mainly interested in the steady state properties of the system. Within the Keldysh formalism expectation values with respect to the steady state are worked out as follows. At $t = 0$ the probe potential, e.g. an electric field, is switched on. The steady state evolves for long time scales ($t \rightarrow \infty$). The advantage of the Keldysh formalism is that there is no need to evaluate the steady state directly, which is a highly nontrivial task for general models.

With the definition of the contour C in Fig. 1.8 the expectation value of the operator O in the steady state is given by

$$\langle O(z = \infty) \rangle = \frac{\text{Tr}(e^{\beta\mu N} T_C e^{-i \int_C dz_1 H(z_1)} O(z = \infty))}{\text{Tr}(e^{\beta\mu N} T_C e^{-i \int_C dz_1 H(z_1)})}, \quad (1.26)$$

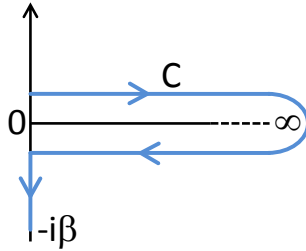


Figure 1.8: Sketch of the Keldysh contour C in the complex time plane (for $t \rightarrow \infty$): the time evolution starts at $t = 0$ and ends at $t = -i\beta$.

where z_1 runs along the contour C from 0 to $-i\beta$ and T_C denotes ordering along the contour. The variable z corresponds to the position (time) on the contour C .

The next step in the Keldysh formalism is introducing non-equilibrium Green's functions. However, since we do not use the Keldysh formalism for our calculation and the next steps in this formalism are rather technical, we refer to one of the many introductions to the Keldysh formalism for further reading, e.g. Refs. [64, 65].

A Keldysh treatment of the Kondo model is highly nontrivial [45, 46]. As we show in this thesis the physical properties of the system - especially the dynamical ones - can be much easier accessed by diagonalizing the Hamiltonian using flow equations.

1.3.3 Scattering State Approaches

Only recently several scattering state approaches focusing on non-equilibrium systems were developed [24–27]. We again denote the unperturbed system by H_0 , the time independent probe potential is denoted by H_p .

The key idea of scattering state approaches is summarized as follows. An incoming eigenstate $|\Phi\rangle$ of H_0 with eigenenergy E scatters off the probe potential and is transferred to the scattering state $|\Psi\rangle$. The scattering state is an eigenstate of $H = H_0 + H_p$. Since we study scattering at impurities (quantum dots), we neglect the small shift of the eigenenergies due to the probe potential:

$$H_0|\Phi\rangle = E|\Phi\rangle \quad \Rightarrow \quad H|\Psi\rangle = E|\Psi\rangle . \quad (1.27)$$

In the limit of vanishing interaction ($H_p \rightarrow 0$) the scattering state is formally given by

$$|\Psi\rangle = |\Phi\rangle + \frac{1}{E - H_0} H_p |\Psi\rangle . \quad (1.28)$$

Since E is an eigenvalue of H_0 the previous equations is singular. The denominator is therefore shifted into the complex plane by a small number ϵ yielding the Lippmann-Schwinger equation

$$|\Psi^\pm\rangle = |\Phi\rangle + \frac{1}{E - H_0 \pm i\epsilon} H_p |\Psi^\pm\rangle . \quad (1.29)$$

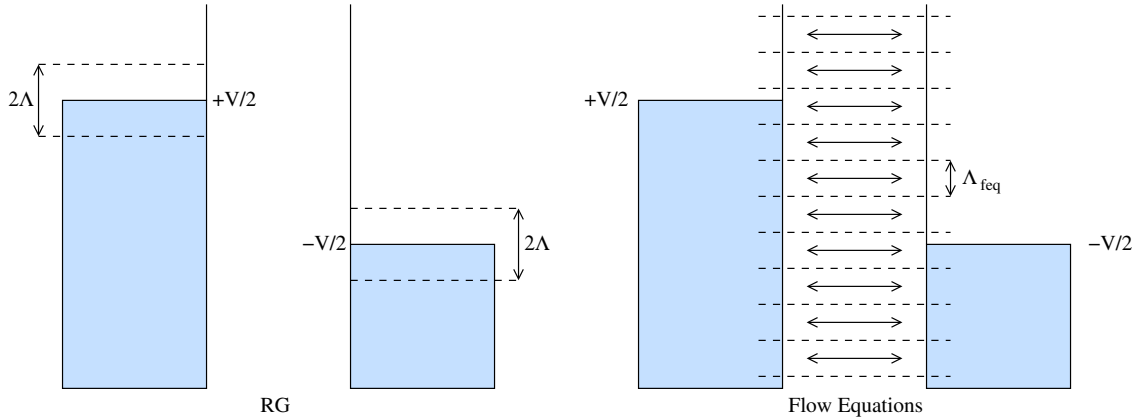


Figure 1.9: If the RG-bandwidth Λ becomes smaller than the voltage bias, energy diagonal scattering processes between the two leads are impossible. In the flow equations picture these are still included in the Hamiltonian.

Note that the scattering eigenstate $|\Psi\rangle$ is equivalent to the steady state of the non-equilibrium system. Again the further calculation is highly nontrivial for general models. We therefore refer to Refs. [24–27] for additional information on constructing the scattering eigenstates.

1.4 The Flow Equation Method

Conventional scaling approaches focus on the states around the chemical potentials. If the scaling parameter Λ becomes smaller than the voltage bias energy conserving interlead scattering processes⁷ - so-called energy diagonal processes - are no longer included in the Hamiltonian, see the sketch in Fig. 1.9. Therefore decoherence effects induced by the current can no longer be studied and one has to stop the scaling at $\Lambda = V$. In the flow equation approach interaction matrix elements are integrated out instead of integrating out states. Since this is done successively from high to small energy transfer, energy diagonal processes remain in the Hamiltonian until the end and decoherence effects by the current are naturally included.

In the following section we discuss the general setup of the flow equation method. The construction of the unitary transformation is shown in Sect. 1.4.2, in Sect. 1.4.3 we give a simple application example to motivate the ansatz for the generator and provide basic concepts to solve the differential equations resulting from the flow equation approach. In Sect. 1.4.4 we discuss the limitations of a perturbative expansion of the flow equation transformation. The normal-ordering procedure is sketched in Sect. 1.4.5.

⁷Since there is no energy dissipation (e.g. phonons) these processes give the main contribution to the current.

1.4.1 General Setup

The flow equation method [66] provides a framework to diagonalize a Hamiltonian using infinitesimal unitary transformations. The diagonalization procedure works as follows. First interaction matrix elements with high energy transfer are eliminated, then successively matrix elements with small energy transfer are integrated out, see Fig. 1.4. We introduce the flow parameter B to label the progress of the diagonalization procedure: the remaining effective bandwidth is given by $\Delta\epsilon = B^{-1/2} = \Lambda_{\text{feq}}$, so at $B = 0$ the Hamiltonian is in the original basis and at $B = \infty$ the Hamiltonian is diagonal.

Constructing such unitary transformations is of course difficult for many particle problems.⁸ It is therefore convenient to work out transformed objects only: the transformed Hamiltonian $H(B) = U(B)HU^\dagger(B)$ is constructed via the ordinary differential equation

$$\frac{dH(B)}{dB} = [\eta(B), H(B)] , \quad (1.30)$$

where the generator $\eta(B)$ is a suitable antihermitian operator $\eta^\dagger(B) = -\eta(B)$. Actually any antihermitian generator leads to a unitary transformation $U^\dagger(B) = U^{-1}(B)$, but of course only a certain set of generators leads to a diagonal Hamiltonian. In the following section we prove that the unitary transformation and its generator are related by

$$\frac{dU(B)}{dB} = \eta(B)U(B) . \quad (1.31)$$

The generic choice for the generator is given by [66]

$$\eta(B) = [H_0(B), H_{\text{int}}(B)] , \quad (1.32)$$

where $H_0(B)$ is the diagonal part of the Hamiltonian and $H_{\text{int}}(B)$ the interaction part. With this choice the flow parameter B and the remaining effective bandwidth $\Delta\epsilon$ are related via $\Delta\epsilon = B^{-1/2}$. Note that a different choice of the generator leads to a different interpretation of the flow parameter. In certain problems processes at specific energy scales dominate the flow of the Hamiltonian. To describe such problems it is essential to take all processes at a given energy scale into account in a controlled way. In contrast to conventional scaling approaches, where states at high energies are integrated out, an intrinsic energy scale separation is included in the flow equation method.

In typical many particle problems the flow equation method generates additional interactions, which are typically of higher order in the interaction parameter. To keep track of these newly generated interactions we introduce a parameter $\lambda = 1$ in the Hamiltonian:

$$H(B) = H_0(B) + \lambda H_{\text{int}}(B) . \quad (1.33)$$

We only take terms into account that enter the flow of the original Hamiltonian up to a certain power of λ . We denote the order of the calculation by loops: a n -loop calculation

⁸Actually this is already nontrivial for simple objects like general real symmetric 3×3 matrices.

takes only terms up to order λ^{n+1} into account. Note that this concept corresponds to a loop expansion in renormalization theory. The interaction parameter as function of the flow parameter is called running coupling.

To work out the commutators (1.30) and (1.32) a suitable operator product expansion is needed. For products of fermionic operators normal-ordering (see Sect. 1.4.5) with respect to the noninteracting ground state is typically a suitable approach. Typically the resulting error is negligible. However, for general models it is of course unclear whether the interacting ground state can be described as a perturbation of the noninteracting one or not.

The unitary transformation is not worked out. Therefore operators have to be transformed into the diagonal ($B = \infty$) basis to work out expectation values. In typical many body problems the eigenstates of the Hamiltonian are very complicated objects. Especially for deriving analytical results it is convenient to have simple eigenstates. Hence it is not cutback that the unitary transformation and therefore also the eigenstates in the original ($B = 0$) basis are not easily accessible.

An operator O is transformed via

$$\frac{dO(B)}{dB} = [\eta(B), O(B)] , \quad (1.34)$$

where again $O(B) = U(B)OU^\dagger(B)$. A general operator generates an infinite number of higher order terms and one has to chose a suitable approximation scheme, which is again perturbative in the running coupling.

We addressed Chap. 3 to the transformation of operators and the calculation of expectation values, see especially Sect. 3.2 for the details. Note that the techniques used in this section are not flow equation specific, any unitary transformation that diagonalizes the given Hamiltonian will do the job.

1.4.2 Infinitesimal Unitary Transformations

The unitary transformation $U(B)$ is constructed from the differential equation for the Hamiltonian (1.30):

$$\begin{aligned} \frac{dH(B)}{dB} &= \left(\frac{dU(B)}{dB} \right) HU^\dagger(B) + U(B)H \left(\frac{dU^\dagger(B)}{dB} \right) \\ &= \left(\frac{dU(B)}{dB} \right) U^\dagger(B)U(B)HU^\dagger(B) + U(B)HU^\dagger(B)U(B) \left(\frac{dU^\dagger(B)}{dB} \right) \\ &\stackrel{!}{=} \eta(B)U(B)HU^\dagger(B) + U(B)HU^\dagger(B)\eta^\dagger(B) \\ &= [\eta(B), H(B)] , \end{aligned} \quad (1.35)$$

where we used $U^\dagger(B) = U^{-1}(B)$ and $\eta^\dagger(B) = -\eta(B)$. The transformation is easily constructed from the differential equation

$$\frac{dU(B)}{dB} = \eta(B)U(B) , \quad (1.36)$$

where $U(B=0) = \mathbb{1}$. Note that the Hamiltonian H in Eq. (1.35) can be replaced by an arbitrary linear operator and that any antihermitian generator $\eta(B)$ leads to a unitary transformation.

In analogy to time evolution in the interaction picture we iterate the solution:

$$\begin{aligned} U(B) &= \mathbb{1} + \int_0^B dB_1 \eta(B_1) U(B_1) \\ &= \mathbb{1} + \int_0^B dB_1 \eta(B_1) + \int_0^B dB_1 \int_0^{B_1} dB_2 \eta(B_1) \eta(B_2) + \dots \end{aligned} \quad (1.37)$$

In the following we introduce Dyson's ordering operator for B -ordering. Using integration by parts we find⁹

$$\begin{aligned} \int_0^B dB_1 \int_0^{B_1} dB_2 \eta(B_1) \eta(B_2) &= \int_0^B dB_1 \int_0^B dB_2 \eta(B_1) \eta(B_2) - \int_0^B dB_1 \int_0^{B_1} dB_2 \eta(B_2) \eta(B_1) \\ &= \int_0^B dB_1 \int_0^B dB_2 \eta(B_2) \eta(B_1) - \int_0^B dB_1 \int_0^{B_1} dB_2 \eta(B_2) \eta(B_1) \\ &= \int_0^B dB_1 \int_{B_1}^B dB_2 \eta(B_2) \eta(B_1) . \end{aligned} \quad (1.38)$$

From this equation follows

$$\begin{aligned} \int_0^B dB_1 \int_0^{B_1} dB_2 \eta(B_1) \eta(B_2) &= \frac{1}{2} \left(\int_0^B dB_1 \int_0^{B_1} dB_2 \eta(B_1) \eta(B_2) + \right. \\ &\quad \left. + \int_0^B dB_1 \int_{B_1}^B dB_2 \eta(B_2) \eta(B_1) \right) \\ &= \frac{1}{2!} T_B \int_0^B dB_1 \int_0^B dB_2 \eta(B_1) \eta(B_2) , \end{aligned} \quad (1.39)$$

where we introduced the Dyson like B -ordering operator T_B . In analogy to time evolution operator products are ordered in such a way that the operators at small B are moved to the right and the ones for large B are moved to the left. The generalization to higher

⁹Hint: $u' = \eta(B_1)$, $v = \int_0^{B_1} dB_2 \eta(B_2)$.

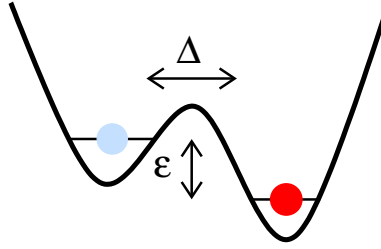


Figure 1.10: Tunneling in an asymmetric double well potential: Two levels with energy splitting ϵ are connected by the tunneling rate Δ .

order terms is trivial. Summing up we arrived at a handy expression for the unitary transformation:

$$U(B) = \sum_{k=0}^{\infty} \frac{1}{k!} T_B \left(\int_0^B dB_1 \eta(B_1) \right)^k = T_B \exp \left(\int_0^B dB_1 \eta(B_1) \right). \quad (1.40)$$

The B -ordering is interpreted as follows. If the flow parameter B can be related to the remaining effective bandwidth $\Delta\epsilon$ via $\Delta\epsilon = B^{-1/2}$ the unitary transformation first acts in such a way that the operators in the generator $\eta(B)$ are applied successively from high to low energies. As already stated above this intrinsic energy scale separation is the key improvement of the flow equation approach compared to conventional scaling approaches.

1.4.3 Tunneling in a Double Well

In this section we discuss tunneling in an asymmetric double well potential using flow equations, see Fig. 1.10. The Hamiltonian is given by

$$H = \frac{\epsilon}{2} \begin{pmatrix} 1 & 0 \\ 0 & -1 \end{pmatrix} - \frac{\Delta}{2} \begin{pmatrix} 0 & 1 \\ 1 & 0 \end{pmatrix} = \frac{\epsilon}{2} \sigma_z - \frac{\Delta}{2} \sigma_x = H_0 + H_{\text{int}}. \quad (1.41)$$

Though this simple model is easily solved using exact diagonalization we discuss it in the flow equation framework to introduce the basic concepts of the method. In the following we assume $\epsilon \neq 0$ since the flow equation method is doomed to fail if all diagonal matrix elements are equal.¹⁰ Using the standard commutation relation for Pauli matrices $[\sigma_a, \sigma_b] = 2i\epsilon_{abc}\sigma_c$ one easily shows

$$\eta(B) = -\frac{\epsilon(B)\Delta(B)}{4} [\sigma_z, \sigma_x] = -i\frac{\epsilon(B)\Delta(B)}{2} \sigma_y. \quad (1.42)$$

¹⁰Then the generator η is zero yielding the unitary transformation $U(B) \equiv \mathbb{1}$.

To derive the flow equations for the double well Hamiltonian (1.41) we have to calculate the commutator $[\eta(B), H(B)]$ yielding

$$\begin{aligned} [\eta(B), H_0(B)] &= -i \frac{\epsilon^2(B)\Delta(B)}{4} [\sigma_y, \sigma_z] = \frac{\epsilon^2(B)\Delta(B)}{2} \sigma_x \\ [\eta(B), H_{\text{int}}(B)] &= i \frac{\epsilon(B)\Delta^2(B)}{4} [\sigma_y, \sigma_x] = \frac{\epsilon(B)\Delta^2(B)}{2} \sigma_z . \end{aligned} \quad (1.43)$$

By comparison with Eq. (1.41) we identify

$$\frac{d\Delta(B)}{dB} = -\epsilon^2(B)\Delta(B) \quad (1.44)$$

$$\frac{d\epsilon(B)}{dB} = \epsilon(B)\Delta^2(B) . \quad (1.45)$$

In the following we use the shorthand notations $\epsilon_0 = \epsilon(B=0)$ and $\Delta_0 = \Delta(B=0)$. Integration of Eq. (1.44) yields

$$\Delta(B) = \Delta_0 \exp \left(- \int_0^B dB_1 \epsilon^2(B_1) \right) . \quad (1.46)$$

The coupling $\Delta(B)$ decays to zero if the integral in the exponential diverges. Using the generic choice of the generator $\eta(B) = [H_0(B), H_{\text{int}}(B)]$ typically leads to an exponential decay of the latter form.

Comment:

In more challenging models the flow equation for an interaction $I(B)$ is usually of the form

$$\frac{dI(B)}{dB} = -\epsilon^2(B)I(B) + f(I(B), B, \dots) . \quad (1.47)$$

The formal solution of this differential equation is given by

$$I(B) = e^{-\int_0^B dB_1 \epsilon^2(B_1)} \left(I(B=0) + \int_0^B dB_1 e^{+\int_0^{B_1} dB_2 \epsilon^2(B_2)} f(I(B_1), B_1, \dots) \right) . \quad (1.48)$$

Here the Hamiltonian is only diagonalized if the exponential decay dominates over the integration of the exponential increase times the function f . The function f usually is proportional to an exponential decay thereby increasing the chances of convergence. In general it is unclear whether a specific model can be solved using the flow equation method or not unless one derived and solved the flow equations.

To solve the flow equations for the Hamiltonian (1.41) we use the relation

$$-2\Delta(B)\frac{d\Delta(B)}{dB} = 2\epsilon(B)\frac{d\epsilon(B)}{dB} \quad (1.49)$$

leading to

$$\Delta^2(B) = \epsilon_0^2 + \Delta_0^2 - \epsilon^2(B) . \quad (1.50)$$

Using this relation with Eq. (1.45) yields

$$\frac{d\epsilon(B)}{dB} = \epsilon(B) (\epsilon_0^2 + \Delta_0^2 - \epsilon^2(B)) . \quad (1.51)$$

One easily shows that the absolute value of $\epsilon(B)$ increases until the flow stops in the fixpoint

$$\epsilon_{\text{fix}} = \text{sgn}(\epsilon_0)\sqrt{\epsilon_0^2 + \Delta_0^2} . \quad (1.52)$$

The eigenvalues of the double well Hamiltonian (1.41) are given by $\lambda_{\pm} = \pm\epsilon_{\text{fix}}/2$, which is easily checked:

$$\det \begin{pmatrix} \epsilon_0/2 - \lambda & -\Delta_0/2 \\ -\Delta_0/2 & -\epsilon_0/2 - \lambda \end{pmatrix} = \frac{1}{4} (-\epsilon_0^2 + 4\lambda^2 - \Delta_0^2) \stackrel{!}{=} 0 . \quad (1.53)$$

We continue the analysis of the flow equations by solving Eq. (1.51):

$$\begin{aligned} \int_0^B dB_1 &= \int_{\epsilon_0}^{\epsilon} d\epsilon_1 \frac{1}{\epsilon_{\text{fix}}^2 \epsilon_1 - \epsilon_1^3} \\ B &= -\frac{1}{2\epsilon_{\text{fix}}^2} \ln \left(\frac{\epsilon^2 - \epsilon_{\text{fix}}^2}{\epsilon_0^2 - \epsilon_{\text{fix}}^2} \right) + \frac{1}{\epsilon_{\text{fix}}^2} \ln \left(\frac{\epsilon}{\epsilon_0} \right) \\ \epsilon(B) &= \epsilon_0 \sqrt{\frac{\epsilon_0^2 + \Delta_0^2}{\epsilon_0^2 + \Delta_0^2 \exp(-2B(\epsilon_0^2 + \Delta_0^2))}} . \end{aligned} \quad (1.54)$$

With Eq. (1.50) follows

$$\Delta(B) = \Delta_0 \sqrt{\frac{\epsilon_0^2 + \Delta_0^2}{\Delta_0^2 + \epsilon_0^2 \exp(2B(\epsilon_0^2 + \Delta_0^2))}} \stackrel{B \rightarrow \infty}{\sim} \exp(-B(\epsilon_0^2 + \Delta_0^2)) \quad (1.55)$$

leading to a diagonal Hamiltonian in the limit $B \rightarrow \infty$. In Fig. 1.11 we plotted $\epsilon(B)$ and $\Delta(B)$ for the initial value $\epsilon_0 = \Delta_0 = 1$. From Eqs. (1.54) and (1.55) one easily identifies a critical value of the flow parameter:

$$B_c = \frac{1}{2} (\epsilon_0^2 + \Delta_0^2)^{-2} . \quad (1.56)$$

If B is much smaller than B_c the system is unchanged and for $B \gg B_c$ the interaction matrix element is integrated out.

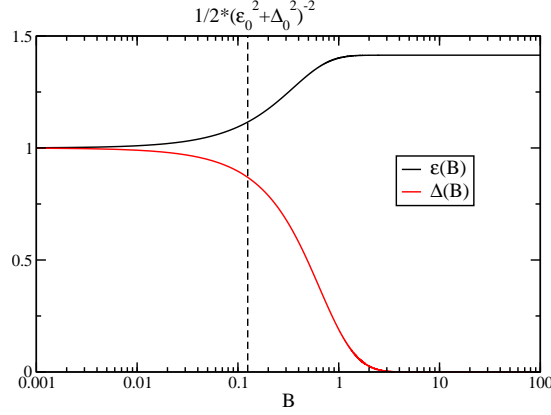


Figure 1.11: Flow of $\epsilon(B)$ and $\Delta(B)$ for the initial values $\epsilon_0 = \Delta_0 = 1$.

As an example for the transformation of an operator we calculate the ground state ($|0\rangle$) expectation value of σ_z . The ground state expectation value of σ_z is denoted as magnetization in the following. We use the Ansatz

$$\sigma_z(B) = h_z(B)\sigma_z + h_x(B)\sigma_x \quad (1.57)$$

for the flow of the operator, where $h_z(B=0) = 1$ and $h_x(B=0) = 0$. The ground state magnetization is then given by

$$\langle \sigma_z \rangle = \langle 0 | U^\dagger(B=\infty) U(B=\infty) \sigma_z U^\dagger(B=\infty) U(B=\infty) | 0 \rangle = -\text{sgn}(\epsilon_0) h_z(B=\infty), \quad (1.58)$$

since $U(B=\infty)|0\rangle$ is either $(1,0)^T$ or $(0,1)^T$ depending on the sign of ϵ_0 . One easily derives the flow equations

$$\begin{aligned} \frac{dh_z(B)}{dB} &= -\epsilon(B)\Delta(B)h_x(B) \\ \frac{dh_x(B)}{dB} &= \epsilon(B)\Delta(B)h_z(B). \end{aligned} \quad (1.59)$$

The solutions $h_z(B)$ and $h_x(B)$ are related by $h_x(B) = \sqrt{1 - h_z^2(B)}$ yielding

$$\begin{aligned} \frac{dh_z(B)}{dB} &= -\epsilon(B)\Delta(B)\sqrt{1 - h_z^2(B)} \\ h_z(B) &= \cos\left(\int_0^B dB_1 \epsilon(B_1)\Delta(B_1)\right). \end{aligned} \quad (1.60)$$

For the remaining integral one finds

$$\int_0^\infty dB \epsilon(B)\Delta(B) = \frac{i}{2} \ln\left(\frac{\epsilon_0 - i\Delta_0}{\epsilon_0 + i\Delta_0}\right) = \frac{1}{2} \text{sgn}(\epsilon_0\Delta_0) \arccos\left(\frac{\epsilon_0^2 - \Delta_0^2}{\epsilon_0^2 + \Delta_0^2}\right). \quad (1.61)$$

The resulting ground state magnetization is given by

$$\langle \sigma_z \rangle = -\frac{\epsilon_0}{\sqrt{\epsilon_0^2 + \Delta_0^2}}. \quad (1.62)$$

In the weak tunneling limit $|\Delta_0| \ll |\epsilon_0|$ the magnetization is given by $\pm \text{sgn}(\epsilon_0)$, in the strong tunneling regime $|\Delta_0| \gg |\epsilon_0|$ the magnetization vanishes.

Since we study a trivial model the unitary transformation is easily calculated. We ignore the B -ordering operator since $[\eta(B_1), \eta(B_2)] = 0$:

$$U(B) = T_B \exp \left(\int_0^B dB_1 \eta(B_1) \right) = \exp \left(\int_0^B dB_1 \eta(B_1) \right) \quad (1.63)$$

yielding (as expected) a simple rotation

$$U(B = \infty) = \begin{pmatrix} \cos(\varphi) & -\sin(\varphi) \\ \sin(\varphi) & \cos(\varphi) \end{pmatrix}, \quad (1.64)$$

$$\varphi = \frac{1}{4} \text{sgn}(\epsilon_0 \Delta_0) \arccos \left(\frac{\epsilon_0^2 - \Delta_0^2}{\epsilon_0^2 + \Delta_0^2} \right).$$

The ground state magnetization (1.62) is easily rederived using this transformation.

1.4.4 Perturbative Truncation of the Unitary Transformation

Obviously one would like to calculate the unitary transformation from Eq. (1.40) also for nontrivial problems. After the diagonalization of the Hamiltonian the flow of the running coupling and the eigenenergies are (at least numerically) accessible on all scales. Therefore also the generator η is known as function of the flow parameter. In contrast to the simple example in Eq. (1.64) one cannot expect to find a closed form for the unitary transformation and one has to give a perturbative expansion of the unitary transformation.

Typically the generator has the structure

$$\eta(B) = \epsilon B^{-c} e^{-B\epsilon^2}, \quad (1.65)$$

where ϵ is some energy scale and $0 < c < 1$. Here the central assumption is that the flow of the interaction is described by a combination of exponential and power law decay, which is the case for the Kondo Hamiltonian. A mathematical problem arises when studying integrals of the form

$$\int_0^B dB_1 \eta(B_1) \quad (1.66)$$

and taking the limits $B \rightarrow \infty$ and $\epsilon \rightarrow 0$ at the same time (assuming a continuous spectrum). For the following discussion we need the integral

$$\begin{aligned}
\int_0^B dB_1 B_1^{-c} e^{-B_1 \epsilon^2} &= \epsilon^{-2} \int_0^{B\epsilon^2} dt \left(\frac{t}{\epsilon^2}\right)^{-c} e^{-t} \\
&= \epsilon^{2(c-1)} \sum_{k=0}^{\infty} \frac{(-1)^k}{k!} \int_0^{B\epsilon^2} dt t^{k-c} \\
&= \sum_{k=0}^{\infty} \frac{(-1)^k}{k!} \frac{B^{k-c+1} \epsilon^{2k}}{k+1-c} \\
&= B^{1-c} \frac{1}{1-c} {}_1F_1(1-c, 2-c, -B\epsilon^2), \tag{1.67}
\end{aligned}$$

where ${}_1F_1(\alpha, \beta, x)$ is the confluent hypergeometric function of the first kind which converges nicely in the relevant parameter regime. To take a controlled limit we first set $\epsilon = B^{-1/2}$ and take the limit $B \rightarrow \infty$ afterwards:

$$\begin{aligned}
\lim_{B \rightarrow \infty} \left(\epsilon \int_0^B dB_1 B_1^{-c} e^{-B_1 \epsilon^2} \Big|_{\epsilon=1/\sqrt{B}} \right) &= \lim_{B \rightarrow \infty} \sum_{k=0}^{\infty} \frac{(-1)^k}{k!(k+1-c)} B^{-c+1/2} \\
&= \text{“finite number”} \times \lim_{B \rightarrow \infty} B^{-c+1/2}. \tag{1.68}
\end{aligned}$$

If $c < 1/2$ already the first order term diverges. An analogue calculation for the second order term yields

$$\begin{aligned}
\int_0^B dB_1 B_1^{-c} e^{-B_1 \epsilon_1^2} \int_0^{B_1} dB_2 B_2^{-c} e^{-B_2 \epsilon_2^2} &= \sum_{k,m=0}^{\infty} \frac{(-\epsilon_1^2)^m (-\epsilon_2^2)^k}{m!k!(k-c+1)} \int_0^B dB_1 B_1^{m+k+1-2c} \\
&= \sum_{k,m=0}^{\infty} \frac{(-1)^m (-1)^k \epsilon_1^{2m} \epsilon_2^{2k}}{m!k!} \times \tag{1.69} \\
&\quad \times \frac{1}{(k+1-c)(k+m+2-2c)} B^{k+m+2-2c}.
\end{aligned}$$

We again find divergence for $c < 1/2$:

$$\begin{aligned}
\lim_{B \rightarrow \infty} \left(\epsilon^2 \int_0^B B_1^{-c} e^{-B_1 \epsilon^2} \int_0^{B_1} dB_2 B_2^{-c} e^{-B_2 \epsilon^2} \Big|_{\epsilon=1/\sqrt{B}} \right) &= \\
&= \lim_{B \rightarrow \infty} \sum_{k,m=0}^{\infty} \frac{(-1)^{m+k}}{m!k!} \frac{1}{(k+1-c)(k+m+2-2c)} B^{1-2c} \\
&= \text{“finite number”} \times \lim_{B \rightarrow \infty} B^{1-2c}. \tag{1.70}
\end{aligned}$$

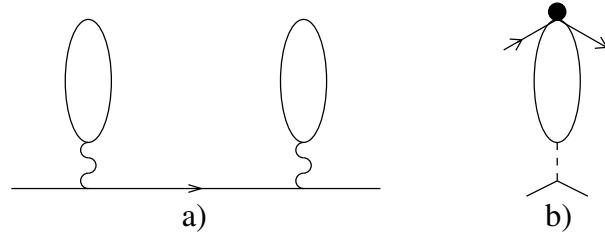


Figure 1.12: Normal-ordering is similar to the reduction of diagrams. While Subfig. a) is reducible to simpler objects (by cutting the straight line) Subfig. b) is irreducible.

In systems with continuous spectrum a perturbative expansion of the flow equation transformation is therefore only possible if the running coupling decays faster than

$$B^{-1/2} \exp(-B\epsilon^2) . \quad (1.71)$$

Note that this observation does not mean that the flow equation transformation does not converge. It is e.g. also impossible to get

$$\lim_{x \rightarrow \infty} e^{-x} = 0 \quad (1.72)$$

by a truncation of the power series for the exponential function. The B -ordered exponential in Eq. (1.40) is just plain not the most clever way to write down the flow equation transformation. Unfortunately, it is the only way known.

1.4.5 Normal-Ordering

The expansion of operator products is a fundamental problem in the flow equation approach. It is of ultimate importance to identify contribution of different scattering processes. In this thesis we use Wick's normal-ordering procedure [67] to expand operator products, the following short introduction to normal-ordering is heavily based on Ref. [41].

The normal-ordering procedure is similar to the reduction of diagrams. If a diagram is reducible to a simpler form (by cutting one internal line) it describes the successive execution of two independent interaction processes. In classical mechanics the successive scattering of a ball at a wall is an example for a reducible process. However, in quantum mechanics also the phase of the wave function is important, the outcome of a single scattering process can affect all successive processes leading to irreducible many particle processes. See Fig. 1.12 for an illustration of reducible and irreducible diagrams. In this spirit normal-ordering is used to differentiate interaction processes by the number of involved irreducible processes.

1.4.5.1 Formalism

In the following A_p denotes creation and annihilation operators, the α 's are C-numbers, and $P(\{A_p\})$ is a product of operators from the set $\{A_p\}$. A normal-ordered operator

product $P(\{A_p\})$ is denoted by $: P(\{A_p\}) :$. The basic rules for Wick's normal-ordering are given by:

1. Numbers are unchanged:

$$: \alpha : = \alpha \quad (1.73)$$

2. Normal-ordering is linear

$$: \alpha_1 P_1(\{A_p\}) + \alpha_2 P_2(\{A_p\}) : = \alpha_1 : P_1(\{A_p\}) : + \alpha_2 : P_2(\{A_p\}) : \quad (1.74)$$

3. Recurrence relation

$$A_q : P(\{A_p\}) : = : A_q P(\{A_p\}) : + \sum_r C_{qr} : \frac{\partial P(\{A_p\})}{\partial A_r} : , \quad (1.75)$$

where the contraction C_{qr} is defined by

$$C_{qr} = \langle \Psi | A_q A_r | \Psi \rangle \quad (1.76)$$

for a pure reference state $|\Psi\rangle$ or

$$C_{qr} = \text{Tr}(\rho A_q A_r) \quad (1.77)$$

for some mixed state described by the density matrix ρ . Typically one choses the ground state or the density matrix of the noninteracting system as reference.

From the recurrence relation (1.75) one can derive Wick's first theorem

$$: A_{p_1} \dots A_{p_n} : = \left(A_{p_1} - \sum_{q_1} C_{p_1 q_1} \frac{\partial}{\partial A_{q_1}} \right) \times \dots \times \left(A_{p_{n-1}} - \sum_{q_{n-1}} C_{p_{n-1} q_{n-1}} \frac{\partial}{\partial A_{q_{n-1}}} \right) A_{p_n} . \quad (1.78)$$

From this relation follows that the commutation of neighboring fermionic operators picks up a minus sign, bosonic operators commute. The product of two normal-ordered objects can be calculated from Wick's second theorem. The fermionic version is given by

$$: P_1(\{A_p\}) :: P_2(\{A_p\}) : = : \exp \left(\sum_{r,s} C_{rs} \frac{\partial^2}{\partial B_s \partial A_r} \right) P_1(\{A_p\}) P_2(\{B_p\}) : \Big|_{B=A} . \quad (1.79)$$

1.4.5.2 Basic Examples

In the following we give certain important examples for normal-ordering of fermionic creation and annihilation operators c_1^\dagger and c_1 . We normal-order with respect to the nonin-

teracting system, so

$$\begin{aligned}
\langle 0|c_{1'}^\dagger c_1|0\rangle &= \delta_{1',1}n(1') , \\
\langle 0|c_1 c_{1'}^\dagger|0\rangle &= \delta_{1',1}(1-n(1')) , \\
\langle 0|c_{1'}^\dagger c_{2'}^\dagger|0\rangle &= \langle 0|c_1 c_2|0\rangle = 0 , \\
\text{Tr}\left(\rho c_{1'}^\dagger c_1\right) &= \delta_{1',1}n(1') , \\
\text{Tr}\left(\rho c_1 c_{1'}^\dagger\right) &= \delta_{1',1}(1-n(1')) , \\
&\vdots
\end{aligned} \tag{1.80}$$

where $|0\rangle$ denotes the ground state and $n(1')$ is the occupation number which is e.g. given by the Fermi function or by Eq. (1.10).

Normal ordering of a single operator simply gives the unchanged operator:

$$:c_{1'}^\dagger: = c_{1'}^\dagger , \quad :c_1: = c_1 . \tag{1.81}$$

All possible combinations for normal-ordered products of two operators are given by

$$\begin{aligned}
:c_{1'}^\dagger c_1: &= c_{1'}^\dagger c_1 - C_{1'1} = c_{1'}^\dagger c_1 - \delta_{1',1}n(1') , \\
:c_{1'}^\dagger c_{2'}^\dagger: &= c_{1'}^\dagger c_{2'}^\dagger , \\
:c_1 c_2: &= c_1 c_2 .
\end{aligned} \tag{1.82}$$

Note that $:c_{1'}^\dagger c_1: = -:c_1 c_{1'}^\dagger:$. The flow equation approach naturally leads to products of (normal-ordered) operators. The most important example (in the context of this thesis) is given by

$$\begin{aligned}
:c_{1'}^\dagger c_1 :: c_{2'}^\dagger c_2: &\stackrel{(1.79)}{=} :c_{1'}^\dagger c_1 c_{2'}^\dagger c_2: + \\
&+ \frac{1}{1!} \left(-C_{1'2'} :c_1 c_2: + C_{1'2} :c_1 c_{2'}^\dagger: + C_{12'} :c_{1'}^\dagger c_2: - C_{12} :c_{1'}^\dagger c_{2'}^\dagger: \right) + \\
&+ \frac{1}{2!} (-C_{1'2'} C_{12} + C_{1'2} C_{12'} + C_{12'} C_{1'2} - C_{12} C_{1'2'}) \\
&= :c_{1'}^\dagger c_1 c_{2'}^\dagger c_2: - \delta_{1',2} n(1') :c_{2'}^\dagger c_1: + \delta_{1,2'} (1-n(1)) :c_{1'}^\dagger c_2: + \\
&+ \delta_{1',2} \delta_{1,2'} n(1') (1-n(1)) ,
\end{aligned} \tag{1.83}$$

yielding the commutator

$$[:c_{1'}^\dagger c_1 :: c_{2'}^\dagger c_2:] = -\delta_{1',2} :c_{2'}^\dagger c_1: + \delta_{1,2'} :c_{1'}^\dagger c_2: + \delta_{1',2} \delta_{1,2'} (n(1') - n(1)) . \tag{1.84}$$

For the commutator we can alternatively work out

$$\begin{aligned}
[c_1^\dagger, c_1, c_2^\dagger, c_2] &= c_1^\dagger c_1 c_2^\dagger c_2 - c_2^\dagger c_2 c_1^\dagger c_1 \\
&= c_1^\dagger c_1 c_2^\dagger c_2 - c_2^\dagger \{c_2, c_1^\dagger\} c_1 + c_2^\dagger c_1^\dagger c_2 c_1 \\
&= \dots \\
&= -\delta_{1',2} c_2^\dagger c_1 + \delta_{2',1} c_1^\dagger c_2 \\
&= -\delta_{1',2} \left(: c_2^\dagger c_1 : + \delta_{2',1} n(1) \right) + \delta_{2',1} \left(: c_1^\dagger c_2 : + \delta_{1',2} n(1') \right) \\
&= -\delta_{1',2} : c_2^\dagger c_1 : + \delta_{2',1} : c_1^\dagger c_2 : + \delta_{1',2} \delta_{2',1} (n(1') - n(1)) \\
&\stackrel{(1.84)}{=} [: c_1^\dagger c_1 :, : c_2^\dagger c_2 :] \tag{1.85}
\end{aligned}$$

without running into any problem. As we show in Chap. 2 in the Kondo model also the anticommutator is needed. Here the situation is more complex since we create an operator product (two creation and two annihilation operators) that is neither included in the Hamiltonian nor in the generator:

$$\begin{aligned}
\{ : c_1^\dagger c_1 :, : c_2^\dagger c_2 : \} &\stackrel{(1.83)}{=} 2 : c_1^\dagger c_1 c_2^\dagger c_2 : + \delta_{1,2'} (1 - 2n(1)) : c_1^\dagger c_2 : + \\
&\quad + \delta_{1',2} (1 - 2n(1')) : c_2^\dagger c_1 : + \delta_{1',2} \delta_{1,2'} (n(1') + n(1) - 2n(1')n(1)) . \tag{1.86}
\end{aligned}$$

Here we see the full power of normal-ordering. The mixture of one- and two-particle operations $\{ : c_1^\dagger c_1 :, : c_2^\dagger c_2 : \}$ is reduced to pure one- and two-particle operations. The two-particle operations belong to new interactions generated during the flow. Without normal-ordering we would be stuck at the point

$$\{ c_1^\dagger, c_1, c_2^\dagger, c_2 \} = 2c_1^\dagger c_1 c_2^\dagger c_2 + \delta_{1',2} c_2^\dagger c_1 - \delta_{1,2'} c_1^\dagger c_2 , \tag{1.87}$$

since we could not distinguish between contributions to the new two-particle interaction and contributions to the one-particle interaction. Without this distinction it is impossible to consistently work out the flow equations.

Generally speaking, if new interactions are generated during the flow it is of ultimate importance to have a suitable operator product expansion at hand. Otherwise one is simply lost. Nevertheless, there is always the option to switch to a more sophisticated operator basis where an adequate operator product expansion exists, e.g. by bosonization [16, 68].

1.5 Summary

The Kondo problem still is a fundamental problem in condensed matter theory. Though the equilibrium problem has been formally solved in the 1980's, still the dynamics of the system is not fully accessible, e.g. for high magnetic field or for high temperature. In thermal equilibrium transport through a Kondo system is well described by linear response theory.

Recent experiments on semiconductor quantum dots in the Coulomb blockade regime opened a new field to Kondo physics, the non-equilibrium Kondo problem. In quantum dots one can apply a voltage bias directly to the Kondo spin. Thereby one can drive a strong current through the Kondo spin without bringing the leads out of the ohmic linear response regime. The current can be tuned to such high values that a description of the system using linear response theory fails. In this far out of equilibrium situation the system is no longer described by its ground state or by its unperturbed density matrix. Instead one has to use the highly excited steady state to describe the system. Another interesting way of driving the quantum dot out of equilibrium is to couple it to two heat baths at different temperature, thereby driving a thermocurrent through the system.

The equilibrium Kondo problem is a low energy problem. The typical energy scale of the system, the so-called Kondo temperature T_K , is usually only of a few Kelvin. Most theoretical methods developed to describe the Kondo problem therefore focus on the low energy properties of the system, features at high energies are typically neglected. If the high energy features of the system are neglected, it becomes impossible to describe the physics of the system in the steady state. Therefore new theoretical approaches have to be developed to describe the non-equilibrium Kondo problem.

Previous perturbation theory calculations using the Keldysh formalism and perturbative renormalization group calculations showed the importance of decoherence effects in the non-equilibrium Kondo model at high voltage bias. The Kondo effect is suppressed by decoherence effects due to the shot noise of the current through the system. Many physical properties of the non-equilibrium system have so far only been calculated in leading order, the subleading corrections that actually contain the Kondo physics are still missing. Very recently it became possible to construct the steady state in Kondo like systems using scattering state approaches. However, a lot of work has still to be done until a full description is available. Summing up, in non-equilibrium so far only rudimentary theoretical knowledge has been obtained.

In this thesis we derive a perturbative scaling picture of the Kondo problem in the weak coupling regime $\max(V, |h|, T) \gg T_K$ using the flow equation method. In this method the Hamiltonian is diagonalized using infinitesimal unitary transformations in an energy scale separated way. First, interaction matrix elements with high energy transfer are successively integrated out while interaction matrix elements with lower energy transfer are still retained in the Hamiltonian. In contrast to usual scaling approaches states are not integrated out. This becomes increasingly important in far out of equilibrium situations where transport processes dominate the system's properties. In such highly excited situations also states

at high energies have to be retained in the Hamiltonian since they contribute to transport processes. If states are integrated out in a scaling approach, the scaling procedure has to be stopped at the energy scale on which transport processes become important. It is therefore nearly impossible to describe the transport properties of a system far out of equilibrium using conventional scaling approaches.

In the flow equation method the unitary transformations that diagonalize the Hamiltonian are not calculated directly, instead transformed operators are worked out. The transformation of the Hamiltonian is constructed from the ordinary differential equation

$$\frac{dH(B)}{dB} = [\eta(B), H(B)] , \quad (1.88)$$

where $H(B=0)$ is the initial Hamiltonian and $H(B=\infty)$ the diagonal one. The generic choice for the antihermitian generator $\eta(B)$ is given by

$$\eta(B) = [H_0(B), H_{\text{int}}(B)] , \quad (1.89)$$

where $H_0(B)$ is the diagonal part of the Hamiltonian and $H_{\text{int}}(B)$ the interaction part. With this choice of the generator the flow parameter B and the remaining effective bandwidth $\Delta\epsilon$ are related via $B^{-1/2} = \Delta\epsilon$.

For general models the unitary transformation generated by the flow equation approach cannot be worked out using a truncation scheme perturbative in the running coupling. Therefore the eigenstates of the Hamiltonian cannot be accessed in the original ($B=0$) basis and one has to transform all operators into the diagonal ($B=\infty$) basis of the Hamiltonian before their expectation values can be worked out. Any operator O is transformed via

$$\frac{dO(B)}{dB} = [\eta(B), O(B)] . \quad (1.90)$$

At this point we want to reveal the general construction principle of the flow equation approach: any antihermitian generator generates an unitary transformation. However, only a certain subclass of generators leads to a diagonal Hamiltonian. For example, another important antihermitian generator is given by $\eta(t) = iH(t)/\hbar$ for $B \equiv t$ yielding time evolution in the Heisenberg picture, of course provided that O does not explicitly depend on time.

In the flow equation approach the partial derivative (appearing in the equation of motion) is zero since the system is not aware of the diagonalization process. The partial derivative has to be taken into account only if the diagonalization process is part of the system, e.g. if we would try to solve the Hamiltonian of the whole universe. However, physics in general “promptly vanishes in a puff of logic” [69] at this point.

Chapter 2

Flow Equation Treatment of the Kondo Hamiltonian

We start the flow equation analysis of the Kondo problem with the diagonalization of the Hamiltonian. The previous derivation of the flow equations for the Kondo model at zero magnetic field [40, 41] and the corresponding scaling analysis are generalized to nonzero magnetic field and anisotropic initial conditions. In the anisotropic Kondo model the SU(2) symmetry of the coupling is broken and one distinguishes the coupling in z -direction J_{\parallel} and the one in x - and y -direction J_{\perp} , where J_{\parallel} is not necessarily equal to J_{\perp} . The anisotropic Kondo model is equivalent to the spin boson model with ohmic dissipation and is therefore considered as an important generalization of the original Kondo problem. For a comprehensive review on the spin boson model and its connection to the Kondo model see Ref. [70]. By nature many of the concepts used in the following sections were borrowed from Refs. [40, 41]. For details on the numerical solution of the flow equations see Appendix A.1.

This chapter is outlined as follows. In Sect. 2.1 we derive and analyze the flow equations in 1-loop (quadratic) order. The 2-loop (third order) flow equations are discussed in Sect. 2.2, in Sect. 2.2.6 we discuss scaling in the anisotropic Kondo model.

2.1 1-loop Flow Equations

2.1.1 Basic Commutation Relations

As a first step we have to derive some preliminary relations. Working out products of spin operators is straightforward using the standard spin operator algebra

$$[S^+, S^-] = 2S^z, \quad [S^z, S^{\pm}] = \pm S^{\pm}, \quad \{S^+, S^-\} = \mathbf{1}. \quad (2.1)$$

For convenience we have set $\hbar = 1$. The relations

$$\begin{aligned} [AS^-, BS^z] &= \frac{1}{2}\{A, B\}S^- \\ [AS^+, BS^z] &= -\frac{1}{2}\{A, B\}S^+ \\ [AS^+, BS^-] &= \{A, B\}S^z + \frac{1}{2}[A, B] \end{aligned} \quad (2.2)$$

are fulfilled for arbitrary (linear) operators A, B that commute with the spin operators. Note that $[AS^z, BS^z] = [A, B]/4$.

Using normal-ordering (see Sect. 1.4.5) the commutator

$$[: f_1^\dagger, f_1 : , : f_2^\dagger, f_2 :] = : f_1^\dagger, f_2 : \delta_{1,2'} - : f_2^\dagger, f_1 : \delta_{1',2} + \delta_{1',2}\delta_{1,2'}(n(1') - n(1)) \quad (2.3)$$

is easily derived. Due to the spin operator algebra (2.2) we also need the anticommutator:

$$\begin{aligned} \{ : f_1^\dagger, f_1 : , : f_2^\dagger, f_2 : \} &= \delta_{1,2'}(1 - 2n(1)) : f_1^\dagger, f_2 : + \delta_{2,1'}(1 - 2n(1')) : f_2^\dagger, f_1 : + \\ &+ 2 : f_1^\dagger, f_1 f_2^\dagger, f_2 : + \delta_{1',2}\delta_{1,2'}(n(1') + n(1) - 2n(1')n(1)) . \end{aligned} \quad (2.4)$$

The above relations hold for general fermionic operators with the anticommutation relations $\{f_1^\dagger, f_2\} = \delta_{12}$ and $\{f_1, f_2\} = 0$.

2.1.2 Generator

The diagonal part of the Kondo Hamiltonian (1.9) is given by

$$H_0 = \sum_{p,\sigma} \epsilon_p : f_{p\sigma}^\dagger f_{p\sigma} : - hS^z , \quad (2.5)$$

the interaction part is

$$\begin{aligned} H_{\text{int}} &= \frac{1}{2} \sum_{p,q} \left(J^\uparrow(p, q) : f_{p\uparrow}^\dagger f_{q\uparrow} : - J^\downarrow(p, q) : f_{p\downarrow}^\dagger f_{q\downarrow} : \right) S^z + \\ &+ \frac{1}{2} \sum_{p,q} J_\perp(p, q) \left(: f_{p\uparrow}^\dagger f_{q\downarrow} : S^- + : f_{q\downarrow}^\dagger f_{p\uparrow} : S^+ \right) \\ &\stackrel{\text{def}}{=} H_{\parallel} + H_{\perp} . \end{aligned} \quad (2.6)$$

Note that we normal order with respect to the system without Kondo impurity since the corrections enter in 3-loop order only. We split the interaction in spin conserving scattering (spin-up and spin-down) and spin flip scattering (perpendicular): $J_{(\perp)}^{(\uparrow/\downarrow)}(p, q, B = 0) = J$ for the isotropic Kondo model. At zero initial magnetic field $h(B = 0) = 0$ the relations $h(B) \equiv 0$, $J^\uparrow(p, q) = J^\downarrow(p, q) = J_\perp(p, q) = J_\perp(q, p)$ are fulfilled during the flow. In the anisotropic Kondo model the initial values are given by $J^{\uparrow/\downarrow}(p, q, B = 0) = J_{\parallel}$ and

$J_{\perp}(p, q, B = 0) = J_{\perp}$, where J_{\parallel} is the coupling in z -direction (parallel) and J_{\perp} the coupling in x - and y -direction (perpendicular). Here the relations $h(B) \equiv 0$, $J^{\uparrow}(p, q) = J^{\downarrow}(p, q)$ and $J_{\perp}(p, q) = J_{\perp}(q, p)$ are fulfilled during the flow at zero initial magnetic field. The relations $J^{\uparrow}(p, q) = J^{\uparrow}(q, p)$ and $J^{\downarrow}(p, q) = J^{\downarrow}(q, p)$ are always fulfilled due to hermicity. Note that

$$(: f_{p\uparrow}^{\dagger} f_{q\downarrow} : S^{-})^{\dagger} = : f_{q\downarrow}^{\dagger} f_{p\uparrow} : S^{+} , \quad (2.7)$$

so the Hamiltonian is always hermitian also if $J_{\perp}(p, q, B) \neq J_{\perp}(q, p, B)$. This is the case for nonzero magnetic field. Using Eq. (2.3) one easily shows

$$\begin{aligned} [H_0, : f_{p\sigma}^{\dagger} f_{q\sigma} : S^z] &= \sum_{k,\alpha} \epsilon_k [: f_{k\alpha}^{\dagger} f_{k\alpha} :, : f_{p\sigma}^{\dagger} f_{q\sigma} :] S^z \\ &= \sum_k \epsilon_k (: f_{p\sigma}^{\dagger} f_{p\sigma} : \delta_{k,p} - : f_{p\sigma}^{\dagger} f_{k\sigma} : \delta_{q,k}) S^z \\ &= (\epsilon_p - \epsilon_q) : f_{p\sigma}^{\dagger} f_{q\sigma} : S^z . \end{aligned} \quad (2.8)$$

For spin flip scattering we find:

$$\begin{aligned} [H_0, : f_{p\uparrow}^{\dagger} f_{q\downarrow} : S^{-}] &= \sum_{k,\sigma} \epsilon_k [: f_{k\sigma}^{\dagger} f_{k\sigma} :, : f_{p\uparrow}^{\dagger} f_{q\downarrow} :] S^{-} - h : f_{p\uparrow}^{\dagger} f_{q\downarrow} : [S^z, S^{-}] \\ &= (\epsilon_p - \epsilon_q + h) : f_{p\uparrow}^{\dagger} f_{q\downarrow} : S^{-} . \end{aligned} \quad (2.9)$$

Note that $[H_0, : f_{p\downarrow}^{\dagger} f_{q\uparrow} : S^{+}] = -([H_0, : f_{p\uparrow}^{\dagger} f_{q\downarrow} : S^{-}])^{\dagger}$. The 1-loop generator is then given by

$$\begin{aligned} \eta_0 &= \frac{1}{2} \sum_{p,q} (\epsilon_p - \epsilon_q) \left(J^{\uparrow}(p, q) : f_{p\uparrow}^{\dagger} f_{q\uparrow} : - J^{\downarrow}(p, q) : f_{p\downarrow}^{\dagger} f_{q\downarrow} : \right) S^z + \\ &\quad + \frac{1}{2} \sum_{p,q} (\epsilon_p - \epsilon_q + h) J_{\perp}(p, q) \left(: f_{p\uparrow}^{\dagger} f_{q\downarrow} : S^{-} - : f_{q\downarrow}^{\dagger} f_{p\uparrow} : S^{+} \right) \\ &= \eta_0^{\parallel} + \eta_0^{\perp} . \end{aligned} \quad (2.10)$$

2.1.3 Flow Equations

The rather lengthy expressions for the 1-loop commutators are given in Appendix C.1. In the following we present the resulting 1-loop flow equations only. From the commutator $[\eta_0^{\perp}, H_{\perp}]$ we find a flow equation for the magnetic field:

$$\frac{dh}{dB} = \frac{1}{2} \sum_{pq} (n_f(p) + n_f(q) - 2n_f(p)n_f(q)) (\epsilon_p - \epsilon_q + h) (J_{\perp}(p, q))^2 . \quad (2.11)$$

We find contributions to the flow of parallel scattering from $[\eta_0, H_0]$ and $[\eta_0^{\perp}, H_{\perp}]$ yielding

$$\begin{aligned} \frac{dJ^{\uparrow}(p, q)}{dB} &= -(\epsilon_p - \epsilon_q)^2 J^{\uparrow}(p, q) + \\ &\quad + \frac{1}{2} \sum_r (1 - 2n_f(r)) (2(\epsilon_r - h) - (\epsilon_p + \epsilon_q)) J_{\perp}(p, r) J_{\perp}(q, r) \end{aligned} \quad (2.12)$$

for spin up scattering and

$$\begin{aligned} \frac{dJ^\downarrow(p, q)}{dB} &= -(\epsilon_p - \epsilon_q)^2 J^\downarrow(p, q) + \\ &+ \frac{1}{2} \sum_r (1 - 2n_f(r)) (2(\epsilon_r + h) - (\epsilon_p + \epsilon_q)) J_\perp(r, p) J_\perp(r, q) \end{aligned} \quad (2.13)$$

for spin down scattering. The flow equation for the perpendicular coupling is given by

$$\begin{aligned} \frac{dJ_\perp(p, q)}{dB} &= -(\epsilon_p - \epsilon_q + h)^2 J_\perp(p, q) + \\ &+ \frac{1}{4} \sum_r (1 - 2n_f(r)) ((2\epsilon_r - (\epsilon_p + \epsilon_q) + h) J_\perp(r, q) J^\uparrow(p, r) + \\ &+ (2\epsilon_r - (\epsilon_p + \epsilon_q) - h) J_\perp(p, r) J^\downarrow(q, r)) \quad , \end{aligned} \quad (2.14)$$

where the commutators $[\eta_0, H_0]$, $[\eta_0^\perp, H_\parallel]$ and $[\eta_0^\parallel, H_\perp]$ contributed. In addition to the terms in the original Hamiltonian (2.5) and (2.6) the generator (2.10) generates new interactions. They are discussed in Sect. 2.1.5.

2.1.4 Scaling Analysis (1-loop)

The full set of flow equations cannot be solved analytically due to the complicated momentum dependence. However qualitative results can be obtained for the low energy properties of the system. They are accessible by studying scattering processes that do not change the energy, so-called energy diagonal processes. In the following we derive a simplified scaling picture using the so-called diagonal parametrization:

$$\begin{aligned} J_\perp(p, q) &= g_{\overline{p\overline{q}}}^\perp e^{-B(\epsilon_p - \epsilon_q + h)^2} \\ J^{\uparrow/\downarrow}(p, q) &= g_{\overline{p\overline{q}}}^{\uparrow/\downarrow} e^{-B(\epsilon_p - \epsilon_q)^2} \end{aligned} \quad (2.15)$$

where $\overline{p\overline{q}} = \overline{\epsilon_p \epsilon_q} = (\epsilon_p + \epsilon_q)/2$. Note that the running coupling $g_p^{\uparrow/\downarrow/\perp}$ does not depend on the momentum index p but on the corresponding energy scale ϵ_p . For convenience we use g_p as shorthand notation for g_{ϵ_p} whenever possible. The energy diagonal equations are easily obtained by setting $\epsilon_q = \epsilon_p$ for the $g^{\uparrow/\downarrow}$ terms and $\epsilon_q = \epsilon_p + h$ in the g^\perp terms. The ansatz (2.15) is motivated by Eq. (1.48). Since the energies ϵ_p are unchanged during the flow the integral in the exponential simply leads to a multiplication with B for $J^{\uparrow/\downarrow}(p, q)$. For $J_\perp(p, q)$ the situation is different since we find a shift of the magnetic field. However the resulting correction dh/dB vanishes for the energy diagonal terms $\epsilon_p - \epsilon_q + h = 0$ since

$$\frac{d}{dB} e^{-B(\epsilon_p - \epsilon_q + h)^2} = - \left((\epsilon_p - \epsilon_q + h)^2 + 2B(\epsilon_p - \epsilon_q + h) \frac{dh}{dB} \right) e^{-B(\epsilon_p - \epsilon_q + h)^2} \quad . \quad (2.16)$$

In the following we qualitatively discuss the flow of the 1-loop equations worked out in the previous section. We find

$$\frac{dh}{dB} = \frac{1}{2} \sum_{p, q} (n_f(p) + n_f(q) - 2n_f(p)n_f(q)) (\epsilon_p - \epsilon_q + h) (g_{\overline{p\overline{q}}}^\perp)^2 e^{-2B(\epsilon_p - \epsilon_q + h)^2} \quad (2.17)$$

for the flow of the magnetic field. Its small shift is discussed in Sect. 2.2. The running coupling for parallel scattering is given by

$$\frac{dg_p^\uparrow}{dB} = - \sum_r (1 - 2n_f(r)) (\epsilon_p - \epsilon_r + h) (g_{\overline{pr}}^\perp)^2 e^{-2B(\epsilon_p - \epsilon_r + h)^2}, \quad (2.18)$$

$$\frac{dg_p^\downarrow}{dB} = - \sum_r (1 - 2n_f(r)) (\epsilon_p - \epsilon_r - h) (g_{\overline{pr}}^\perp)^2 e^{-2B(\epsilon_p - \epsilon_r - h)^2}, \quad (2.19)$$

and for spin-flip scattering one finds

$$\begin{aligned} \frac{dg_p^\perp}{dB} = & -\frac{1}{2} \sum_r (1 - 2n_f(r)) \left(\epsilon_p - \epsilon_r - \frac{h}{2} \right) g_{\epsilon_r(\epsilon_p+h/2)}^\perp g_{(\epsilon_p-h/2)\epsilon_r}^\uparrow e^{-2B(\epsilon_p - \epsilon_r - h/2)^2} - \\ & -\frac{1}{2} \sum_r (1 - 2n_f(r)) \left(\epsilon_p - \epsilon_r + \frac{h}{2} \right) g_{\epsilon_r(\epsilon_p-h/2)}^\perp g_{(\epsilon_p+h/2)\epsilon_r}^\downarrow e^{-2B(\epsilon_p - \epsilon_r + h/2)^2}. \end{aligned} \quad (2.20)$$

At zero temperature the flow of the running coupling is simplified using

$$f(x) \exp(-2B(x - c)^2) \approx f(c) \exp(-2B(x - c)^2) \quad (2.21)$$

to remove the ϵ_r dependence of the running coupling. The summations in (2.18)-(2.20) then lead to ($\rho = 1$ sets the energy scale):

$$\int_{-D}^D d\epsilon (1 - 2n_f(\epsilon)) (\epsilon + c) e^{-2B(\epsilon+c)^2} \stackrel{D \rightarrow \infty}{=} \frac{1}{2B} \left(\frac{e^{-2B(c-V/2)^2}}{1+R} + \frac{e^{-2B(c+V/2)^2}}{1+1/R} \right). \quad (2.22)$$

Using this approximation for parallel scattering yields

$$\frac{dg_p^\uparrow}{dB} = \frac{(g_{\epsilon_p+h/2}^\perp)^2}{2B} \left(\frac{e^{-2B(\epsilon_p+h+V/2)^2}}{1+R} + \frac{e^{-2B(\epsilon_p+h-V/2)^2}}{1+1/R} \right), \quad (2.23)$$

$$\frac{dg_p^\downarrow}{dB} = \frac{(g_{\epsilon_p-h/2}^\perp)^2}{2B} \left(\frac{e^{-2B(\epsilon_p-h+V/2)^2}}{1+R} + \frac{e^{-2B(\epsilon_p-h-V/2)^2}}{1+1/R} \right). \quad (2.24)$$

For spin-flip scattering we find

$$\begin{aligned} \frac{dg_p^\perp}{dB} = & \frac{g_p^\perp g_{\epsilon_p-h/2}^\uparrow}{4B} \left(\frac{e^{-2B(\epsilon_p-h/2+V/2)^2}}{1+R} + \frac{e^{-2B(\epsilon_p-h/2-V/2)^2}}{1+1/R} \right) + \\ & + \frac{g_p^\perp g_{\epsilon_p+h/2}^\downarrow}{4B} \left(\frac{e^{-2B(\epsilon_p+h/2+V/2)^2}}{1+R} + \frac{e^{-2B(\epsilon_p+h/2-V/2)^2}}{1+1/R} \right). \end{aligned} \quad (2.25)$$

The flow of the running coupling is cut off by the exponential decay unless $\epsilon_p = -(h \pm V/2)$ for g_p^\uparrow , $\epsilon_p = h \pm V/2$ for g_p^\downarrow , and $\epsilon_p = \pm(h \pm V)/2$ for g_p^\perp . As a consequence the running coupling is strongly peaked at these energy scales. The terms in 2-loop order cut off this strong-coupling behavior as we show in the 2-loop section. Replacing the exponentials in Eqs. (2.23)-(2.25) by Θ -step-functions, these equations are equivalent to the perturbative RG equations derived in Refs. [37, 38]. The different momentum dependency of the running coupling only leads to subleading corrections.

At nonzero temperature ($T > 0, V = 0$) the situation is a bit more tricky since one cannot give a closed expression for

$$\int_{-\infty}^{\infty} d\epsilon \tanh\left(\frac{\epsilon}{2T}\right) (\epsilon + c) e^{-2B(\epsilon+c)^2}. \quad (2.26)$$

We therefore only discuss the asymptotic result for $T \gg |h|$. Since we are mainly interested in small energy scales $\epsilon_p \rightarrow 0$, we study the running coupling at the Fermi level only: $g = g_{\epsilon_p=0}^{\uparrow/\downarrow}$. For $B \ll T^{-2}$ the terms at high energies $\epsilon \gg T$ give the main contribution to the integral and we obtain the usual zero temperature scaling equation [35]

$$\frac{dg}{dB} = \frac{g^2}{2B}. \quad (2.27)$$

Note that $\Lambda_{\text{feq}} = B^{-1/2}$. For $B \gg T^{-2}$ only energies $\epsilon \ll T$ contribute to the integral, since higher energies are cut off by the exponential. Therefore we linearize the hyperbolic tangent in this case yielding

$$\frac{dg}{dB} = \frac{g^2}{B} \frac{\sqrt{2\pi}}{16} \frac{1}{T\sqrt{B}}. \quad (2.28)$$

The flow of the running coupling stops for $B \gg T^{-2}$ or $T\sqrt{B} \gg 1$ respectively.

2.1.5 Newly Generated Terms

The additionally generated number from $[\eta_0^\parallel, H_\parallel]$ and $[\eta_0^\perp, H_\perp]$ is dropped since it has no influence on the flow. From the commutators $[\eta_0^\parallel, H_\parallel]$ and $[\eta_0^\perp, H_\perp]$ arises a potential scattering term:

$$H_{\text{pot}} = \sum_{pq} (V_{pq}^\uparrow : f_{p\uparrow}^\dagger f_{q\uparrow} : + V_{pq}^\downarrow : f_{p\downarrow}^\dagger f_{q\downarrow} :). \quad (2.29)$$

The corresponding flow equations are given by

$$\begin{aligned} \frac{dV_{pq}^\uparrow}{dB} &= \frac{1}{16} \sum_r (\epsilon_p + \epsilon_q - 2\epsilon_r) J^\uparrow(p, r) J^\uparrow(r, q) + \\ &+ \frac{1}{8} \sum_r (\epsilon_p + \epsilon_q - 2\epsilon_r + 2h) J_\perp(p, r) J_\perp(q, r) \end{aligned} \quad (2.30)$$

for the spin up component and by

$$\begin{aligned} \frac{dV_{pq}^\downarrow}{dB} &= \frac{1}{16} \sum_r (\epsilon_p + \epsilon_q - 2\epsilon_r) J^\downarrow(p, r) J^\downarrow(r, q) + \\ &+ \frac{1}{8} \sum_r (\epsilon_p + \epsilon_q - 2\epsilon_r - 2h) J_\perp(r, p) J_\perp(r, q) \end{aligned} \quad (2.31)$$

for the spin down one. Using diagonal parametrization and the standard approximation $f(x)e^{-B(x-c)^2} \approx f(c)e^{-B(x-c)^2}$ one easily shows

$$\begin{aligned} \frac{dV_{pq}^{\uparrow/\downarrow}}{dB} &\sim \int_{-D}^D d\epsilon_r (\epsilon_p + \epsilon_q - 2\epsilon_r + 2c) e^{-B(\epsilon_p - \epsilon_r + c)^2} e^{-B(\epsilon_q - \epsilon_r + c)^2} \\ &\stackrel{D \rightarrow \infty}{=} -\frac{1}{2} \left(\int_{D^2}^0 dx + \int_0^{D^2} dx \right) e^{-Bx} = 0. \end{aligned} \quad (2.32)$$

The potential scattering term therefore only leads to finite bandwidth effects and does not affect the universal low energy properties of the system. We accordingly neglect it in the following.

An important contribution is given by the newly generated ‘‘two particle’’ interactions. We find three contributions, namely

$$H_K^\uparrow = \sum_{p,q,r,s} K^\uparrow(p, q, r, s) (: f_{p\uparrow}^\dagger f_{q\downarrow} f_{r\uparrow}^\dagger f_{s\uparrow} : S^- + : f_{q\downarrow}^\dagger f_{p\uparrow} f_{s\uparrow}^\dagger f_{r\uparrow} : S^+) \quad (2.33)$$

from $[\eta_0^\perp, H_\parallel]$ and $[\eta_0^\parallel, H_\perp]$,

$$H_K^\downarrow = \sum_{p,q,r,s} K^\downarrow(p, q, r, s) (: f_{p\uparrow}^\dagger f_{q\downarrow} f_{r\downarrow}^\dagger f_{s\downarrow} : S^- + : f_{q\downarrow}^\dagger f_{p\uparrow} f_{s\downarrow}^\dagger f_{r\downarrow} : S^+) \quad (2.34)$$

from $[\eta_0^\perp, H_\parallel]$, $[\eta_0^\parallel, H_\perp]$ and

$$H_K^\perp = \sum_{p,q,r,s} K_\perp(p, q, r, s) : f_{p\uparrow}^\dagger f_{q\downarrow} f_{r\downarrow}^\dagger f_{s\uparrow} : S^z \quad (2.35)$$

from $[\eta_0^\perp, H_\perp]$. Note that $K_\perp(p, q, r, s) = K_\perp(s, r, q, p)$ for hermicity. We discuss the influence of the new interactions K on the flow of the Hamiltonian in the following section. For completeness we sum up the generating flow equations:

$$\begin{aligned} \frac{dK^\uparrow(p, q, r, s)}{dB} &= \frac{1}{4} (\epsilon_p - \epsilon_q - \epsilon_r + \epsilon_s + h) J_\perp(p, q) J^\uparrow(r, s), \\ \frac{dK^\downarrow(p, q, r, s)}{dB} &= -\frac{1}{4} (\epsilon_p - \epsilon_q - \epsilon_r + \epsilon_s + h) J_\perp(p, q) J^\downarrow(r, s), \\ \frac{dK_\perp(p, q, r, s)}{dB} &= -\frac{1}{2} (\epsilon_p - \epsilon_q - \epsilon_r + \epsilon_s + 2h) J_\perp(p, q) J_\perp(s, r). \end{aligned} \quad (2.36)$$

2.2 2-loop Flow Equations

2.2.1 Basic Commutation Relations

In addition to the relations (2.2), (2.3) and (2.4) we will need the corresponding commutation relations for single and two particle terms. In the following we neglect terms with four or six fermionic operators on the rhs. since they would enter the calculation in 3-loop order only. Again we need both the commutator

$$\begin{aligned}
[:c_{1'}^\dagger c_1 :, :c_2^\dagger c_2 c_{3'}^\dagger c_3 :] &= \delta_{1',2} \delta_{1,2'} (n(1') - n(1)) :c_{3'}^\dagger c_3 : - \\
&\quad - \delta_{1',2} \delta_{1,3'} (n(1') - n(1)) :c_2^\dagger c_3 : - \\
&\quad - \delta_{1',3} \delta_{1,2'} (n(1') - n(1)) :c_{3'}^\dagger c_2 : + \\
&\quad + \delta_{1',3} \delta_{1,3'} (n(1') - n(1)) :c_2^\dagger c_2 : \quad (2.37)
\end{aligned}$$

and the anticommutator

$$\begin{aligned}
\{ :c_{1'}^\dagger c_1 :, :c_2^\dagger c_2 c_{3'}^\dagger c_3 : \} &= \delta_{1',2} \delta_{1,2'} (n(1') + n(1) - 2n(1')n(1)) :c_{3'}^\dagger c_3 : - \\
&\quad - \delta_{1',2} \delta_{1,3'} (n(1') + n(1) - 2n(1')n(1)) :c_2^\dagger c_3 : - \\
&\quad - \delta_{1',3} \delta_{1,2'} (n(1') + n(1) - 2n(1')n(1)) :c_{3'}^\dagger c_2 : + \\
&\quad + \delta_{1',3} \delta_{1,3'} (n(1') + n(1) - 2n(1')n(1)) :c_2^\dagger c_2 : \quad (2.38)
\end{aligned}$$

for the following calculation.

2.2.2 Ansatz Hamiltonian and Generator

We again define the diagonal part of the Hamiltonian by

$$H_0 = \sum_{p,\sigma} \epsilon_p : f_{p\sigma}^\dagger f_{p\sigma} : - h S^z . \quad (2.39)$$

For the interaction part we use the Ansatz

$$H_{\text{int}} = H_{\parallel} + H_{\perp} + H_K^\uparrow + H_K^\downarrow + H_K^\perp , \quad (2.40)$$

where the parallel scattering is given by

$$H_{\parallel} = \frac{1}{2} \sum_{p,q} \left(J^\uparrow(p,q) : f_{p\uparrow}^\dagger f_{q\uparrow} : - J^\downarrow(p,q) : f_{p\downarrow}^\dagger f_{q\downarrow} : \right) S^z$$

and the perpendicular one by

$$H_{\perp} = \frac{1}{2} \sum_{p,q} J_{\perp}(p,q) \left(: f_{p\uparrow}^\dagger f_{q\downarrow} : S^- + : f_{q\downarrow}^\dagger f_{p\uparrow} : S^+ \right) .$$

The two particle scattering enters in three flavors: spin flip times spin up scattering

$$H_K^\uparrow = \sum_{p,q,r,s} K^\uparrow(p, q, r, s) (: f_{p\uparrow}^\dagger f_{q\downarrow} f_{r\uparrow}^\dagger f_{s\uparrow} : S^- + : f_{q\downarrow}^\dagger f_{p\uparrow} f_{s\uparrow}^\dagger f_{r\uparrow} : S^+) ,$$

spin flip times spin down scattering

$$H_K^\downarrow = \sum_{p,q,r,s} K^\downarrow(p, q, r, s) (: f_{p\uparrow}^\dagger f_{q\downarrow} f_{r\downarrow}^\dagger f_{s\downarrow} : S^- + : f_{q\downarrow}^\dagger f_{p\uparrow} f_{s\downarrow}^\dagger f_{r\downarrow} : S^+) ,$$

and finally double spin flip scattering

$$H_K^\perp = \sum_{p,q,r,s} K_\perp(p, q, r, s) : f_{p\uparrow}^\dagger f_{q\downarrow} f_{r\downarrow}^\dagger f_{s\uparrow} : S^z .$$

Note that $K_{(\perp)}^{\uparrow/\downarrow}(p, q, r, s, B=0) = 0$, $J^{\uparrow/\downarrow}(p, q, B=0) = J_\parallel$ and $J_\perp(p, q, B=0) = J_\perp$. For zero initial magnetic field the relations $h(B) \equiv 0$, $J^\uparrow(p, q) = J^\downarrow(p, q) = J_\perp(p, q) = J_\perp(q, p)$, and $K^\uparrow(p, q, r, s) = -K^\downarrow(p, q, r, s) = -K^\perp(p, q, r, s)/2$ are fulfilled during the flow in the isotropic Kondo model. In the anisotropic Kondo model the relations $h(B) \equiv 0$, $J^\uparrow(p, q) = J^\downarrow(p, q)$, $J_\perp(p, q) = J_\perp(q, p)$ and $K^\uparrow(p, q, r, s) = -K^\downarrow(p, q, r, s)$ are fulfilled during the flow at zero initial magnetic field. The relations $J^\uparrow(p, q) = J^\uparrow(q, p)$, $J^\downarrow(p, q) = J^\downarrow(q, p)$ and $K_\perp(p, q, r, s) = K_\perp(s, r, q, p)$ are always fulfilled due to hermicity.

We split the generator into several parts:

$$\eta_{2\text{-loop}} = \eta_0^\parallel + \eta_0^\perp + \eta_K^\uparrow + \eta_K^\downarrow + \eta_K^\perp . \quad (2.41)$$

The 1-loop contributions are given by

$$\eta_0^\parallel = \frac{1}{2} \sum_{p,q} (\epsilon_p - \epsilon_q) \left(J^\uparrow(p, q) : f_{p\uparrow}^\dagger f_{q\uparrow} : - J^\downarrow(p, q) : f_{p\downarrow}^\dagger f_{q\downarrow} : \right) S^z \quad (2.42)$$

for parallel scattering and

$$\eta_0^\perp = \frac{1}{2} \sum_{p,q} (\epsilon_p - \epsilon_q + h) J_\perp(p, q) \left(: f_{p\uparrow}^\dagger f_{q\downarrow} : S^- - : f_{q\downarrow}^\dagger f_{p\uparrow} : S^+ \right) \quad (2.43)$$

for perpendicular scattering. The 2-loop parts of the generator are easily calculated using Eqs. (2.37) and (2.38). We find

$$\eta_K^\uparrow = \sum_{p,q,r,s} (\epsilon_p - \epsilon_q + \epsilon_r - \epsilon_s + h) K^\uparrow(p, q, r, s) \times \quad (2.44)$$

$$\times (: f_{p\uparrow}^\dagger f_{q\downarrow} f_{r\uparrow}^\dagger f_{s\uparrow} : S^- - : f_{q\downarrow}^\dagger f_{p\uparrow} f_{s\uparrow}^\dagger f_{r\uparrow} : S^+) \quad (2.45)$$

for spin flip times spin up scattering and

$$\eta_K^\downarrow = \sum_{p,q,r,s} (\epsilon_p - \epsilon_q + \epsilon_r - \epsilon_s + h) K^\downarrow(p, q, r, s) \times \quad (2.46)$$

$$\times (: f_{p\uparrow}^\dagger f_{q\downarrow} f_{r\downarrow}^\dagger f_{s\downarrow} : S^- - : f_{q\downarrow}^\dagger f_{p\uparrow} f_{s\downarrow}^\dagger f_{r\downarrow} : S^+) \quad (2.47)$$

for spin flip times spin down scattering. The double spin flip component is given by

$$\eta_K^\perp = \sum_{p,q,r,s} (\epsilon_p - \epsilon_q + \epsilon_r - \epsilon_s) K_\perp(p, q, r, s) : f_{p\uparrow}^\dagger f_{q\downarrow} f_{r\downarrow}^\dagger f_{s\uparrow} : S^z . \quad (2.48)$$

2.2.3 Flow Equations

Again we banned the lengthy expressions for the commutators to the appendix (C.2). In the following we give the flow equations in 2-loop order. The flow of the magnetic field is induced by the commutator $[\eta_0^\perp, H_\perp]$ (no 2-loop contribution):

$$\frac{dh}{dB} = \frac{1}{2} \sum_{p,q} (n_f(p) + n_f(q) - 2n_f(p)n_f(q)) (\epsilon_p - \epsilon_q + h) (J_\perp(p, q))^2 . \quad (2.49)$$

Note that the rhs. of this equation is zero if $h(B=0) = 0$ since then $J_\perp(p, q) = J_\perp(q, p)$. Therefore no additional magnetic field is generated, only an existing one is shifted. For the flow of $J^\uparrow(p, q)$ we find contributions from $[\eta_0, H_0]$, $[\eta_0^\perp, H_\perp]$, $[\eta_K^\uparrow, H_\perp]$ and $[\eta_0, H_K^\uparrow]$

$$\begin{aligned} \frac{dJ^\uparrow(p, q)}{dB} &= -(\epsilon_p - \epsilon_q)^2 J^\uparrow(p, q) + \\ &+ \frac{1}{2} \sum_r (1 - 2n_f(r)) (2(\epsilon_r - h) - (\epsilon_p + \epsilon_q)) J_\perp(p, r) J_\perp(q, r) - \\ &- \sum_{r,s} (n_f(r) + n_f(s) - 2n_f(r)n_f(s)) J_\perp(r, s) \times \\ &\times ((\epsilon_p - \epsilon_q + 2(\epsilon_r - \epsilon_s + h))(K^\uparrow(r, s, p, q) - K^\uparrow(p, s, r, q)) - \\ &- (\epsilon_p - \epsilon_q - 2(\epsilon_r - \epsilon_s + h))(K^\uparrow(r, s, q, p) - K^\uparrow(q, s, r, p))) . \end{aligned} \quad (2.50)$$

The commutators $[\eta_0, H_0]$, $[\eta_0^\perp, H_\perp]$, $[\eta_K^\downarrow, H_\perp]$ and $[\eta_0, H_K^\downarrow]$ lead to the $J^\downarrow(p, q)$ flow equation

$$\begin{aligned} \frac{dJ^\downarrow(p, q)}{dB} &= -(\epsilon_p - \epsilon_q)^2 J^\downarrow(p, q) + \\ &+ \frac{1}{2} \sum_r (1 - 2n_f(r)) (2(\epsilon_r + h) - (\epsilon_p + \epsilon_q)) J_\perp(r, p) J_\perp(r, q) + \\ &+ \sum_{r,s} (n_f(r) + n_f(s) - 2n_f(r)n_f(s)) J_\perp(r, s) \times \\ &\times ((\epsilon_p - \epsilon_q + 2(\epsilon_r - \epsilon_s + h))(K^\downarrow(r, s, p, q) - K^\downarrow(r, q, p, s)) - \\ &- (\epsilon_p - \epsilon_q - 2(\epsilon_r - \epsilon_s + h))(K^\downarrow(r, s, q, p) - K^\downarrow(r, p, q, s))) . \end{aligned} \quad (2.51)$$

Using the flow equations for the K -terms (shown below) one easily derives $J^{\uparrow/\downarrow}(p, q) = J^{\uparrow/\downarrow}(q, p)$. For the spin flip coupling $J_\perp(p, q)$ we find contributions from $[\eta_0, H_0]$, $[\eta_0^\perp, H_\perp]$,

$[\eta_0^\parallel, H_\perp], [\eta_K^\uparrow, H_\parallel], [\eta_K^\downarrow, H_\parallel], [\eta_K^\perp, H_\perp], [\eta_0, H_K^\uparrow], [\eta_0, H_K^\downarrow]$ and $[\eta_0, H_K^\perp]$

$$\begin{aligned}
\frac{dJ_\perp(p, q)}{dB} &= -(\epsilon_p - \epsilon_q + h)^2 J_\perp(p, q) + \\
&+ \frac{1}{4} \sum_r (1 - 2n_f(r)) ((2\epsilon_r - (\epsilon_p + \epsilon_q) + h) J_\perp(r, q) J^\uparrow(p, r) + \\
&+ (2\epsilon_r - (\epsilon_p + \epsilon_q) - h) J_\perp(p, r) J^\downarrow(q, r)) + \\
&+ \frac{1}{2} \sum_{r, s} (n_f(r) + n_f(s) - 2n_f(r)n_f(s)) (\epsilon_p - \epsilon_q + 2(\epsilon_r - \epsilon_s) + h) \times \\
&\times ((K^\uparrow(p, q, r, s) - K^\uparrow(r, q, p, s)) J^\uparrow(s, r) - \\
&- (K^\downarrow(p, q, r, s) - K^\downarrow(p, s, r, q)) J^\downarrow(s, r)) - \\
&- \frac{1}{2} \sum_{r, s} (n_f(r) + n_f(s) - 2n_f(r)n_f(s)) (\epsilon_p - \epsilon_q + 2(\epsilon_r - \epsilon_s) - h) \times \\
&\times K_\perp(p, q, r, s) J_\perp(s, r) . \tag{2.52}
\end{aligned}$$

In the case of zero magnetic field one easily shows $J_\perp(p, q) = J_\perp(q, p)$. The flow equations for the two particle interaction are given by contributions from $[\eta_K^\uparrow, H_0], [\eta_0^\perp, H_\parallel]$ and $[\eta_0^\parallel, H_\perp]$ for K^\uparrow

$$\begin{aligned}
\frac{dK^\uparrow(p, q, r, s)}{dB} &= -(\epsilon_p - \epsilon_q + \epsilon_r - \epsilon_s + h)^2 K^\uparrow(p, q, r, s) + \\
&+ \frac{1}{4} (\epsilon_p - \epsilon_q - \epsilon_r + \epsilon_s + h) J_\perp(p, q) J^\uparrow(r, s) , \tag{2.53}
\end{aligned}$$

$[\eta_K^\downarrow, H_0], [\eta_0^\perp, H_\parallel]$ and $[\eta_0^\parallel, H_\perp]$ for K^\downarrow

$$\begin{aligned}
\frac{dK^\downarrow(p, q, r, s)}{dB} &= -(\epsilon_p - \epsilon_q + \epsilon_r - \epsilon_s + h)^2 K^\downarrow(p, q, r, s) - \\
&- \frac{1}{4} (\epsilon_p - \epsilon_q - \epsilon_r + \epsilon_s + h) J_\perp(p, q) J^\downarrow(r, s) , \tag{2.54}
\end{aligned}$$

and $[\eta_K^\perp, H_0]$ and $[\eta_0^\perp, H_\perp]$ for K_\perp

$$\begin{aligned}
\frac{dK_\perp(p, q, r, s)}{dB} &= -(\epsilon_p - \epsilon_q + \epsilon_r - \epsilon_s)^2 K_\perp(p, q, r, s) - \\
&- \frac{1}{2} (\epsilon_p - \epsilon_q - \epsilon_r + \epsilon_s + 2h) J_\perp(p, q) J_\perp(s, r) . \tag{2.55}
\end{aligned}$$

2.2.4 Diagonal Parametrization

We again use the diagonal parametrization defined in Eq. (2.15) to discuss the flow equations in 2-loop order. As first step we simplify the flow equations for the K -terms. In the following we discuss the approximations in detail for the K_\perp term only, the other terms are evaluated using an analogue argumentation. The approximation for the K -terms is summarized as follows:

- We neglect the small B -dependence of the magnetic field which is of $\mathcal{O}(1/\ln(1/\sqrt{B}T_K))$ corresponding to a 3-loop correction.
- We assume a weak dependence of the running coupling g on B . It is of $\mathcal{O}(1/\ln(1/\sqrt{B}T_K))$ for small B and of $\mathcal{O}(B^{-1/c})$ for large B with $2 \leq c \leq 4$. (We give definitions for small and large B in the following sections.)

We use the ansatz (1.48) to “solve” Eq. (2.55):

$$\begin{aligned}
K_\perp(p, q, r, s) &= -\frac{1}{2}(\epsilon_p - \epsilon_q - \epsilon_r + \epsilon_s + 2h)e^{-B(\epsilon_p - \epsilon_q + \epsilon_r - \epsilon_s)^2} \times \\
&\quad \times \int_0^B dB_1 e^{B_1(\epsilon_p - \epsilon_q + \epsilon_r - \epsilon_s)^2} g_{pq}^\perp(B_1) g_{rs}^\perp(B_1) e^{-B_1(\epsilon_p - \epsilon_q + h)^2} e^{-B_1(\epsilon_r - \epsilon_s - h)^2} \\
&= -\frac{1}{2}(\epsilon_p - \epsilon_q - \epsilon_r + \epsilon_s + 2h)e^{-B(\epsilon_p - \epsilon_q + \epsilon_r - \epsilon_s)^2} \times \\
&\quad \times \int_0^B dB_1 e^{2B_1(\epsilon_p - \epsilon_q + h)(\epsilon_r - \epsilon_s - h)} g_{pq}^\perp(B_1) g_{rs}^\perp(B_1) . \tag{2.56}
\end{aligned}$$

In the next step we replace the running coupling by an average value:

$$\begin{aligned}
K_\perp(p, q, r, s) &= -\frac{1}{2}(\epsilon_p - \epsilon_q - \epsilon_r + \epsilon_s + 2h)e^{-B(\epsilon_p - \epsilon_q + \epsilon_r - \epsilon_s)^2} \times \\
&\quad \times \left(\int_0^B dB_1 e^{2B_1(\epsilon_p - \epsilon_q + h)(\epsilon_r - \epsilon_s - h)} \right) \frac{1}{B} \left(\int_0^B dB_2 g_{pq}^\perp(B_2) g_{rs}^\perp(B_2) \right) , \tag{2.57}
\end{aligned}$$

since it depends only weakly on B (in comparison with the exponential). The exponential is easily integrated yielding

$$\begin{aligned}
K_\perp(p, q, r, s) &= -\frac{1}{4B} \left(\int_0^B dB_1 g_{pq}^\perp g_{rs}^\perp \right) \frac{(\epsilon_p - \epsilon_q + h) - (\epsilon_r - \epsilon_s - h)}{(\epsilon_p - \epsilon_q + h)(\epsilon_r - \epsilon_s - h)} \times \\
&\quad \times (e^{-B((\epsilon_p - \epsilon_q + h)^2 + (\epsilon_r - \epsilon_s - h)^2)} - e^{-B((\epsilon_p - \epsilon_q + h) + (\epsilon_r - \epsilon_s - h))^2}) . \tag{2.58}
\end{aligned}$$

For the remaining K -terms we find

$$K^\uparrow(p, q, r, s) = \frac{1}{8B} \left(\int_0^B dB_1 g_{pq}^\perp g_{rs}^\uparrow \right) \frac{(\epsilon_p - \epsilon_q + h) - (\epsilon_r - \epsilon_s)}{(\epsilon_p - \epsilon_q + h)(\epsilon_r - \epsilon_s)} \times \\ \times (e^{-B((\epsilon_p - \epsilon_q + h)^2 + (\epsilon_r - \epsilon_s)^2)} - e^{-B((\epsilon_p - \epsilon_q + h) + (\epsilon_r - \epsilon_s))^2}), \quad (2.59)$$

$$K^\downarrow(p, q, r, s) = -\frac{1}{8B} \left(\int_0^B dB_1 g_{pq}^\perp g_{rs}^\downarrow \right) \frac{(\epsilon_p - \epsilon_q + h) - (\epsilon_r - \epsilon_s)}{(\epsilon_p - \epsilon_q + h)(\epsilon_r - \epsilon_s)} \times \\ \times (e^{-B((\epsilon_p - \epsilon_q + h)^2 + (\epsilon_r - \epsilon_s)^2)} - e^{-B((\epsilon_p - \epsilon_q + h) + (\epsilon_r - \epsilon_s))^2}). \quad (2.60)$$

Using these relations and

$$\lim_{b \rightarrow 0} \frac{a-b}{ab} (e^{-B(a^2+b^2)} - e^{-B(a+b)^2}) = 2aB e^{-Ba^2} \quad (2.61)$$

one easily derives the 2-loop flow equations in diagonal parametrization.

For the magnetic field we again find

$$\frac{dh}{dB} = \frac{1}{2} \sum_{pq} (n_f(p) + n_f(q) - 2n_f(p)n_f(q)) (\epsilon_p - \epsilon_q + h) (g_{pq}^\perp)^2 e^{-2B(\epsilon_p - \epsilon_q + h)^2}. \quad (2.62)$$

The spin up component of the running coupling is given by

$$\frac{dg_p^\uparrow}{dB} = - \sum_r (1 - 2n_f(r)) (\epsilon_p - \epsilon_r + h) (g_{pr}^\perp)^2 e^{-2B(\epsilon_p - \epsilon_r + h)^2} - \\ - \sum_{r,s} (n_f(r) + n_f(s) - 2n_f(r)n_f(s)) (\epsilon_r - \epsilon_s + h)^2 e^{-2B(\epsilon_r - \epsilon_s + h)^2} \times \\ \times g_{rs}^\perp \int_0^B dB_1 g_{rs}^\perp g_p^\uparrow + \text{blue terms up} \quad (2.63)$$

$$\text{blue terms up} = \frac{1}{2} \sum_{r,s} (n_f(r) + n_f(s) - 2n_f(r)n_f(s)) \times \\ \times (\epsilon_r - \epsilon_s + h) \frac{(\epsilon_p - \epsilon_s + h) - (\epsilon_r - \epsilon_p)}{(\epsilon_p - \epsilon_s + h)(\epsilon_r - \epsilon_p)} e^{-B(\epsilon_r - \epsilon_s + h)^2} \times \\ \times (e^{-B((\epsilon_p - \epsilon_s + h)^2 + (\epsilon_r - \epsilon_p)^2)} - e^{-B(\epsilon_r - \epsilon_s + h)^2}) g_{rs}^\perp \frac{1}{B} \int_0^B dB_1 g_{ps}^\perp g_{rp}^\uparrow. \quad (2.64)$$

We will show below that the blue terms do not lead to an important contribution. For the spin down component we find

$$\begin{aligned}
\frac{dg_p^\downarrow}{dB} &= - \sum_r (1 - 2n_f(r))(\epsilon_p - \epsilon_r - h)(g_{pr}^\perp)^2 e^{-2B(\epsilon_r - \epsilon_p + h)^2} - \\
&- \sum_{r,s} (n_f(r) + n_f(s) - 2n_f(r)n_f(s))(\epsilon_r - \epsilon_s + h)^2 e^{-2B(\epsilon_r - \epsilon_s + h)^2} \times \\
&\times g_{rs}^\perp \int_0^B dB_1 g_{rs}^\perp g_p^\downarrow + \text{blue terms down}
\end{aligned} \tag{2.65}$$

$$\begin{aligned}
\text{blue terms down} &= \frac{1}{2} \sum_{r,s} (n_f(r) + n_f(s) - 2n_f(r)n_f(s)) \times \\
&\times (\epsilon_r - \epsilon_s + h) \frac{(\epsilon_r - \epsilon_p + h) - (\epsilon_p - \epsilon_s)}{(\epsilon_r - \epsilon_p + h)(\epsilon_p - \epsilon_s)} e^{-B(\epsilon_r - \epsilon_s + h)^2} \times \\
&\times (e^{-B((\epsilon_r - \epsilon_p + h)^2 + (\epsilon_p - \epsilon_s)^2)} - e^{-B(\epsilon_r - \epsilon_s + h)^2}) g_{rs}^\perp \frac{1}{B} \int_0^B dB_1 g_{pr}^\perp g_{ps}^\downarrow .
\end{aligned} \tag{2.66}$$

The flow equation for the spin flip coupling is given by

$$\begin{aligned}
\frac{dg_p^\perp}{dB} &= \frac{1}{2} \sum_r (1 - 2n_f(r))(\epsilon_r - \epsilon_p + \frac{h}{2}) e^{-2B(\epsilon_r - \epsilon_p + h/2)^2} g_{\epsilon_r(\epsilon_p + h/2)}^\perp g_{(\epsilon_p - h/2)\epsilon_r}^\uparrow + \\
&+ \frac{1}{2} \sum_r (1 - 2n_f(r))(\epsilon_r - \epsilon_p - \frac{h}{2}) e^{-2B(\epsilon_r - \epsilon_p - h/2)^2} g_{\epsilon_r(\epsilon_p - h/2)}^\perp g_{(\epsilon_p + h/2)\epsilon_r}^\downarrow - \\
&- \frac{1}{4} \sum_{r,s} (n_f(r) + n_f(s) - 2n_f(r)n_f(s))(\epsilon_r - \epsilon_s)^2 e^{-2B(\epsilon_r - \epsilon_s)^2} \times \\
&\times \left(g_{rs}^\uparrow \int_0^B dB_1 g_p^\perp g_{rs}^\uparrow + g_{rs}^\downarrow \int_0^B dB_1 g_p^\perp g_{rs}^\downarrow \right) - \\
&- \frac{1}{2} \sum_{r,s} (n_f(r) + n_f(s) - 2n_f(r)n_f(s))(\epsilon_r - \epsilon_s - h)^2 e^{-2B(\epsilon_r - \epsilon_s - h)^2} \times \\
&\times g_{rs}^\perp \int_0^B dB_1 g_p^\perp g_{rs}^\perp + \text{blue terms perp}
\end{aligned} \tag{2.67}$$

$$\begin{aligned}
\text{blue terms perp} &= \frac{1}{8} \sum_{r,s} (n_f(r) + n_f(s) - 2n_f(r)n_f(s))(\epsilon_r - \epsilon_s) e^{-B(\epsilon_r - \epsilon_s)^2} \times \\
&\times \left[g_{rs}^\uparrow \left(\frac{1}{B} \int_0^B dB_1 g_{\epsilon_r(\epsilon_p+h/2)}^\perp g_{(\epsilon_p-h/2)\epsilon_s}^\uparrow \right) \times \right. \\
&\times \frac{-(\epsilon_r - \epsilon_p + h/2) + (\epsilon_p - \epsilon_s - h/2)}{(\epsilon_r - \epsilon_p + h/2)(\epsilon_s - \epsilon_p + h/2)} \times \\
&\times (e^{-B((\epsilon_r - \epsilon_p + h/2)^2 + (\epsilon_p - \epsilon_s - h/2)^2)} - e^{-B(\epsilon_r - \epsilon_s)^2}) + \\
&+ g_{rs}^\downarrow \left(\frac{1}{B} \int_0^B dB_1 g_{(\epsilon_p-h/2)\epsilon_s}^\perp g_{\epsilon_r(\epsilon_p+h/2)}^\downarrow \right) \times \\
&\times \frac{(\epsilon_p - \epsilon_s + h/2) - (\epsilon_r - \epsilon_p - h/2)}{(\epsilon_p - \epsilon_s + h/2)(\epsilon_r - \epsilon_p - h/2)} \times \\
&\left. \times (e^{-B((\epsilon_p - \epsilon_s + h/2)^2 + (\epsilon_r - \epsilon_p - h/2)^2)} - e^{-B(\epsilon_r - \epsilon_s)^2}) \right]. \quad (2.68)
\end{aligned}$$

The blue terms cannot be easily taken into account analytically, however they can be easily studied numerically. In the following we only discuss the spin up contribution (2.64), the calculation for the other terms is analogue. As first observation we note that the blue term vanishes for zero magnetic field:

$$\begin{aligned}
&\sum_{r,s} (n_f(r) + n_f(s) - 2n_f(r)n_f(s))(\epsilon_r - \epsilon_s + h) \frac{(\epsilon_p - \epsilon_s + h) - (\epsilon_r - \epsilon_p)}{(\epsilon_p - \epsilon_s + h)(\epsilon_r - \epsilon_p)} \times \quad (2.69) \\
&\times e^{-B(\epsilon_r - \epsilon_s + h)^2} (e^{-B((\epsilon_p - \epsilon_s + h)^2 + (\epsilon_r - \epsilon_p)^2)} - e^{-B(\epsilon_r - \epsilon_s + h)^2}) \stackrel{h \rightarrow 0}{=} \\
&- \sum_{r,s} (n_f(r) + n_f(s) - 2n_f(r)n_f(s))(\epsilon_r - \epsilon_s) \frac{(\epsilon_p - \epsilon_s) + (\epsilon_p - \epsilon_r)}{(\epsilon_p - \epsilon_s)(\epsilon_p - \epsilon_r)} \times \\
&\times e^{-B(\epsilon_r - \epsilon_s)^2} (e^{-B((\epsilon_p - \epsilon_s)^2 + (\epsilon_p - \epsilon_r)^2)} - e^{-B(\epsilon_r - \epsilon_s)^2}) = 0,
\end{aligned}$$

since the latter expression is antisymmetric under the exchange $r \leftrightarrow s$. In addition the contributions from the poles at $\epsilon_p = \epsilon_r$ and $\epsilon_p = \epsilon_s - h$ cancel each other. Using numerical integration one easily shows

$$\begin{aligned}
&\sum_{r,s} (n_f(r) + n_f(s) - 2n_f(r)n_f(s))(\epsilon_r - \epsilon_s + h) \frac{(\epsilon_p - \epsilon_s + h) - (\epsilon_r - \epsilon_p)}{(\epsilon_p - \epsilon_s + h)(\epsilon_r - \epsilon_p)} \times \quad (2.70) \\
&\times e^{-B(\epsilon_r - \epsilon_s + h)^2} (e^{-B((\epsilon_p - \epsilon_s + h)^2 + (\epsilon_r - \epsilon_p)^2)} - e^{-B(\epsilon_r - \epsilon_s + h)^2}) \sim B^{-3/2}
\end{aligned}$$

and

$$\sum_{r,s} (n_f(r) + n_f(s) - 2n_f(r)n_f(s))(\epsilon_r - \epsilon_s + h)^2 e^{-2B(\epsilon_r - \epsilon_s + h)^2} \sim B^{-3/2}. \quad (2.71)$$

Since the blue term (2.70) has an additional B^{-1} factor in (2.64) it is less important for the flow at large B than the black 2-loop term (2.71). We will therefore neglect the blue terms in the following analytical discussion. In addition we assume

$$\int_0^B dB_1 g_p(B_1) g_q(B_1) = B g_p(B) g_q(B) , \quad (2.72)$$

where g is a shorthand notation for $g^{\uparrow/\downarrow}$. This approximation is motivated by the weak B dependence of the running coupling which is logarithmic for small B and a power law for large B . In Fig. 2.1 we plotted the flow of $J^\downarrow(p, q)$ at nonzero magnetic field ($h = 0.25$, $V = T = 0$) both from the full set of flow equations (2.50) and from diagonal parametrization without the blue terms (2.64). We find excellent agreement, also for other parameter regimes.

2.2.5 Scaling Analysis (2-loop), Isotropic Model

2.2.5.1 Magnetic field only

The flow of the 2-loop equations can only be hardly described analytically due to complicated momentum dependence. In the 1-loop section (2.1.4) we learned that the running coupling is strongly peaked at $\epsilon_p = \mp h$ for $g_p^{\uparrow/\downarrow}$ and $\epsilon_p = \pm h/2$ for g_p^\perp ($V = T = 0$). For a qualitative discussion it is sufficient to restrict the analysis of the flow equations to the peak positions of the running couplings. This can be interpreted as a “worst case study”. We define

$$g_{\parallel} = g_{-h}^{\uparrow} = g_h^{\downarrow} , \quad g_{\perp} = g_{-h/2}^{\perp} = g_{h/2}^{\perp} \quad (2.73)$$

and replace the momentum dependent coupling by the latter expressions. The straightforward but lengthy evaluation of the momentum sums is given in Appendix B.1. Using the results from Sec. 2.1.4 and Eq. (B.4) the 2-loop flow equations simplify to

$$\begin{aligned} \frac{dg_{\parallel}}{dB} &= \frac{g_{\perp}^2}{2B} - \frac{g_{\perp}^2 g_{\parallel}}{8B} \left(2e^{-2Bh^2} + \sqrt{2\pi B} \operatorname{herf}(\sqrt{2B}h) \right) \\ \frac{dg_{\perp}}{dB} &= \frac{g_{\perp} g_{\parallel}}{4B} \left(1 + e^{-2Bh^2} \right) - \frac{g_{\perp} g_{\parallel}^2}{8B} - \frac{g_{\perp}^3}{16B} \left(2e^{-2Bh^2} + \sqrt{2\pi B} \operatorname{herf}(\sqrt{2B}h) \right) . \end{aligned} \quad (2.74)$$

We identify two important limits namely $B \ll h^{-2}$ and $B \gg h^{-2}$. For small B we are left with the flow equations

$$\begin{aligned} \frac{dg_{\parallel}}{dB} &= \frac{g_{\perp}^2}{2B} - \frac{g_{\perp}^2 g_{\parallel}}{4B} \\ \frac{dg_{\perp}}{dB} &= \frac{g_{\perp} g_{\parallel}}{2B} - \frac{g_{\perp} g_{\parallel}^2}{8B} - \frac{g_{\perp}^3}{8B} , \end{aligned} \quad (2.75)$$

since

$$\lim_{x \rightarrow 0} e^{-x^2} = 1 , \quad \lim_{x \rightarrow 0} x \operatorname{erf}(x) = 0 . \quad (2.76)$$

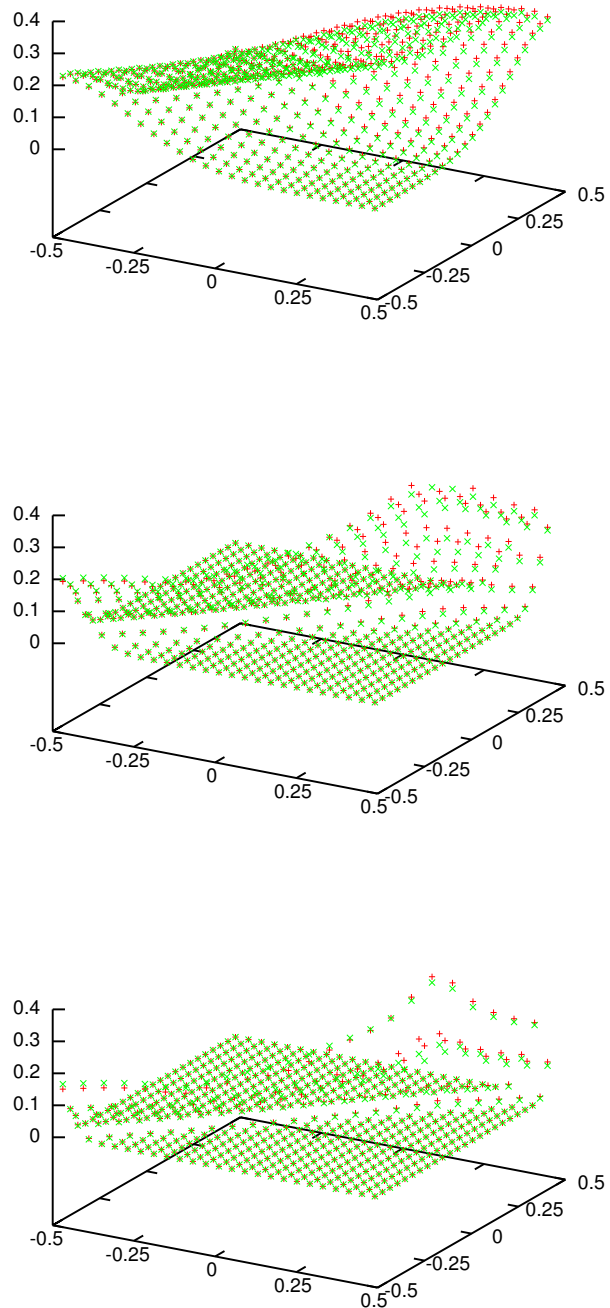


Figure 2.1: Flow of $J^\downarrow(p, q)$ at $h = 0.25$ ($V = T = 0$) for $B = 10, 100, 500$ from top to bottom. Red points: full system, green points: diagonal parametrization (see text).

Eqs. (2.75) are the usual 2-loop scaling equations for the anisotropic Kondo Model [71]. Since we started with isotropic initial values $g_{\parallel}(B=0) = g_{\perp}(B=0)$ Eqs. (2.75) can be simplified to

$$\frac{dg}{dB} = \frac{g^2}{2B} - \frac{g^3}{4B}, \quad (2.77)$$

where $g = g_{\perp/\parallel}$. The solution of the 1-loop part is given by

$$g(B) = \frac{1}{\ln(1/(\sqrt{B}T_K^{1\text{-loop}}))}, \quad (2.78)$$

where $T_K^{1\text{-loop}} = D \exp(-1/J)$ is the 1-loop Kondo temperature. The derivation of the solution for general anisotropic initial values is given in Sec. 2.2.6. For convenience we have set $\rho = 1$ in the expression for T_K . In the limit $J \ll 1$ the main effect of the 2-loop term is a redefinition of the Kondo temperature [72–74]:

$$T_K = D\sqrt{J} \exp(-1/J). \quad (2.79)$$

In addition one finds an unphysical fixed point at $g(B) = 2$ that will be shifted or removed by higher order terms [71]. The simple mathematical background is as follows: In RG approaches one typically defines a β -function by

$$\frac{dg(\Lambda)}{d\ln(\Lambda)} = \beta(g(\Lambda)), \quad (2.80)$$

where the flow parameter Λ is identified with $B^{-1/2}$ in the flow equation approach. In perturbative RG approaches the β -function is not calculated directly, instead one derives a power series corresponding to the Taylor expansion of the β -function in g . If one uses a perturbative truncation scheme only the first few powers of this Taylor expansion are calculated. Then the β -function simply is a polynomial in g .

In the Kondo problem this polynomial does not contain a zeroth order contribution g^0 , therefore $g = 0$ is an obvious root of the polynomial. If one takes only the leading term of the β -function into account then $g = 0$ is the only root of the problem. Due to the fundamental theorem of algebra one finds at least one additional root on the complex plane if higher order terms are included. Of course, the roots depend on the details of the polynomial, so the inclusion of higher order terms in general leads to shifts of the roots on the complex plane and typically also to additional roots. It is therefore impossible to predict the roots of a n th order expansion of the β -function.

This provides a fundamental problem in perturbative RG approaches: it is clearly not sufficient to only search for fixpoints in the flow of the running coupling, one also has to check their physical interpretation. Otherwise one studies the mathematical properties of the truncation scheme and not the physical properties of the model.

The appearance of the fixpoint $g = 2$ in the scaling equation (2.77) is simply luck. Since this fixpoint cuts off the logarithmic divergence of the running coupling (yielding a rather small running coupling), we leave it up to the reader whether it should be considered good

or bad luck.

The flow equation for the magnetic field is given by

$$\frac{dh}{dB} = -\frac{g_{\perp}^2}{16B^{3/2}}\sqrt{2\pi}\operatorname{erf}\left(\sqrt{2B}h\right). \quad (2.81)$$

The error function is linear for small argument

$$\operatorname{erf}(x) \stackrel{|x|\ll 1}{=} \frac{2}{\sqrt{\pi}}x. \quad (2.82)$$

Using this expansion Eq. (2.81) for $B \ll h^{-2}$ yields

$$\frac{dh}{dB} = -\frac{h}{2} \frac{g_{\perp}^2}{2B}. \quad (2.83)$$

Using $dg_{\parallel}/dB = g_{\perp}^2/(2B)$ we find a shift of

$$h(B) = h_0 \exp\left(-\frac{1}{2}\left(\frac{1}{\ln(1/(\sqrt{B}T_K))} - \frac{1}{\ln(D/T_K)}\right)\right), \quad (2.84)$$

where $h_0 = h(B=0)$. The impurity spectral function is strongly peaked at the magnetic field (see discussion in Sect. 3.4). Previous Bethe Ansatz calculations [17] predicted a shift of the peaks to $h^* \approx h_0(1 - 1/(2 \ln(|h_0|/T_K)))$. The flow of the magnetic field stops at $B \approx h_0^{-2}$ as we show in the following discussion. In the scaling limit $D/T_K \rightarrow \infty$ Eq. (2.84) yields a shift of the magnetic field to $h^* = h(B=\infty) \approx h_0 \exp(1 - 1/(2 \ln(|h_0|/T_K)))$ which is consistent with the previous Bethe Ansatz result.

For $B \gg h^{-2}$ we use the approximations

$$e^{-x^2} \stackrel{x \gg 1}{\rightarrow} 0, \quad \operatorname{erf}(x) \stackrel{x \gg 1}{\rightarrow} 1 \quad (2.85)$$

to derive the flow equations

$$\begin{aligned} \frac{dg_{\parallel}}{dB} &= -g_{\perp}^2 g_{\parallel} \frac{\sqrt{2\pi}}{8} \frac{|h^*|}{\sqrt{B}} \\ \frac{dg_{\perp}}{dB} &= -g_{\perp}^3 \frac{\sqrt{2\pi}}{16} \frac{|h^*|}{\sqrt{B}}. \end{aligned} \quad (2.86)$$

We neglected the 1-loop terms since they only contribute in $\mathcal{O}(g^2/B)$. As initial values we define $g_{\parallel}^* = g_{\parallel}(B = (h^*)^{-2})$ and $g_{\perp}^* = g_{\perp}(B = (h^*)^{-2})$. The flow of the magnetic field is nearly zero¹ for $B \gg h^{-2}$:

$$\frac{dh}{dB} = -\frac{g_{\perp}^2}{16B^{3/2}}\sqrt{2\pi}. \quad (2.87)$$

¹The shift is only of $\mathcal{O}(h_0/(\ln(h_0/T_K))^2)$.

We therefore set the magnetic field to $h^* = h(B = h_0^{-2})$ for $B \gg h_0^{-2}$, where $h(B)$ is defined in Eq. (2.84). The flow equation for g_\perp is easily integrated:

$$\begin{aligned} \frac{dg_\perp}{dB} &= cg_\perp^3 B^{-1/2} \\ \int_{g_\perp^*}^{g_\perp} \frac{dg}{g^3} &= c \int_{B_0}^B \frac{dB_1}{B_1^{1/2}} \\ -\frac{1}{2}(g_\perp^{-2} - (g_\perp^*)^{-2}) &= 2c(\sqrt{B} - \sqrt{B_0}) \\ g_\perp &= \frac{g_\perp^*}{\sqrt{1 + \Gamma_\perp(\sqrt{B} - \sqrt{B_0})}}, \end{aligned} \quad (2.88)$$

where $B_0 = (h^*)^{-2}$, $c = -|h^*|\sqrt{2\pi}/16$ and

$$\Gamma_\perp = \frac{\sqrt{2\pi}}{4}(g_\perp^*)^2 h^*. \quad (2.89)$$

The solution for parallel scattering is then given by

$$g_\parallel = \frac{g_\parallel^*}{1 + \Gamma_\perp(\sqrt{B} - \sqrt{B_0})}. \quad (2.90)$$

In the limit $B \rightarrow \infty$ the running coupling obviously decays to zero. This is even true if the previous limitation $|h| \gg T_K$ is not fulfilled. Then however the running coupling becomes of $\mathcal{O}(1)$ during the flow and the perturbative truncation leads to an uncontrolled error. Due to the slow decay of g_\perp ($\sim B^{-1/4}$) one cannot give a perturbative expansion of the flow equation transformation, see Sect. 1.4.4 for more information.

2.2.5.2 Voltage Bias, Temperature, and Combinations with Magnetic Field

The situation is even more tricky for combinations of magnetic field and voltage bias since the running coupling shows a multi peak structure. Then the local maxima of the running coupling can no longer be used to describe the flow. Instead one has to find a suitable average over the splitting of the peaks. For zero magnetic field

$$g_{\parallel/\perp} = \frac{1}{V} \int_{-V/2}^{V/2} d\epsilon_p g_p^{\parallel/\perp} \quad (2.91)$$

is a suitable choice, for nonzero magnetic field one has to shift the limits of the integral by $\pm h$ for parallel and by $\pm h/2$ for perpendicular scattering.

Note that a qualitative description of the flow is easily given without going too much into the averaging details since the 2-loop terms are p -independent after replacing g_p with

some averaged value. (The 1-loop terms are neglected anyway.) Additional information on how to work out the momentum summations of the 2-loop terms is given in Appendix B.1. At zero temperature and $V \geq 0$ we find (see Eq. (B.4)):

$$\begin{aligned} & \sum_{r,s} (n_f(\epsilon_r) + n_f(\epsilon_s) - 2n_f(\epsilon_r)n_f(\epsilon_s))(\epsilon_r - \epsilon_s + h)^2 e^{-2B(\epsilon_r - \epsilon_s + h)^2} = \\ & = \frac{1}{8B^2} \frac{1}{(1+R)(1+1/R)} \left(2(R+1/R)e^{-2Bh^2} + 2e^{-2B(V+h)^2} + \right. \\ & \quad + 2e^{-2B(V-h)^2} + (R+1/R)\sqrt{2\pi B} \operatorname{erf}(\sqrt{2B}h) + \\ & \quad \left. + \sqrt{2\pi B}(V+h)\operatorname{erf}(\sqrt{2B}(V+h)) + \sqrt{2\pi B}(V-h)\operatorname{erf}(\sqrt{2B}(V-h)) \right). \end{aligned} \quad (2.92)$$

As in the previous section we do an expansion for small and large B . The relevant energy scales are easily identified as $|V+h^*|$, $|V-h^*|$ and $|h^*|$. In the flow equation for g_\perp one also finds a contribution without magnetic field. Here the relevant energy scale is simply given by V .

In equilibrium at nonzero temperature we again use the peak positions of the running coupling to discuss the flow. We find (see Eq. (B.5)):

$$\begin{aligned} & \sum_{r,s} (n_f(\epsilon_r) + n_f(\epsilon_s) - 2n_f(\epsilon_r)n_f(\epsilon_s))(\epsilon_r - \epsilon_s + h)^2 e^{-2B(\epsilon_r - \epsilon_s + h)^2} = \\ & = \frac{\sqrt{2\pi}}{8B^{3/2}} h \coth\left(\frac{h}{2T}\right). \end{aligned} \quad (2.93)$$

The relevant energy scales are given by T and $h \coth(h/(2T))$ for $h \neq 0$. At zero magnetic field the temperature T is the only relevant energy scale.

For the initial flow (small B) we again find the usual scaling equations for the anisotropic Kondo model (2.75) and a small shift of the magnetic field. Unfortunately an analytic evaluation of the latter shift can only be hardly done for general parameters. For simplicity we restrict the following discussion to the flow at very large flow parameter $B \gg \Lambda_0^{-2}$, where $\Lambda_0 = B_0^{-1/2}$ is the nonzero minimum of the set $\{|V+h|, |V-h|, V, |h|\}$ in non-equilibrium, the nonzero minimum of the set $\{T, h \coth(h/(2T))\}$ in equilibrium for $h \neq 0$, or the temperature T in equilibrium at zero magnetic field. In the regime $B \gg \Lambda_0^{-2}$ the 1-loop contributions are negligible since they are only of $\mathcal{O}(g^2/B)$. We are then left with the flow equations

$$\begin{aligned} \frac{dg_\perp}{dB} &= -\frac{g_\parallel^2 g_\perp}{2\sqrt{B}} c_1 - \frac{g_\perp^3}{2\sqrt{B}} c_2 \\ \frac{dg_\parallel}{dB} &= -\frac{g_\perp^2 g_\parallel}{\sqrt{B}} c_2. \end{aligned} \quad (2.94)$$

The initial values are $g_{\parallel/\perp}(B_0) = g_{\parallel/\perp}^*$ and the constants are given by

$$\begin{aligned} c_1(h^*, V) &= \frac{\sqrt{2\pi}}{4} \frac{V}{(1+R)(1+1/R)} \\ c_2(h^*, V) &= \frac{\sqrt{2\pi}}{8} \frac{|V+h^*| + |V-h^*| + |h^*|(R+1/R)}{(1+R)(1+1/R)} \end{aligned} \quad (2.95)$$

in non-equilibrium and by

$$\begin{aligned} c_1(h^*, T) &= \frac{\sqrt{2\pi}}{4} T \\ c_2(h^*, T) &= \frac{\sqrt{2\pi}}{8} h^* \coth\left(\frac{h^*}{2T}\right) \end{aligned} \quad (2.96)$$

in equilibrium, where we defined $h^* = h(B_0)$. Eqs. (2.94) are easily rewritten to

$$\begin{aligned} \frac{dg_{\parallel}}{dB} &= -\frac{g_{\parallel}^3}{\sqrt{B}} c_1 - \frac{g_{\parallel}^2}{\sqrt{B}} \left(\frac{(g_{\perp}^*)^2}{g_{\parallel}^*} c_2 - g_{\parallel}^* c_1 \right) \\ g_{\perp} &\stackrel{(2.94)}{=} \sqrt{-\frac{\sqrt{B}}{c_2 g_{\parallel}} \frac{dg_{\parallel}}{dB}} = \sqrt{g_{\parallel}^2 \frac{c_1}{c_2} + g_{\parallel} \left(\frac{(g_{\perp}^*)^2}{g_{\parallel}^*} - g_{\parallel}^* \frac{c_1}{c_2} \right)}. \end{aligned} \quad (2.97)$$

The straightforward derivation is given in Appendix B.2, in the following we give the much shorter mathematical proof “only”. The differential equation for g_{\parallel} in (2.97) is obviously equivalent to the one in (2.94). Also the initial values for g_{\parallel} and g_{\perp} are the same for both versions. To show the identity of the two representations we therefore only have to show that g_{\perp} as defined in (2.97) solves the ordinary differential equation for g_{\perp} in (2.94). Using the relation

$$g_{\perp} = \sqrt{ag_{\parallel}^2 + bg_{\parallel}} \quad \Rightarrow \quad \frac{dg_{\perp}}{dB} = \frac{1}{2g_{\perp}} (2ag_{\parallel} + b) \frac{dg_{\parallel}}{dB} \quad (2.98)$$

we find

$$\frac{dg_{\perp}}{dB} = -\frac{g_{\parallel}^2 g_{\perp}}{\sqrt{B}} c_1 - \left(\frac{(g_{\perp}^*)^2}{g_{\parallel}^*} c_2 - g_{\parallel}^* c_1 \right) \frac{g_{\parallel} g_{\perp}}{2\sqrt{B}}. \quad (2.99)$$

Comparing the right hand side of the latter equation with the right hand side of the flow equation for g_{\perp} (2.94), the following relation has to be fulfilled:

$$\begin{aligned} \frac{g_{\parallel}^2 g_{\perp} c_1}{2\sqrt{B}} - \frac{g_{\perp}^3 c_2}{2\sqrt{B}} &\stackrel{!}{=} -\left(\frac{(g_{\perp}^*)^2}{g_{\parallel}^*} c_2 - g_{\parallel}^* c_1 \right) \frac{g_{\parallel} g_{\perp}}{2\sqrt{B}} \\ g_{\parallel}^2 c_1 - g_{\perp}^2 c_2 &\stackrel{!}{=} -g_{\parallel} \left(\frac{(g_{\perp}^*)^2}{g_{\parallel}^*} c_2 - g_{\parallel}^* c_1 \right) \\ g_{\perp} &\stackrel{!}{=} \sqrt{g_{\parallel}^2 \frac{c_1}{c_2} + g_{\parallel} \left(\frac{(g_{\perp}^*)^2}{g_{\parallel}^*} - g_{\parallel}^* \frac{c_1}{c_2} \right)}. \end{aligned} \quad (2.100)$$

The last relation is the definition of g_{\perp} in (2.97).

The remaining flow equation is an Abel differential equation of the first kind whose general solution is unknown. Therefore only asymptotic results can be obtained. Note that the nontrivial fixed point $g_{\parallel}(B) = g_{\parallel}^* - c_2(g_{\perp}^*)^2/(g_{\parallel}^*c_1)$ in Eq. (2.97) can only be reached in the anisotropic Kondo model with initial values $g_{\perp}(B=0) < |g_{\parallel}(B=0)|$ and $|h| \lesssim V, T$. The scaling in the anisotropic model is discussed in Sect. 2.2.6. The equilibrium zero temperature result has already been discussed above. For zero magnetic field we find

$$g(B) = \frac{g^*}{\sqrt{1 + 4(g^*)^2 c_1 (\sqrt{B} - \sqrt{B_0})}}, \quad (2.101)$$

where $g = g_{\parallel} = g_{\perp}$. Here the corresponding decoherence rate Γ is given by

$$\Gamma = 4(g^*)^2 c_1. \quad (2.102)$$

In general we find a competition between the cubic and the quadratic term in (2.97). For very small energies the quadratic term dominates the flow (if existing) and the running couplings decay like $g_{\parallel} \sim B^{-1/2}$ and $g_{\perp} \sim B^{-1/4}$. If the cubic term dominates both running couplings are proportional to $B^{-1/4}$. Again one cannot give a perturbative expansion of the flow equation transformation due to the slow decay of g_{\perp} ($\sim B^{-1/4}$), see Sect. 1.4.4 for more information.

For small magnetic fields $V, T \gg |h|$ Eqs. (2.94) are approximately solved by

$$g_{\parallel/\perp}(B) = \frac{g_{\parallel/\perp}^*}{\sqrt{1 + \Gamma_{\parallel/\perp} (\sqrt{B} - \sqrt{B_0})}}, \quad (2.103)$$

since $g_{\parallel}^* \approx g_{\perp}^*$ and $c_1 \approx c_2$. In the high voltage regime the decoherence rates are given by

$$\begin{aligned} \Gamma_{\parallel}(h^*, V) &= \sqrt{2\pi} (g_{\parallel}^*)^2 \frac{V}{(1+R)(1+1/R)} \\ \Gamma_{\perp}(h^*, V) &= \frac{\sqrt{2\pi}}{2} (g_{\perp}^*)^2 \frac{|V+h^*| + |V-h^*| + |h^*|(R+1/R)}{(1+R)(1+1/R)}. \end{aligned} \quad (2.104)$$

Note that only the spin flip coupling sees both the magnetic field and the voltage bias in its decoherence rate. We find similar behavior at nonzero temperature:

$$\begin{aligned} \Gamma_{\parallel}(h^*, T) &= \sqrt{2\pi} (g_{\parallel}^*)^2 T \\ \Gamma_{\perp}(h^*, T) &= \frac{\sqrt{2\pi}}{2} (g_{\perp}^*)^2 h^* \coth\left(\frac{h^*}{2T}\right). \end{aligned} \quad (2.105)$$

2.2.5.3 Decoherence Effects and Higher Orders

The logarithmic divergence in the 1-loop scaling approach induced by coherent spin-flip scattering is cut off by decoherence effects embedded in the 2-loop corrections, provided $\max(|h|, V, T) \gg T_K$. The corresponding decoherence rates (2.89), (2.102), (2.104) and (2.105) can be related to spin relaxation rates. As we show in Sect. 3.3 the decoherence rates give the energy scales on which the spin operators decay.

In perturbative RG approaches one usually assumes that (at least) the qualitative features of the flow are given by the RG equation in lowest order, provided the running coupling stays small during the flow. It is therefore surprising that for large B the flow is dominated by the terms cubic in the running coupling (2-loop) and not by the quadratic ones (1-loop). The reason for this unexpected behavior is given by the dimensionful parameters h , V , T and their combinations (see above). It is not sufficient to use only the running coupling as control parameter, also expressions of the form $h\sqrt{B}$ (analogue for voltage bias and temperature) have to be considered in the perturbative expansion since they become uncontrolled for $B \gg h^{-2}$ or $h\sqrt{B} \gg 1$ respectively.

This naturally raises questions on the effect of higher order terms. Answering these questions turns out to be nontrivial. While we do not expect qualitative changes in the solution of the isotropic Kondo model ($g_{\perp}(B=0) = g_{\parallel}(B=0)$) we indeed find indications that higher order terms will become important in certain parameter regimes of the anisotropic Kondo model ($g_{\perp}(B=0) \neq g_{\parallel}(B=0)$) as depicted in the following section.

2.2.6 Scaling Analysis, Anisotropic Model

In this section we generalize the previous scaling analysis of the Kondo model with isotropic initial values $g_{\parallel}(B=0) = g_{\perp}(B=0)$ to anisotropic ones where $g_{\parallel}(B=0)$ and $g_{\perp}(B=0)$ might differ.

Note that one assumes $g_{\perp} \geq 0$ since a sign change of g_{\perp} corresponds to a rotation of π around the z -axis. The simple mathematical background is as follows (use your hands as illustration!): assume we have a given right hand basis of a three dimensional space. If we change the direction of two basis vectors - corresponding to a sign change - we are still in a right hand system, we just have to rotate our hand by π around one axis (finger). If we instead change the sign of one axis only (or three) we end up in a left hand system. Since g_{\perp} is the coupling in x - and y -direction a sign change can be absorbed in a rotation of the system. If one absorbs a change in the sign of g_{\parallel} into the spin operator one ends up in a left hand system with a different spin operator algebra than in the original system. In the anisotropic Kondo Model this leads to a quantum phase transition² between the so-called weak and strong coupling regimes, see Fig. 2.2.

²In contrast to classical phase transitions a quantum phase transition occurs at zero temperature.

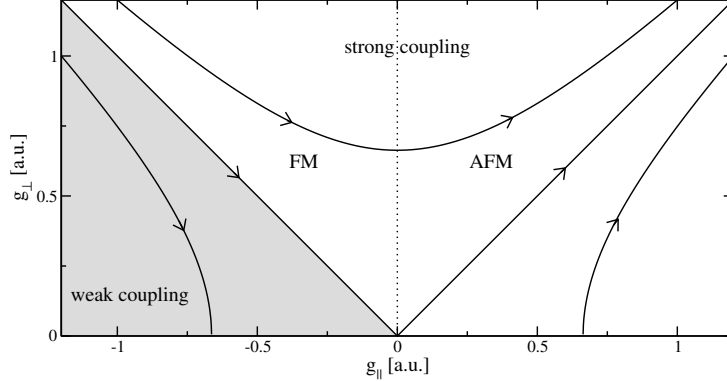


Figure 2.2: Phase portrait for the 1-loop scaling equations of the anisotropic Kondo model. There exist two important regimes, the (white) strong coupling regime where the running coupling flows to infinity and the weak coupling regime where g_{\perp} flows to zero. In the literature the parameter regime $g_{\parallel} > 0$ is typically called antiferromagnetic (AFM) regime, $g_{\parallel} < 0$ is the ferromagnetic (FM) regime.

2.2.6.1 General 1-loop scaling

For small B the 1-loop scaling equations are given by

$$\begin{aligned} \frac{dg_{\parallel}}{dB} &= \frac{g_{\perp}^2}{2B} \\ \frac{dg_{\perp}}{dB} &= \frac{g_{\parallel}g_{\perp}}{2B}, \end{aligned} \quad (2.106)$$

see the derivation of Eq. (2.75). In Fig. 2.2 we show the corresponding phase portrait. The solution is constructed as follows. First we use the symmetry

$$g_{\parallel} \frac{dg_{\parallel}}{dB} = g_{\perp} \frac{dg_{\perp}}{dB} \quad (2.107)$$

to relate the flow of the running couplings by

$$g_{\parallel}^2 - (g_{\parallel}^0)^2 = g_{\perp}^2 - (g_{\perp}^0)^2. \quad (2.108)$$

Here $g_{\parallel/\perp}^0$ are the initial values of $g_{\parallel/\perp}$ at $B = B_0 = D^{-2}$. In the following we use the shorthand notation

$$c = (g_{\parallel}^0)^2 - (g_{\perp}^0)^2. \quad (2.109)$$

The flow equation for parallel scattering

$$\frac{dg_{\parallel}}{dB} = \frac{g_{\parallel}^2 + c}{2B} \quad (2.110)$$

is easily integrated using the substitution $x = g_{\parallel}/\sqrt{c}$. We find

$$g_{\parallel}(B) = \frac{g_{\parallel}^0 + \sqrt{c} \tan\left(\sqrt{c} \ln\left(\sqrt{B/B_0}\right)\right)}{1 - \frac{g_{\parallel}^0}{\sqrt{c}} \tan\left(\sqrt{c} \ln\left(\sqrt{B/B_0}\right)\right)}. \quad (2.111)$$

The flow of the perpendicular coupling is given by $g_{\perp}(B) = \sqrt{g_{\parallel}^2(B) - c}$. We distinguish three parameter regimes, namely $c = 0$, $c < 0$ and $c > 0$.

For $c = 0$ or respectively $|g_{\parallel}^0| = g_{\perp}^0$ Eq. (2.111) simplifies to

$$g_{\parallel}(B) = \frac{g_{\parallel}^0}{1 - g_{\parallel}^0 \ln\left(\sqrt{B/B_0}\right)}. \quad (2.112)$$

For $g_{\parallel}^0 > 0$ the running coupling diverges at the 1-loop Kondo temperature

$$B_{\text{Kondo}}^{-1/2} = T_K^{1\text{-loop}} = D e^{-1/g_{\parallel}^0} \quad (2.113)$$

and Eq. (2.112) is easily reduced to

$$g(B) = g_{\parallel}(B) = g_{\perp}(B) = \frac{1}{\ln\left(1/\left(\sqrt{B} T_K^{1\text{-loop}}\right)\right)}. \quad (2.114)$$

For $g_{\parallel}^0 < 0$ the divergence is shifted to the energy scale $D \exp(+1/|g_{\parallel}^0|)$, which is larger than the band cutoff and is therefore not reached within a scaling approach. In the latter case the running coupling decays to zero for $B \rightarrow \infty$.

At $c < 0$ or $|g_{\parallel}^0| < g_{\perp}$ Eq. (2.111) has to be rewritten to

$$g_{\parallel}(B) = \frac{g_{\parallel}^0 - \sqrt{|c|} \tanh\left(\sqrt{|c|} \ln\left(\sqrt{B/B_0}\right)\right)}{1 - \frac{g_{\parallel}^0}{\sqrt{|c|}} \tanh\left(\sqrt{|c|} \ln\left(\sqrt{B/B_0}\right)\right)}. \quad (2.115)$$

Again we find a divergence for $g_{\parallel}^0 > 0$ at a certain energy scale

$$B_{\text{Kondo}(2)}^{-1/2} = T_K^{1\text{-loop}(2)} = D e^{-\text{atanh}(\sqrt{|c|}/g_{\parallel}^0)/\sqrt{|c|}}. \quad (2.116)$$

For $g_{\parallel}^0 < 0$ there is no divergence but the solution is not limited from above for $B \rightarrow \infty$.

In the case $c > 0$ or $|g_{\parallel}^0| > g_{\perp}^0$ the 1-loop Kondo temperature is given by

$$B_{\text{Kondo}(3)}^{-1/2} = T_K^{1\text{-loop}(3)} = D e^{-\text{atan}(\sqrt{c}/g_{\parallel}^0)/\sqrt{c}}. \quad (2.117)$$

For $g_{\parallel}^0 > 0$ the solution diverges, for $g_{\parallel}^0 < 0$ the solution (2.111) exists only for

$$B \leq B_0 e^{\pi/\sqrt{c}}. \quad (2.118)$$

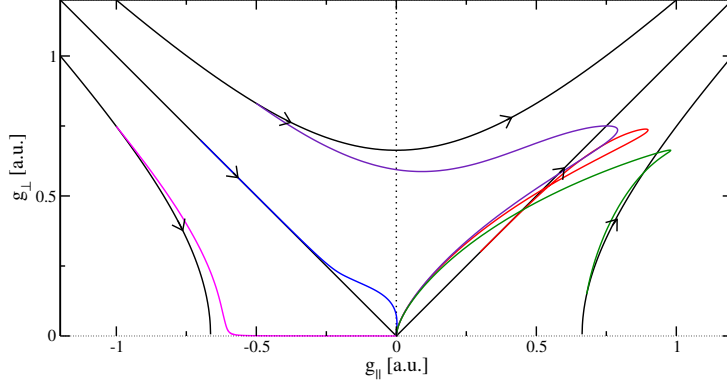


Figure 2.3: Comparison 2-loop scaling equations of the anisotropic Kondo model in a magnetic field with the standard 1-loop scaling equations in zero magnetic field. Note that the 2-loop phase portrait is not universal, the colored curves were calculated for $h = 0.05$ and $B_0 = D^{-2} = 1$.

The reason for this obscure behavior lies in the equation $g_{\perp} = \sqrt{g_{\parallel}^2 - c}$. If $g_{\parallel}^2 < c$ the perpendicular coupling becomes a complex number. Therefore the flow has to stop at $g_{\perp}(B_c) = 0$ or $g_{\parallel}(B_c) = -\sqrt{c}$, where

$$B_c = B_0 \exp \left(\frac{2}{\sqrt{c}} \operatorname{atan} \left(\frac{g_{\parallel}^0 + \sqrt{c}}{g_{\parallel}^0 - \sqrt{c}} \right) \right). \quad (2.119)$$

Note that the stop of the flow at $g_{\perp}(B_c) = 0$ follows immediately from Eqs. (2.107).

2.2.6.2 2-loop Scaling, Magnetic Field Only

In Fig. 2.3 we plotted a typical phase portrait of the 2-loop scaling equations for nonzero magnetic field. In contrast to the 1-loop result discussed in the previous section the running coupling always decays to zero, which actually follows from Eqs. (2.88) and (2.90). Nevertheless the 2-loop scaling analysis in the anisotropic is more tricky than the previous discussion leading to the flow equations (2.86), since we also have to consider the case $g_{\parallel} \rightarrow 0$, where the 2-loop term in the g_{\parallel} equation is zero and the 1-loop term dominates the flow. However since even the solution of

$$\begin{aligned} \frac{dg_{\parallel}}{dB} &= \frac{g_{\perp}^2}{2B} \\ \frac{dg_{\perp}}{dB} &= -g_{\perp}^3 \frac{\sqrt{2\pi} |h^*|}{16 \sqrt{B}} \end{aligned} \quad (2.120)$$

is well behaved

$$g_{\parallel}(B) = g_{\parallel}^* + \frac{(g_{\perp}^*)^2}{1 - \Gamma_{\perp} \sqrt{B_0}} \ln \left(\frac{\sqrt{B/B_0}}{1 + \Gamma_{\perp} (\sqrt{B} - \sqrt{B_0})} \right), \quad (2.121)$$

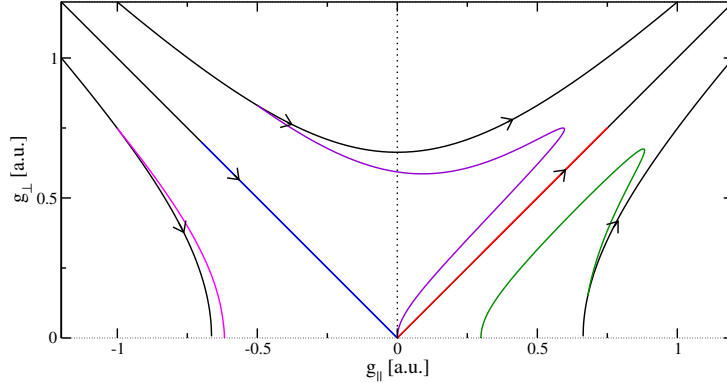


Figure 2.4: Comparison 2-loop scaling equations of the non-equilibrium anisotropic Kondo model with the standard 1-loop scaling equations. The colored curves were calculated for $V = 0.05$, $R = 1$ and $B_0 = D^{-2} = 1$.

we do not expect nontrivialities from this parameter regime. Another issue is the weak coupling regime. As we learned in the previous section the 1-loop scaling equations have a nontrivial fixpoint at a critical value B_c . For $|h| \gg B_c^{-2}$ or equivalently $|h| \rightarrow 0$ the perpendicular coupling might have already fully decayed to zero before the 2-loop terms become large, leading to a stop of the flow.

2.2.6.3 2-loop Scaling Voltage Bias Temperature and Combinations with Magnetic Field

Again the flow of the running coupling can be described using the scaling equations (2.97) derived in the section on the isotropic model. The scaling equations at large B are equivalent for the isotropic and the anisotropic model. The running coupling g_{\parallel} has a nontrivial fixpoint if

$$g_{\parallel}(B) = g_{\parallel}^* - c_2(g_{\perp}^*)^2 / (g_{\parallel}^* c_1) . \quad (2.122)$$

As shown in Figs. 2.4 and 2.5 this fixpoint is reached for scaling at zero magnetic field if $g_{\perp}^0 < |g_{\parallel}^0|$. Here the inclusion of higher order terms might lead to a decay of the running coupling to zero. In the parameter regime $g_{\perp} \geq |g_{\parallel}^0|$ the running couplings always decay to zero.

Discussing the flow for general combinations of magnetic field and voltage bias or temperature is a nontrivial task if $g_{\perp}^0 < |g_{\parallel}^0|$. While in the regime $|h| \gg V, T$ the running coupling decays to zero, the flow stops in the nontrivial fixpoint (2.122) for $|h| \lesssim V, T$. For $g_{\perp} \geq |g_{\parallel}^0|$ the running coupling always decays to zero, also for combinations of magnetic field with voltage bias or temperature. The power laws in the various regimes of the decay have already been discussed in the previous section on the isotropic model.

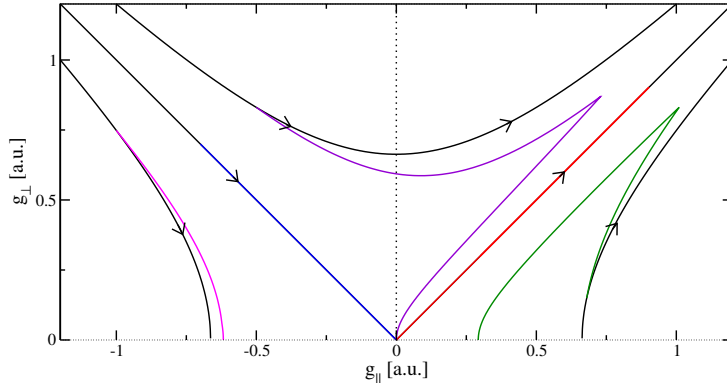


Figure 2.5: Comparison 2-loop scaling equations of the anisotropic Kondo model at $T > 0$ with the standard 1-loop scaling equations. The colored curves were calculated for $T = 0.05$ and $B_0 = D^{-2} = 1$.

2.3 Summary

In lowest (quadratic) order the perturbative RG equation for the running coupling in the isotropic Kondo model ($J_{\parallel} = J_{\perp} = J$) is in equilibrium at zero magnetic field and zero temperature ($V = h = T = 0$) given by

$$\frac{dJ(B)}{dB} = -\frac{J^2(B)}{2B} \quad (2.123)$$

yielding a logarithmic divergence at large flow parameter $B \gg D^{-2}$, where $2D$ is the bandwidth:

$$J(B) = \frac{J(B = D^{-2})}{1 - J(B = D^{-2}) \ln(D\sqrt{B})}, \quad B \in [D^{-2}, \infty). \quad (2.124)$$

At nonzero magnetic field (or nonzero voltage bias) a scaling description with a momentum independent coupling is no longer sufficient and one has to introduce a momentum dependent running coupling [11, 37]. In the flow equation approach the running coupling becomes momentum dependent by construction (see Sect. 1.4). In the weak coupling regime $\max(V, |h|, T) \gg T_K$ the logarithmic divergence is already cut off in lowest order, except for certain resonant energy scales like the chemical potentials or the magnetic field strength. The running coupling at these resonant scales is cut off by the decoherence rate which is naturally introduced if the flow equations are derived in cubic order in the running coupling and $\max(V, |h|, T) \gg T_K$. This natural inclusion of decoherence effects in the flow equation method is the key enhancement to previous approaches where the decoherence rate had to be included by hand [11, 37]. By further analysis we showed that the cubic terms dominate the flow of the running coupling at large flow parameter leading to the diagonalization of the Hamiltonian if $\max(V, |h|, T) \gg T_K$. If $\max(V, |h|, T) \ll T_K$ the

running coupling becomes of order one during the RG flow and our perturbative truncation scheme becomes uncontrolled.

In the anisotropic Kondo model we found a nontrivial fixed point in the flow of the running coupling for certain parameter combinations, namely $J_{\perp} < |J_{\parallel}|$ and $V, T \gtrsim |h|$. In all other situations the Hamiltonian is diagonalized as in the isotropic model. If the flow of the running coupling stops in the nontrivial fixed point the Hamiltonian becomes energy diagonal but not diagonal. As consequence these energy diagonal terms have to be included in the further calculation. For example, in time evolution the inclusion of the remaining energy diagonal interaction terms leads to secular terms since in the Kondo problem also large timescales $t \gg 1/J$ give important contributions. We expect that the inclusion of terms in higher than third order will lead to the diagonalization of the Hamiltonian in the full parameter regime of the anisotropic Kondo model, provided $\max(V, |h|, T) \gg T_K$.

Chapter 3

Observables

3.1 Introduction

The T-Matrix T_σ describes the scattering of conduction band electrons at the impurity:

$$\mathcal{G}_{k,k',\sigma}(\omega) = \mathcal{G}_{k,k',\sigma}^{(0)}(\omega)\delta_{k,k'} + \mathcal{G}_{k,k,\sigma}^{(0)}(\omega)\mathcal{T}_\sigma(\omega)\mathcal{G}_{k',k',\sigma}^{(0)}(\omega), \quad (3.1)$$

where $\mathcal{G}_{k,k',\sigma}(\omega)$ is the Greens function of the interacting system and $\mathcal{G}_{k,k',\sigma}^{(0)}(\omega)$ the Greens function of the noninteracting one. For a dc-biased Kondo dot the T-Matrix and the Greens function become lead dependent. However, if the system's Hamiltonian is derived from an Anderson impurity model only one eigenvalue of the T-Matrix is nonzero [45]. In linear response the resistivity ρ is related to the imaginary part of the T-Matrix via

$$\rho^{-1} = \frac{ne^2}{2mc} \sum_\sigma \int_{-\infty}^{\infty} d\omega A_\sigma^{-1}(\omega) \left(-\frac{\partial f}{\partial \omega} \right), \quad (3.2)$$

where n is the conduction band electron concentration, e the electronic charge, m the mass of the conduction band electrons, c is the small concentration of Kondo impurities in the host metal, and f is the Fermi function. The spectral function

$$A_\sigma(\omega) = -\frac{1}{\pi} \text{Im} [T_\sigma(\omega + i\delta)] \quad (3.3)$$

can be measured directly by tunneling experiments [54]. In equilibrium the spectral function of the Kondo model is well studied [9, 11–13, 17], so far only preliminary results were published in non-equilibrium [45]. Within the flow equation approach a derivation of the spectral function in both equilibrium and non-equilibrium is feasible. We extend the previously known results to the full parameter regime $\max(V, |h|, T) \gg T_K$.

The dynamics of the impurity (dot) spin is described by the spin-spin correlation function and the corresponding response function. The response function can be measured by nuclear magnetic resonance [56, 57] and electron spin resonance [58–60] experiments. The

static properties of the spin are given by the magnetization and the static spin susceptibility. Again in equilibrium the physical properties of the impurity (dot) spin are well studied. The magnetization and the static spin susceptibility in equilibrium are accessible by solving the exact Bethe Ansatz equations [7, 8]. In non-equilibrium only zeroth order results have been obtained [46, 53], the logarithmic corrections containing the Kondo physics are considered as inaccessible in these approaches. Within the flow equation approach the leading logarithmic corrections to the zeroth order result are accessible.

The spin-spin correlation function and the corresponding response function are well studied objects [14, 15, 45, 55], also in the context of the spin boson model. They are easily accessed within the flow equation framework. At zero magnetic field we use the spin-spin correlation function to relate the decoherence rate Γ with the spin relaxation time. The static spin susceptibility is calculated from the imaginary part of the response function using a Kramers-Kronig relation.

The outline of this chapter is as follows. In Sect. 3.2 we derive a simple approach to calculate expectation values and correlation functions within the flow equation framework. Many of the concepts we use in this section are well understood, for convenience we use the notation from Ref. [41]. The transformation of the impurity (dot) spin operator into the diagonal basis is derived in Sect. 3.3. For convenience we restrict the numerical results shown in this section to $V = T = 0$. We rederive the asymptotic Bethe Ansatz result for the zero temperature equilibrium magnetization in Sect. 3.3.2, the spin-spin correlation function and the corresponding response function are derived in Sect. 3.3.3. The T-matrix is constructed in Sect. 3.4, again we restrict the numerical results to $V = T = 0$. In Sect. 3.5 we study in detail the spin-spin correlation function and the imaginary part of the T-Matrix as functions of voltage bias, temperature, and magnetic field and discuss the dependence of the magnetization and the static spin susceptibility on the voltage bias and the temperature.

3.2 The Flow Equation Way

Despite the sections name, the following discussion actually is independent of the diagonalization procedure. Any unitary transformation that diagonalizes the given Hamiltonian does the job. For the readers convenience we use the notation from Ref. [41].

In quantum mechanics many measurable quantities are calculated by taken the expectation value of an operator or an operator product. At zero temperature a equilibrium system is described by its ground state, at nonzero temperature the system is described by the density matrix.

3.2.1 Zero Temperature

The ground state expectation value of a given operator O is defined as

$$\langle O \rangle = \langle 0|O|0 \rangle, \quad (3.4)$$

where we denoted the ground state by $|0\rangle$. The ground state is easily identified in the diagonal ($B = \infty$) basis since eigenvalues (E) are basis independent

$$H|\Psi\rangle = E|\Psi\rangle \Leftrightarrow \underbrace{(UHU^\dagger)}_{\tilde{H}} \underbrace{(U|\Psi\rangle)}_{|\tilde{\Psi}\rangle} = E \underbrace{(U|\Psi\rangle)}_{|\tilde{\Psi}\rangle} \quad (3.5)$$

and the eigenstates in the diagonal basis are trivial. Unless stated otherwise U denotes a general unitary transformation throughout this thesis. The flow equation transformation is always denoted by $U(B)$ or by $\tilde{U} = U(B = \infty)$. Eq. (3.4) is then simplified to

$$\langle O \rangle = (\langle 0|U^\dagger(B = \infty)) \underbrace{(U(B = \infty)OU^\dagger(B = \infty))}_{O(B=\infty)} (U(B = \infty)|0\rangle) . \quad (3.6)$$

The remaining task is to transform the operator into the diagonal basis which turns out to be challenging for nontrivial problems.

3.2.2 Nonzero Temperature

The thermal expectation value of a given operator O is defined as

$$\langle O \rangle_\beta = \text{Tr}(\rho(\beta)O) , \quad (3.7)$$

where the trace is taken over all states in the Hilbert space. We use the textbook definition of the density matrix $\rho(\beta)$ via the partition function $Z(\beta)$ and the inverse temperature β ($k_B = 1$):

$$\rho(\beta) = \frac{1}{Z(\beta)} e^{-\beta H} , \quad Z(\beta) = \text{Tr}(e^{-\beta H}) , \quad \beta = \frac{1}{T} . \quad (3.8)$$

The eigenstates are trivial and orthonormal in the diagonal ($B = \infty$) basis

$$H(B = \infty)|n\rangle = E_n|n\rangle , \quad \langle n|m\rangle = \delta_{nm} . \quad (3.9)$$

We therefore take the trace in the diagonal basis. Eq. (3.7) then yields

$$\langle O \rangle_\beta = \frac{1}{Z(\beta)} \sum_n \langle n|e^{-\beta \tilde{H}} \tilde{O}|n\rangle = \frac{1}{Z(\beta)} \sum_n e^{-\beta E_n} \langle n|\tilde{O}|n\rangle = \frac{1}{Z(\beta)} \sum_n e^{-\beta E_n} \langle n|\tilde{U}O\tilde{U}^\dagger|n\rangle , \quad (3.10)$$

where the tilde is a shorthand notation for operator at $B = \infty$. The partition function is simplified to

$$Z(\beta) = \sum_n e^{-\beta E_n} . \quad (3.11)$$

A common source of error lies in the evaluation of the eigenenergies. Since the transformation of the Hamiltonian is typically truncated using some perturbative argument also the calculated eigenenergies are only correct up to some order in the expansion parameter. This might lead to an uncontrolled error in the evaluation of the Boltzmann weights since the exponential function reacts strongly on small changes of its argument. For single impurity models like the Kondo model the renormalization of the eigenenergies can typically be neglected.

3.2.3 Non-Equilibrium

In non-equilibrium situations expectation values have to be evaluated with respect to the steady state instead of the ground state. Since the steady state is usually unknown, we evaluate expectation values with respect to the non-interacting preparation state of the system. For dc-voltage bias the preparation state is given by the well defined ground state of the non-interacting system. If the dot is coupled to two leads at different temperature, we assume non-interacting leads described by the usual temperature dependent Fermi functions.

3.2.4 Time Evolution

In the Heisenberg picture the time evolution of a time independent operator O is given by

$$O(t) = e^{iHt} O e^{-iHt} . \quad (3.12)$$

Using the identities

$$U A^n U^\dagger = (U A U^\dagger)^n , \quad n = 0, 1, 2, \dots \Rightarrow e^A = U^\dagger e^{U A U^\dagger} U , \quad (3.13)$$

where A is an operator, Eq. (3.12) is easily rewritten to

$$O(t) = \tilde{U}^\dagger e^{i\tilde{H}t} \tilde{O} e^{-i\tilde{H}t} \tilde{U} , \quad (3.14)$$

where again the tilde denotes operator at $B = \infty$. It is convenient to commute the left exponential with the \tilde{O} operator and to combine it afterwards with the right exponential. To do so we first have to take a closer look at the structure of a transformed operator. We split it up in a linear combination of specific operations T_a :

$$O(B = \infty) = \sum_a t_a(O) T_a , \quad (3.15)$$

where the coefficients $t_a(O)$ are numbers that depend on the operator O . The operations T_a are chosen such that

$$[H(B = \infty), T_a] = \Omega_a T_a , \quad (3.16)$$

where Ω_a is a number. Ω_a is interpreted as the energy transfer by the operation T_a . Since $H(B = \infty)$ is a diagonal operator such a decomposition is always possible. Typical choices for T_a are single operators like c_p or operator products like $c_p^\dagger c_q^\dagger c_r c_s$.

If the relation

$$[A, B] = BD \Leftrightarrow AB = B(A + D) \quad (3.17)$$

is fulfilled for the operators A, B, D then immediately follows

$$A^n B = B(A + D)^n , \quad n = 0, 1, 2, \dots \Rightarrow e^A B = B e^{A+D} . \quad (3.18)$$

Using the definitions (3.15) and (3.16) we rewrite Eq. (3.14) to

$$\begin{aligned} O(t) &= \sum_a t_a(O) \tilde{U}^\dagger e^{i\tilde{H}t} T_a e^{-i\tilde{H}t} \tilde{U} \stackrel{(3.18)}{=} \sum_a t_a(O) \tilde{U}^\dagger T_a e^{i(\tilde{H}+\Omega_a)t} e^{-i\tilde{H}t} \tilde{U} \\ &= \tilde{U}^\dagger \left(\sum_a t_a(O) e^{i\Omega_a t} T_a \right) \tilde{U}. \end{aligned} \quad (3.19)$$

Note that we combined the operator-valued exponentials since their arguments commute. Both the ground state expectation value (3.6) and thermal averages (3.10) of Eq. (3.19) are easily evaluated within the flow equation framework.

Again a perturbative truncation of the flow equations might lead to an uncontrolled error since the eigenenergies are only known up to some power of the expansion parameter. For very long timescales ($t \rightarrow \infty$) any small error $\Delta\Omega_a$ might become important since $|\Delta\Omega_a t|$ is not limited from above.

In the following two sections we derive some simple and handy expressions for general correlation functions both at zero and nonzero temperature.

3.2.5 Zero Temperature Correlation Functions

We start with the zero temperature correlation function of two Operators O_1, O_2 :

$$C_{\text{gs}}(t_1, t_2) = \langle 0 | O_1(t_1) O_2(t_2) | 0 \rangle. \quad (3.20)$$

Again we denoted the groundstate by $|0\rangle$. Since we study time independent Hamiltonians, the correlation function depends on the time difference $\tau = t_1 - t_2$ only (see also Eq. (3.22)). Using Eq. (3.19) we find

$$C_{\text{gs}}(t_1, t_2) = \sum_{a_1, a_2} t_{a_1}(O_1) t_{a_2}(O_2) e^{i\Omega_{a_1} t_1} e^{i\Omega_{a_2} t_2} \langle 0 | \tilde{U}^\dagger T_{a_1} T_{a_2} \tilde{U} | 0 \rangle. \quad (3.21)$$

Note that $\tilde{U}|0\rangle$ is the groundstate in the diagonal basis. Since Ω_a measures by definition (3.16) the energy transfer for the operation T_a , terms with $\Omega_{a_1} \neq -\Omega_{a_2}$ vanish:

$$C_{\text{gs}}(t_1, t_2) = \sum_{a_1, a_2} t_{a_1}(O_1) t_{a_2}(O_2) e^{-i\Omega_{a_2}(t_1-t_2)} \langle 0 | \tilde{U}^\dagger T_{a_1} T_{a_2} \tilde{U} | 0 \rangle. \quad (3.22)$$

We are mainly interested in the spin-spin correlation function where $O_1 = O_2 = O$, e.g. $O = S^z$. The symmetrized correlation function is given by

$$\begin{aligned} C_{\text{gs}}^{(\text{sym})}(\tau) &= \frac{1}{2} \langle \{O(\tau), O(0)\} \rangle \\ &= \sum_{a_1, a_2} t_{a_1}(O) t_{a_2}(O) \cos(\Omega_{a_2} \tau) \langle 0 | \tilde{U}^\dagger T_{a_1} T_{a_2} \tilde{U} | 0 \rangle, \end{aligned} \quad (3.23)$$

where we used the time difference $\tau = t_1 - t_2$ for convenience. Fourier transform yields

$$\begin{aligned} C_{\text{gs}}^{(\text{sym})}(\omega) &= \int d\tau e^{i\omega\tau} C_{\text{gs}}^{(\text{sym})}(\tau) \\ &= \pi \sum_{a_1, a_2} t_{a_1}(O) t_{a_2}(O) \langle 0 | \tilde{U}^\dagger T_{a_1} T_{a_2} \tilde{U} | 0 \rangle (\delta(\omega - \Omega_{a_2}) + \delta(\omega + \Omega_{a_2})) . \end{aligned} \quad (3.24)$$

The response function is defined by

$$R_{\text{gs}}(\tau) = -i\Theta(\tau) \langle \{O(\tau), O(0)\} \rangle . \quad (3.25)$$

For the Fourier transform of the imaginary part one finds

$$\Im(R_{\text{gs}}(\omega)) = \pi \sum_{a_1, a_2} t_{a_1}(O) t_{a_2}(O) \langle 0 | \tilde{U}^\dagger T_{a_1} T_{a_2} \tilde{U} | 0 \rangle (\delta(\omega - \Omega_{a_2}) - \delta(\omega + \Omega_{a_2})) . \quad (3.26)$$

3.2.6 Nonzero Temperature Correlation Functions

The nonzero temperature correlation function is defined as

$$C_\beta(t_1, t_2) = \frac{1}{Z(\beta)} \text{Tr}(\rho(\beta) O_1(t_1) O_2(t_2)) . \quad (3.27)$$

From Eqs. (3.10) and (3.19) immediately follows

$$C_\beta(t_1, t_2) = \frac{1}{Z(\beta)} \sum_n \sum_{a_1, a_2} t_{a_1}(O_1) t_{a_2}(O_2) e^{-\beta E_n} e^{i\Omega_{a_1} t_1} e^{i\Omega_{a_2} t_2} \langle n | T_{a_1} T_{a_2} | n \rangle , \quad (3.28)$$

where the partition function is given by (3.11). The summation runs over all eigenstates of the diagonal Hamiltonian (labeled by n). The Fourier transform of the symmetrized correlation function in the special case $O_1 = O_2 = O$ is easily derived:

$$C_\beta^{(\text{sym})}(\omega) = \frac{\pi}{Z(\beta)} \sum_n \sum_{a_1, a_2} t_{a_1}(O) t_{a_2}(O) e^{-\beta E_n} \langle n | T_{a_1} T_{a_2} | n \rangle (\delta(\omega - \Omega_{a_2}) + \delta(\omega + \Omega_{a_2})) . \quad (3.29)$$

For the imaginary part of the response function (Fourier transformed) one finds

$$\Im(R_\beta^{(\text{sym})}(\omega)) = \frac{\pi}{Z(\beta)} \sum_n \sum_{a_1, a_2} t_{a_1}(O) t_{a_2}(O) e^{-\beta E_n} \langle n | T_{a_1} T_{a_2} | n \rangle (\delta(\omega - \Omega_{a_2}) - \delta(\omega + \Omega_{a_2})) . \quad (3.30)$$

3.3 Spin Operator

In this section we transform the spin operator into the diagonal basis of the Hamiltonian. We use the expressions derived above to derive the spin-spin correlation function and the corresponding response function. The outline of this section is as follows. In Sect. 3.3.1 we in detail derive and analyze the transformation of the S^z -operator. The zero temperature equilibrium magnetization is derived in Sect. 3.3.2, the spin-spin correlation function is derived in Sect. 3.3.3. In Sect. 3.3.4 we depict the results for the transformation of $S^{x/y}$ and the corresponding spin-spin correlation function and the response function.

3.3.1 Transformation of S^z

We make the following ansatz for S^z :

$$\begin{aligned} S^z(B) &= h^z(B)S^z + \frac{M(B)}{2} + \sum_{p,q} \gamma_{pq}(B) (: f_{p\uparrow}^\dagger f_{q\downarrow} : S^- + : f_{q\downarrow}^\dagger f_{p\uparrow} : S^+) \quad (3.31) \\ &\stackrel{\text{def}}{=} h^z(B)S^z + \frac{M(B)}{2} + S^\perp, \end{aligned}$$

where $h^z(B=0) = 1$, $\gamma_{pq}(B=0) = 0$ and $M(B=0) = 0$. For the transformation of the spin operator it is sufficient to use only the 1-loop generator (2.10), the commutators are given in Appendix C.3. In this order the decay of the operator ($h^z(\infty) = 0$) is given by

$$\frac{dh^z}{dB} = - \sum_{p,q} (n_f(p) + n_f(q) - 2n_f(p)n_f(q)) (\epsilon_p - \epsilon_q + h) J_\perp(p, q)(B) \gamma_{pq}(B). \quad (3.32)$$

For the flow of the newly generated number we find

$$\frac{dM}{dB} = \sum_{p,q} (n_f(p) - n_f(q)) (\epsilon_p - \epsilon_q + h) J_\perp(p, q)(B) \gamma_{pq}(B). \quad (3.33)$$

For zero magnetic field the relations $J_\perp(p, q) = J_\perp(q, p)$ and $\gamma_{pq} = -\gamma_{qp}$ are fulfilled. Using these relations one easily shows $M(B) \equiv 0$. The number M becomes only nonzero during the flow if a magnetic field is applied.

The flow of the newly generated operators is given by

$$\begin{aligned} \frac{d\gamma_{pq}}{dB} &= \frac{h^z}{2} (\epsilon_p - \epsilon_q + h) J_\perp(p, q)(B) + \frac{1}{4} \sum_r (1 - 2n_f(r)) \times \quad (3.34) \\ &\quad \times ((\epsilon_r - \epsilon_p) J^\uparrow(p, r)(B) \gamma_{rq}(B) + (\epsilon_r - \epsilon_q) J^\downarrow(r, q)(B) \gamma_{pr}(B)). \end{aligned}$$

In the following discussion we show $h^z(B = \infty) = 0$ corresponding to a full decay of the spin operator. If the spin operator would not fully decay we would have to include it in the calculation of the spin-spin correlation function yielding a zero frequency delta peak. The physical interpretation of a zero frequency delta peak is as follows: assume

we prepared the dot level in (e.g.) the spin-up configuration. At zero magnetic field this spin configuration must fully decay (in the Kondo model). A zero frequency delta peak in the spin-spin correlation indicates that the prepared spin configuration does not fully decay even on infinite timescales yielding a wrong description of the physical model. At nonzero magnetic field the prepared spin configuration does not fully decay since the magnetization of the dot is nonzero. It is therefore far from obvious that h^z has to decay to zero for $B \rightarrow \infty$ at nonzero magnetic field. Note that it is impossible to show the full decay of the spin operator by numerically solving the flow equations, since one would have to integrate up to $B = \infty$. In the following we assume $V = T = 0$, the generalization to $V, T \neq 0$ is trivial, see also Ref. [41]. For $B \ll h^{-2}$ the flow of h^z is given by

$$\frac{dh^z}{dB} = -\frac{g_{\perp}^2}{4B} = -\frac{1}{2} \frac{dg_{\parallel}}{dB}. \quad (3.35)$$

This yields only a small change of h^z proportional to $(g_{\perp}(B=0) - g_{\perp}(B))$. Note that $h^z = \mathcal{O}(1)$ and $g_{\perp}(B) \ll 1$. To derive Eq. (3.35) we used

$$\begin{aligned} J_{\perp}(p, q) &= g_{\perp} e^{-B(\epsilon_p - \epsilon_q + h)^2} \\ \gamma_{pq} &= \frac{1}{2} \frac{g_{\perp}}{\epsilon_p - \epsilon_q + h} \left(1 - e^{-B(\epsilon_p - \epsilon_q + h)^2}\right). \end{aligned} \quad (3.36)$$

The latter expression for γ_{pq} follows directly from the first order term in Eq. (3.34) assuming $h^z \approx 1$. For $B \gg h^{-2}$ we have to use an improved description for γ_{pq} , since h^z begins to decay. In lowest order we find

$$\gamma_{pq} = \frac{1}{2} (\epsilon_p - \epsilon_q + h) \int_0^B dB_1 h^z(B_1) J_{\perp}(p, q, B_1). \quad (3.37)$$

Inserting this result in the flow equation for h^z (3.32) yields

$$\begin{aligned} \frac{dh^z}{dB} &= -\frac{1}{2} \sum_{p,q} (n_f(p) + n_f(q) - 2n_f(p)n_f(q)) (\epsilon_p - \epsilon_q + h)^2 J_{\perp}(p, q, B) \times \\ &\quad \times \int_0^B dB_1 h^z(B_1) J_{\perp}(p, q, B_1) \\ &= -\frac{1}{2} g_{\perp}(B) \int_0^B dB_1 h^z(B_1) g_{\perp}(B_1) \sum_{r,s} (n_f(r) + n_f(s) - 2n_f(r)n_f(s)) \times \\ &\quad \times (\epsilon_r - \epsilon_s + h)^2 e^{-(B+B_1)(\epsilon_r - \epsilon_s + h)^2} \\ &= -h \frac{\sqrt{\pi}}{4} g_{\perp}(B) \int_0^B dB_1 h^z(B_1) g_{\perp}(B_1) (B + B_1)^{-3/2} \\ &\approx -(2 - \sqrt{2}) \frac{\sqrt{\pi}}{4} h B^{-3/2} g_{\perp}(B) \int_0^B dB_1 h^z(B_1) g_{\perp}(B_1). \end{aligned} \quad (3.38)$$

Note the similarity with the 2-loop flow equation for g_{\parallel} (2.86). With Eq. (2.88) follows:

$$h^z(B) \approx \frac{1}{\left(1 + \Gamma_{\perp} \left(\sqrt{B} - \sqrt{B_0}\right)\right)^{\sqrt{2}}}, \quad (3.39)$$

where B_0 is the flow parameter at the decoherence scale. The decay of the spin operator S^z sets in on the same energy scale as the decay of g_{\parallel} , also for nonzero voltage bias or nonzero temperature. Upon analyzing the flow equations for the S^x - and the S^y -operator given in Sect. 3.3.4 we find that their decay sets in on the same energy scale as the decay of g_{\perp} .

It is this observation that relates the decoherence rates Γ_{\parallel} and Γ_{\perp} to the spin relaxation rates. Though one typically defines the spin relaxations rates $1/T_1$ and $1/T_2$ by the broadening of the resonance poles in the longitudinal and the transverse dynamical spin susceptibilities [45], there is no need to explicitly calculate these expressions. This is due to the intrinsic energy scale separation of the flow equation method. For $B \sim \Gamma_{\parallel/\perp}^{-2}$ all excitations with energy transfer much larger than the decoherence rate are integrated out. Since the spin operator does not decay on this high energy scales, these scales cannot contribute to the broadening of the resonance pole. They “see” unbroadened resonance poles. Only energy scales on which the spin operator decays can contribute to a broadening of the resonance poles. The width of the broadening of the resonance poles is therefore (up to an uninteresting prefactor) automatically given by the decoherence rates defined in Chap. 2.

Note that Eq. (3.39) only holds for $h^z > 0$. If B becomes sufficiently large h^z does not directly decay to zero but instead performs an oscillation around zero unless g_{\perp} is zero. From Eq. (3.38) follows that the flow of h^z stops if g_{\perp} is zero, it does not stop if h^z is zero since the integral is nonzero.

To estimate errors due to the perturbative truncation of the flow equation transformation we study the sumrule

$$\langle (S^z(B))^2 \rangle \stackrel{!}{=} \frac{1}{4}. \quad (3.40)$$

From the ansatz for the spin operator (3.31) directly follows

$$\begin{aligned} \langle (S^z(B))^2 \rangle &= \left\langle \left(h^z S^z + \sum_{p,q} \gamma_{pq} (: f_{p\uparrow}^{\dagger} f_{q\downarrow} : S^{-} + : f_{q\downarrow}^{\dagger} f_{p\uparrow} : S^{+}) + \frac{M}{2} \right) \times \right. \\ &\quad \left. \times \left(h^z S^z + \sum_{r,s} \gamma_{rs} (: f_{r\uparrow}^{\dagger} f_{s\downarrow} : S^{-} + : f_{s\downarrow}^{\dagger} f_{r\uparrow} : S^{+}) + \frac{M}{2} \right) \right\rangle \\ &= \frac{(h^z)^2 + M^2}{4} + M h^z \langle S^z \rangle - \\ &\quad - \sum_{p,q} (n_f(p)(1 - n_f(q)) - n_f(q)(1 - n_f(p))) \gamma_{pq}^2 \langle S^z \rangle + \\ &\quad + \frac{1}{2} \sum_{p,q} (n_f(p)(1 - n_f(q)) + n_f(q)(1 - n_f(p))) \gamma_{pq}^2. \end{aligned} \quad (3.41)$$

In the limit $h \rightarrow +\infty$ the spin expectation value is given by $\langle S^z \rangle = +1/2$ yielding

$$\langle (S^z(B))^2 \rangle = \frac{(h^z + M)^2}{4} + \sum_{p,q} n_f(q)(1 - n_f(p))\gamma_{pq}^2. \quad (3.42)$$

At $B = 0$ the sumrule is obviously fulfilled. To study deviations from the sumrule we look at the derivative:

$$\begin{aligned} \frac{d\langle (S^z(B))^2 \rangle}{dB} &= \frac{h^z + M}{2} \left(\frac{dh^z}{dB} + \frac{dM}{dB} \right) + 2 \sum_{p,q} n_f(q)(1 - n_f(p))\gamma_{pq} \frac{d\gamma_{pq}}{dB} \\ &= -M \sum_{p,q} n_f(q)(1 - n_f(p))(\epsilon_p - \epsilon_q + h)J_{\perp}(p, q)\gamma_{p,q} + \mathcal{O}(J^3). \end{aligned} \quad (3.43)$$

One easily shows that $M(B) \approx 0$ for $B \ll h^{-2}$. As we show in the following section the sum in the last equation is zero for $B \gg h^{-2}$. In the limit of a high magnetic field the error is therefore of $\mathcal{O}(J^3)$ thereby providing a stable perturbative expansion of the spin operators transformation. By an analogue argumentation one finds similar results for nonzero voltage bias / temperature, see also Ref. [41].

3.3.2 Magnetization

The magnetization of the dot spin is given by $M(B = \infty)$ which follows directly from the ansatz (3.31). However, as we already discussed above the S^z operator decays only slowly with B and therefore also the magnetization converges slowly, making an analytical analysis difficult. Nevertheless, by using a mathematical trick (telescoping series) one easily rederives the equilibrium zero temperature Bethe Ansatz result in leading logarithmic order. The magnetization is given by

$$\begin{aligned} 2\langle S^z \rangle &= 2h^z(B = \infty)\langle 0|\tilde{U}^\dagger S^z \tilde{U}|0\rangle + M(B = \infty) \\ &= h^z(B = \infty)\text{sgn}(h(B = \infty)) + M(B = \infty), \end{aligned} \quad (3.44)$$

where $\tilde{U}|0\rangle$ is the ground state of $H_0(B = \infty)$. Note that $h^z(\infty) = 0$ as shown in the previous section. For convenience we assume $h > 0$ in the following. We rewrite Eq. (3.44) to the form

$$\begin{aligned} 2\langle S^z \rangle &= h^z(0) + M(0) + \int_0^\infty dB \frac{d(h^z(B) + M(B))}{dB} \\ &= 1 - 2 \int_0^\infty dB \sum_{pq} n_f(q)(1 - n_f(p))(\epsilon_p - \epsilon_q + h)J_{\perp}(p, q)(B)\gamma_{pq}(B). \end{aligned} \quad (3.45)$$

Using the parametrization

$$\begin{aligned} J_{\perp}(p, q) &\approx g_{\perp} e^{-B(\epsilon_p - \epsilon_q + h)^2} \\ \gamma_{pq} &\approx \frac{g_{\perp}}{2(\epsilon_p - \epsilon_q + h)} \left(1 - e^{-B(\epsilon_p - \epsilon_q + h)^2} \right) \end{aligned} \quad (3.46)$$

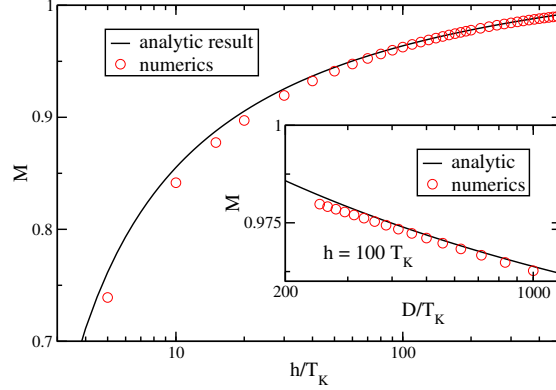


Figure 3.1: Comparison magnetization from Eq. (3.51) with numerical results for $D = 10^3 T_K$. The inset shows the bandwidth dependence of the magnetization at $h = 100 T_K$.

we find

$$2\langle S^z \rangle \approx 1 - \int_{D^{-2}}^{\infty} dB \frac{g_{\perp}^2(B)}{4B} f(B), \quad (3.47)$$

where the function $f(B)$ is given by

$$f(B) = -2h\sqrt{\pi}\sqrt{B} + h\sqrt{2\pi}\sqrt{B} + 2h\sqrt{\pi}\sqrt{B}\text{Berf}(\sqrt{B}h) + 2e^{-Bh^2} - h\sqrt{2\pi}\sqrt{B}\text{Berf}(\sqrt{2B}h) - e^{-2Bh^2}. \quad (3.48)$$

Expansion in the usual limits yields

$$f(B) = \begin{cases} 1 & , \text{ for } B \ll h^{-2} \\ 0 & , \text{ for } B \gg h^{-2} \end{cases}. \quad (3.49)$$

Neglecting higher order corrections we find

$$2\langle S^z \rangle \approx 1 - \int_{D^{-2}}^{h^{-2}} dB \frac{g_{\perp}^2(B)}{4B} \quad (3.50)$$

and with $dg_{\parallel}(B)/dB = g_{\perp}^2(B)/(2B)$ we find

$$2\langle S^z \rangle \approx 1 - \frac{1}{2\ln(h/T_K)} + \frac{1}{2\ln(D/T_K)}, \quad (3.51)$$

which in the scaling limit $D/T_K \rightarrow \infty$ is to leading logarithmic order the asymptotic Bethe Ansatz result [75]. Fig. 3.1 shows the excellent agreement between the analytical expression and numerical results for high magnetic fields. For fields of $\mathcal{O}(10 T_K)$ we see deviations from the analytical result due to the perturbative nature of our approach. The inset shows the bandwidth dependence of the magnetization in good agreement with Eq. (3.51). An analytic calculation of the magnetization for $T, V > 0$ is difficult, since the exact flow of the running couplings is unknown. We present numerical results in Sect. 3.5.3.

3.3.3 Spin-Spin Correlation Function

The symmetrized correlation function is defined as $C(t_1, t_2) = \frac{1}{2}\langle\{O(t_1), O(t_2)\}\rangle$ and the response function as $\chi(t_1, t_2) = -i\Theta(t_1 - t_2)\langle[O(t_1), O(t_2)]\rangle$. In the following we derive the spin-spin correlation function in the spirit of Sect. 3.2. We start with the energy transfer, both the number M and the spin operator S^z commute with $H(B = \infty)$:

$$\Omega_z = \Omega_M = 0 . \quad (3.52)$$

Note that we neglect higher order corrections from the energy diagonal K -terms that still remain in the Hamiltonian at $B = \infty$. From

$$\begin{aligned} [H_0, \gamma_{pq}(: f_{p\uparrow}^\dagger f_{q\downarrow} : S^- + : f_{q\downarrow}^\dagger f_{p\uparrow} : S^+)] &= (\epsilon_p - \epsilon_q + h)\gamma_{pq} : f_{p\uparrow}^\dagger f_{q\downarrow} : S^- - \\ &\quad - (\epsilon_p - \epsilon_q + h)\gamma_{pq} : f_{q\downarrow}^\dagger f_{p\uparrow} : S^+ \end{aligned} \quad (3.53)$$

directly follows the energy transfer for γ_{pq} :

$$\begin{aligned} \Omega_{\gamma_{pq}^-} &= (\epsilon_p - \epsilon_q + h) \\ \Omega_{\gamma_{pq}^+} &= -(\epsilon_p - \epsilon_q + h) . \end{aligned} \quad (3.54)$$

To calculate the correlation function we also need to consider expectation values of the spin operator and of products of spin operators. One easily shows:

$$\begin{aligned} \langle S^- S^+ \rangle &= -\langle S^z \rangle + \frac{1}{2} \\ \langle S^+ S^- \rangle &= \langle S^z \rangle + \frac{1}{2} . \end{aligned} \quad (3.55)$$

The expectation value of S^z in the diagonal basis is given by

$$\langle S^z \rangle = \langle 0|U^\dagger(B = \infty)S^z(B = 0)U(B = \infty)|0\rangle = \frac{1}{2}\text{sgn}(h) = \frac{1}{2} \begin{cases} +1, & h > 0 \\ 0, & h = 0 \\ -1, & h < 0 \end{cases} , \quad (3.56)$$

where $U(B = \infty)|0\rangle$ is the ground state of the diagonal Hamiltonian. Since we use the eigenstates of the non-interacting system as reference states the spin is always decoupled from the lead(s) and there is no energy dissipation between the subsystems. In the non-interacting system therefore only the conduction band electrons “see” the temperature, the spin temperature is always zero. So there is no need to do thermal averaging for the spin expectation value. Inserting the relations above in the general expression for the zero temperature spin-spin correlation function (3.24) yields:

$$\begin{aligned} C^z(\omega) &= \pi \left(\sum_{p,q,r,s} \gamma_{pq}\gamma_{rs} (\langle 0|U^\dagger(B = \infty) : f_{p\uparrow}^\dagger f_{q\downarrow} : f_{s\downarrow}^\dagger f_{r\uparrow} : S^- S^+ U(B = \infty)|0\rangle \times \right. \\ &\quad \times (\delta(\omega + (\epsilon_r - \epsilon_s + h)) + \delta(\omega - (\epsilon_r - \epsilon_s + h))) + \\ &\quad \langle 0|U^\dagger(B = \infty) : f_{q\downarrow}^\dagger f_{p\uparrow} : f_{r\uparrow}^\dagger f_{s\downarrow} : S^+ S^- U^\dagger(B = \infty)|0\rangle \times \\ &\quad \times (\delta(\omega - (\epsilon_r - \epsilon_s + h)) + \delta(\omega + (\epsilon_r - \epsilon_s + h)))) + \\ &\quad \left. + \frac{1}{2}M^2\delta(\omega) \right) . \end{aligned} \quad (3.57)$$

From the products of normal ordered fermionic operators only the number survives. Doing a similar calculation at nonzero temperature the spin-spin correlation function is given by a single expression for all cases:¹

$$\begin{aligned}
C^z(\omega) = & \frac{\pi(1 - \text{sgn}(\tilde{h}))}{2} \sum_p \left(\tilde{\gamma}_{\epsilon_p, \epsilon_p + \omega + \tilde{h}}^2 n_f(\epsilon_p)(1 - n_f(\epsilon_p + \omega + \tilde{h})) + \right. \\
& \left. + \tilde{\gamma}_{\epsilon_p, \epsilon_p - \omega + \tilde{h}}^2 n_f(\epsilon_p)(1 - n_f(\epsilon_p - \omega + \tilde{h})) \right) + \\
& + \frac{\pi(1 + \text{sgn}(\tilde{h}))}{2} \sum_p \left(\tilde{\gamma}_{\epsilon_p, \epsilon_p + \omega + \tilde{h}}^2 n_f(\epsilon_p + \omega + \tilde{h})(1 - n_f(\epsilon_p)) + \right. \\
& \left. + \tilde{\gamma}_{\epsilon_p, \epsilon_p - \omega + \tilde{h}}^2 n_f(\epsilon_p - \omega + \tilde{h})(1 - n_f(\epsilon_p)) \right) \\
& + \frac{\pi}{2} \tilde{M}^2 \delta(\omega) .
\end{aligned} \tag{3.58}$$

Here again the tilde denotes function at $B = \infty$. The corresponding imaginary part of the Fourier transformed response function is given by

$$\begin{aligned}
\chi''(\omega) = & \frac{\pi(1 - \text{sgn}(\tilde{h}))}{2} \sum_p \left(\tilde{\gamma}_{\epsilon_p, \epsilon_p + \omega + \tilde{h}}^2 n_f(\epsilon_p)(1 - n_f(\epsilon_p + \omega + \tilde{h})) - \right. \\
& \left. - \tilde{\gamma}_{\epsilon_p, \epsilon_p - \omega + \tilde{h}}^2 n_f(\epsilon_p)(1 - n_f(\epsilon_p - \omega + \tilde{h})) \right) \\
& + \frac{\pi(1 + \text{sgn}(\tilde{h}))}{2} \sum_p \left(\tilde{\gamma}_{\epsilon_p, \epsilon_p + \omega + \tilde{h}}^2 n_f(\epsilon_p + \omega + \tilde{h})(1 - n_f(\epsilon_p)) - \right. \\
& \left. - \tilde{\gamma}_{\epsilon_p, \epsilon_p - \omega + \tilde{h}}^2 n_f(\epsilon_p - \omega + \tilde{h})(1 - n_f(\epsilon_p)) \right) ,
\end{aligned} \tag{3.59}$$

the real part is accessible via a Kramers-Kronig transformation. The spin-spin correlation function is a symmetric function of ω , the imaginary part of the response function is antisymmetric. Both functions do not depend on the sign of h . In equilibrium the fluctuation dissipation theorem [76] relates the imaginary part of the response function and the spin-spin correlation function by $\chi''(\omega) = \tanh(\omega/(2T))C^z(\omega)$. In non-equilibrium the fluctuation dissipation theorem is violated in general. For completeness we show the transformation of $S^{x/y}$ and the corresponding expressions for the spin-spin correlation function and the response function in the following section.

Typical curves for the equilibrium zero temperature spin-spin correlation functions are shown in Fig. 3.2. We find a zero frequency δ -peak weighted with $M^2(B = \infty)\pi/2$ in the correlation function (3.58). It is not plotted for obvious reasons. For convenience we assume $h > 0$ in the following discussion. We find a power law behavior for the maxima of the sharp asymmetric features at $|\omega| \sim h$. For $|\omega| \lesssim h^*$ the correlation function vanishes, for $|\omega| \gg h$ we find $C^z(\omega) \sim |\omega|^{-1}/(\ln(|\omega|/T_K))^2$. See Appendix A.2.1 for additional information on the numerical evaluation.

¹We assume that the reference state in non-equilibrium is given by the non-interacting preparation state of the system, see Sect. 3.2.3 for more details.

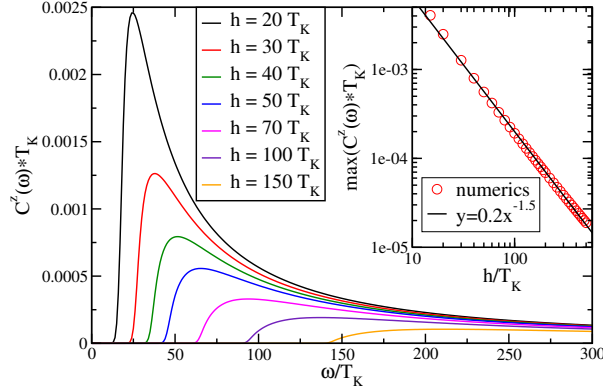


Figure 3.2: S^z correlation function for various magnetic fields ($V=T=0$). The inset shows the power law behavior of the peak height as function of the magnetic field.

3.3.4 Transformation of $S^{x/y}$

For the transformation of S^x we make the ansatz

$$\begin{aligned}
S^x(B) &= h^{xy} S^x + i \sum_{p,q} \mu^\uparrow(p,q) : f_{p\uparrow}^\dagger f_{q\uparrow} : S^y + i \sum_{p,q} \mu^\downarrow(p,q) : f_{p\downarrow}^\dagger f_{q\downarrow} : S^y + \\
&+ \sum_{p,q} \mu^z(p,q) (: f_{p\uparrow}^\dagger f_{q\downarrow} : + : f_{q\downarrow}^\dagger f_{p\uparrow} :) S^z \\
&\stackrel{\text{def}}{=} h^x S^x + S_\uparrow^x + S_\downarrow^x + S_z^x .
\end{aligned} \tag{3.60}$$

As expected from the rotational symmetry (z-axis) of the problem, the couplings in the ansatz for S^x can be recycled for the transformation of S^y . One easily shows

$$\begin{aligned}
S^y(B) &= h^{xy} S^y - i \sum_{p,q} \mu^\uparrow(p,q) : f_{p\uparrow}^\dagger f_{q\uparrow} : S^x - i \sum_{p,q} \mu^\downarrow(p,q) : f_{p\downarrow}^\dagger f_{q\downarrow} : S^x - \\
&- i \sum_{p,q} \mu^z(p,q) (: f_{p\uparrow}^\dagger f_{q\downarrow} : - : f_{q\downarrow}^\dagger f_{p\uparrow} :) S^z ,
\end{aligned} \tag{3.61}$$

in Appendix C.4 we give the relevant commutators for the transformation of S^x . For the decay of the spin operator we find:

$$\begin{aligned}
\frac{dh^{xy}}{dB} &= \frac{1}{4} \sum_{p,q} (n_f(p) + n_f(q) - 2n_f(p)n_f(q)) (\epsilon_p - \epsilon_q) (J^\uparrow(p,q) \mu_{qp}^\uparrow - J^\downarrow(p,q) \mu_{qp}^\downarrow) + \\
&+ \frac{1}{2} \sum_{p,q} (n_f(p) + n_f(q) - 2n_f(p)n_f(q)) (\epsilon_p - \epsilon_q + h) J_\perp(p,q) \mu_{pq}^z .
\end{aligned} \tag{3.62}$$

The flow of the newly generated operators is given by

$$\begin{aligned} \frac{d\mu_{pq}^\uparrow}{dB} &= \frac{h^{xy}}{2}(\epsilon_p - \epsilon_q)J^\uparrow(p, q) - \frac{1}{4} \sum_r (1 - 2n_f(r))(\epsilon_p - \epsilon_r + h)J_\perp(p, r)\mu_{qr}^z \\ &\quad + \frac{1}{4} \sum_r (1 - 2n_f(r))(\epsilon_q - \epsilon_r + h)J_\perp(q, r)\mu_{pr}^z \end{aligned} \quad (3.63)$$

for the spin up component and

$$\begin{aligned} \frac{d\mu_{pq}^\downarrow}{dB} &= -\frac{h^{xy}}{2}(\epsilon_p - \epsilon_q)J^\downarrow(p, q) - \frac{1}{4} \sum_r (1 - 2n_f(r))(\epsilon_r - \epsilon_q + h)J_\perp(r, q)\mu_{rp}^z \\ &\quad + \frac{1}{4} \sum_r (1 - 2n_f(r))(\epsilon_r - \epsilon_p + h)J_\perp(r, p)\mu_{rq}^z \end{aligned} \quad (3.64)$$

for spin down. For the spin flip component we find

$$\begin{aligned} \frac{d\mu_{pq}^z}{dB} &= -\frac{h^{xy}}{2}(\epsilon_p - \epsilon_q + h)J_\perp(p, q) - \frac{1}{4} \sum_r (1 - 2n_f(r))(\epsilon_r - \epsilon_q + h)J_\perp(r, q)\mu_{pr}^\uparrow \\ &\quad - \frac{1}{4} \sum_r (1 - 2n_f(r))(\epsilon_p - \epsilon_r + h)J_\perp(p, r)\mu_{rq}^\downarrow. \end{aligned} \quad (3.65)$$

The spin-spin correlation function for both x - and y -direction is given by the lengthy formula

$$\begin{aligned} C^\perp(\omega) &= \frac{\pi(1 + \text{sgn}(\tilde{h}))}{8} \sum_p ((\tilde{\mu}_{\epsilon_p, \epsilon_p + \omega - \tilde{h}}^\uparrow)^2 + (\tilde{\mu}_{\epsilon_p, \epsilon_p + \omega - \tilde{h}}^\downarrow)^2) n_f(\epsilon_p)(1 - n_f(\epsilon_p + \omega - \tilde{h})) \\ &\quad + \frac{\pi(1 + \text{sgn}(\tilde{h}))}{8} \sum_p ((\tilde{\mu}_{\epsilon_p, \epsilon_p - \omega - \tilde{h}}^\uparrow)^2 + (\tilde{\mu}_{\epsilon_p, \epsilon_p - \omega - \tilde{h}}^\downarrow)^2) n_f(\epsilon_p)(1 - n_f(\epsilon_p - \omega - \tilde{h})) \\ &\quad + \frac{\pi(1 - \text{sgn}(\tilde{h}))}{8} \sum_p ((\tilde{\mu}_{\epsilon_p, \epsilon_p + \omega + \tilde{h}}^\uparrow)^2 + (\tilde{\mu}_{\epsilon_p, \epsilon_p + \omega + \tilde{h}}^\downarrow)^2) n_f(\epsilon_p)(1 - n_f(\epsilon_p + \omega + \tilde{h})) \\ &\quad + \frac{\pi(1 - \text{sgn}(\tilde{h}))}{8} \sum_p ((\tilde{\mu}_{\epsilon_p, \epsilon_p - \omega + \tilde{h}}^\uparrow)^2 + (\tilde{\mu}_{\epsilon_p, \epsilon_p - \omega + \tilde{h}}^\downarrow)^2) n_f(\epsilon_p)(1 - n_f(\epsilon_p - \omega + \tilde{h})) \\ &\quad + \frac{\pi}{4} \sum_p (\tilde{\mu}_{\epsilon_p, \epsilon_p + \omega}^z)^2 (n_f(\epsilon_p)(1 - n_f(\epsilon_p + \omega)) + n_f(\epsilon_p + \omega)(1 - n_f(\epsilon_p))) \\ &\quad + \frac{\pi}{4} \sum_p (\tilde{\mu}_{\epsilon_p, \epsilon_p - \omega}^z)^2 (n_f(\epsilon_p)(1 - n_f(\epsilon_p - \omega)) + n_f(\epsilon_p - \omega)(1 - n_f(\epsilon_p))). \end{aligned} \quad (3.66)$$

For the imaginary part of the response function we find

$$\begin{aligned}
\chi''_{\perp}(\omega) &= \frac{\pi(1 + \text{sgn}(\tilde{h}))}{8} \sum_p ((\tilde{\mu}_{\epsilon_p, \epsilon_p + \omega - \tilde{h}}^{\uparrow})^2 + (\tilde{\mu}_{\epsilon_p, \epsilon_p + \omega - \tilde{h}}^{\downarrow})^2) n_f(\epsilon_p) (1 - n_f(\epsilon_p + \omega - \tilde{h})) \\
&\quad - \frac{\pi(1 + \text{sgn}(\tilde{h}))}{8} \sum_p ((\tilde{\mu}_{\epsilon_p, \epsilon_p - \omega - \tilde{h}}^{\uparrow})^2 + (\tilde{\mu}_{\epsilon_p, \epsilon_p - \omega - \tilde{h}}^{\downarrow})^2) n_f(\epsilon_p) (1 - n_f(\epsilon_p - \omega - \tilde{h})) \\
&\quad + \frac{\pi(1 - \text{sgn}(\tilde{h}))}{8} \sum_p ((\tilde{\mu}_{\epsilon_p, \epsilon_p + \omega + \tilde{h}}^{\uparrow})^2 + (\tilde{\mu}_{\epsilon_p, \epsilon_p + \omega + \tilde{h}}^{\downarrow})^2) n_f(\epsilon_p) (1 - n_f(\epsilon_p + \omega + \tilde{h})) \\
&\quad - \frac{\pi(1 - \text{sgn}(\tilde{h}))}{8} \sum_p ((\tilde{\mu}_{\epsilon_p, \epsilon_p - \omega + \tilde{h}}^{\uparrow})^2 + (\tilde{\mu}_{\epsilon_p, \epsilon_p - \omega + \tilde{h}}^{\downarrow})^2) n_f(\epsilon_p) (1 - n_f(\epsilon_p - \omega + \tilde{h})) \\
&\quad + \frac{\pi}{4} \sum_p (\tilde{\mu}_{\epsilon_p, \epsilon_p + \omega}^z)^2 (n_f(\epsilon_p) (1 - n_f(\epsilon_p + \omega)) - n_f(\epsilon_p + \omega) (1 - n_f(\epsilon_p))) \\
&\quad - \frac{\pi}{4} \sum_p (\tilde{\mu}_{\epsilon_p, \epsilon_p - \omega}^z)^2 (n_f(\epsilon_p) (1 - n_f(\epsilon_p - \omega)) - n_f(\epsilon_p - \omega) (1 - n_f(\epsilon_p))) . \quad (3.67)
\end{aligned}$$

At zero magnetic field and isotropic initial values for the running coupling the flow equations and the correlation functions for $S^{x/y}$ are equivalent to their S^z - counterparts (see Sect. 3.3.1). One easily shows that the decay of h^x is related to the decay of g_{\perp} , the calculation is analogue to the one for h^z in Sect. 3.3.1.

3.4 T-Matrix

In this section we construct the T-Matrix. The basic parts of the construction are given in Sect. 3.4.1. In Sect. 3.4.2 we derive the flow equation transformation of the involved operators, numerical results for $V = T = 0$ are presented in Sect. 3.4.3. Results for $V, T > 0$ are given in Sect. 3.5.2.

3.4.1 Construction

The imaginary part of the T-Matrix is given by [5, 9]

$$\Im(\hat{T}_{\sigma}(\omega)) = - \int_{-\infty}^{\infty} dt \Theta(t) \langle \{O_{\sigma}(t), O_{\sigma}^{\dagger}(0)\} \rangle e^{i\omega t} , \quad (3.68)$$

where

$$\begin{aligned}
O_{\uparrow}(B) &= \sum_k (U_k^{\downarrow} f_{k\downarrow} S^{-} + U_k^{\uparrow} f_{k\uparrow} S^z) = O_{\uparrow}^{\perp} + O_{\uparrow}^{\parallel} \\
O_{\downarrow}(B) &= \sum_k (V_k^{\downarrow} f_{k\uparrow} S^{+} - V_k^{\uparrow} f_{k\downarrow} S^z) = O_{\downarrow}^{\perp} + O_{\downarrow}^{\parallel}
\end{aligned} \quad (3.69)$$

and $U_k^{\perp/\uparrow}(B=0) = V_k^{\perp/\downarrow}(B=0) = J_{\perp/\parallel}/2$. The real part is simply given by $J_{\parallel}\langle S^z \rangle/2$. As for the correlation function in Sect. 3.2 the strategy is to calculate the time evolution $\exp(-iHt)$ in the diagonal basis and to simplify the expression by commuting the latter exponentials with the O_σ -operators. If the relation $[A, B] = BD$ is fulfilled for arbitrary operators A, B, D then

$$e^A B = B e^{A+D} \quad (3.70)$$

is easily derived, see Sect. 3.2.4. The energy transfers are given by:

$$[H_0, f_{p\downarrow} S^-] = -(\epsilon_p - h) f_{p\downarrow} S^- , \quad [H_0, f_{p\uparrow} S^z] = -\epsilon_p f_{p\uparrow} S^z . \quad (3.71)$$

At zero temperature the spin up part is easily derived (implying $B = \infty$):

$$\begin{aligned} & \langle \{O_\uparrow(B = \infty, t), O_\uparrow^\dagger(B = \infty, t = 0)\} \rangle = \\ & = \langle e^{iH_0 t} O_\uparrow e^{-iH_0 t} O_\uparrow^\dagger + O_\uparrow^\dagger e^{iH_0 t} O_\uparrow e^{-iH_0 t} \rangle \\ & = \langle \sum_{p,q} \left(e^{iH_0 t} (U_p^\perp f_{p\downarrow} S^- + U_p^\uparrow f_{p\uparrow} S^z) e^{-iH_0 t} (U_q^\perp f_{q\downarrow}^\dagger S^+ + U_q^\uparrow f_{q\uparrow}^\dagger S^z) \right) + \\ & \quad + \sum_{p,q} \left((U_q^\perp f_{q\downarrow}^\dagger S^+ + U_q^\uparrow f_{q\uparrow}^\dagger S^z) e^{iH_0 t} (U_p^\perp f_{p\downarrow} S^- + U_p^\uparrow f_{p\uparrow} S^z) e^{-iH_0 t} \right) \rangle \\ & = \sum_{p,q} \langle (U_p^\perp f_{p\downarrow} S^- e^{-i(\epsilon_p - h)t} + U_p^\uparrow f_{p\uparrow} S^z e^{-i\epsilon_p t}) (U_q^\perp f_{q\downarrow}^\dagger S^+ + U_q^\uparrow f_{q\uparrow}^\dagger S^z) + \\ & \quad + (U_q^\perp f_{q\downarrow}^\dagger S^+ + U_q^\uparrow f_{q\uparrow}^\dagger S^z) (U_p^\perp f_{p\downarrow} S^- e^{-i(\epsilon_p - h)t} + U_p^\uparrow f_{p\uparrow} S^z e^{-i\epsilon_p t}) \rangle \\ & = \sum_p \left((U_p^\perp)^2 e^{-i(\epsilon_p - h)t} (1 - n_f(p)) \langle S^- S^+ \rangle + \frac{1}{4} (U_p^\uparrow)^2 e^{-i\epsilon_p t} (1 - n_f(p)) + \right. \\ & \quad \left. + (U_p^\perp)^2 e^{-i(\epsilon_p - h)t} n_f(p) \langle S^+ S^- \rangle + \frac{1}{4} (U_p^\uparrow)^2 e^{-i\epsilon_p t} n_f(p) \right) \\ & = \frac{1}{4} \sum_p (U_p^\uparrow)^2 e^{-i\epsilon_p t} + \frac{1}{2} \sum_p (U_p^\perp)^2 e^{-i(\epsilon_p - h)t} (1 + 2\langle S^z \rangle (2n_f(p) - 1)) . \quad (3.72) \end{aligned}$$

Again the calculation for nonzero temperature leads to the same result. Doing an analogue calculation for the spin down part we find

$$\begin{aligned} & \langle \{O_\downarrow(B = \infty, t), O_\downarrow^\dagger(B = \infty, t = 0)\} \rangle = \quad (3.73) \\ & = \frac{1}{4} \sum_p (V_p^\downarrow)^2 e^{-i\epsilon_p t} + \frac{1}{2} \sum_p (V_p^\perp)^2 e^{-i(\epsilon_p + h)t} (1 - 2\langle S^z \rangle (2n_f(p) - 1)) , \end{aligned}$$

where we used

$$[H_0, f_{p\uparrow} S^+] = -(\epsilon_p + h) f_{p\uparrow} S^+ , \quad [H_0, f_{p\downarrow} S^z] = -\epsilon_p f_{p\downarrow} S^z . \quad (3.74)$$

Fourier transform of Eqs. (3.72) and (3.73) yields

$$\begin{aligned} \Im(\hat{T}_\uparrow(\omega)) & = -\frac{\pi}{4} \left((U_\omega^\uparrow)^2 + 2(U_{\omega+h}^\perp)^2 (1 + 2\langle S^z \rangle (2n_f(\omega + h) - 1)) \right) \\ \Im(\hat{T}_\downarrow(\omega)) & = -\frac{\pi}{4} \left((V_\omega^\downarrow)^2 + 2(V_{\omega-h}^\perp)^2 (1 - 2\langle S^z \rangle (2n_f(\omega - h) - 1)) \right) . \quad (3.75) \end{aligned}$$

3.4.2 Flow Equations

3.4.2.1 Lowest Order

The relevant commutators are worked given in Appendix C.5. In lowest order the flow equations for the spin up component are given by

$$\frac{dU_p^\uparrow}{dB} = -\frac{1}{2} \sum_r (1 - 2n_f(r)) (\epsilon_p - \epsilon_r + h) U_p^\perp J_\perp(r, p), \quad (3.76)$$

$$\begin{aligned} \frac{dU_p^\perp}{dB} &= -\frac{1}{4} \sum_r (1 - 2n_f(r)) (\epsilon_p - \epsilon_r + h) U_r^\uparrow J_\perp(k, p) - \\ &\quad -\frac{1}{4} \sum_r (1 - 2n_f(r)) (\epsilon_p - \epsilon_r) U_p^\perp J^\downarrow(r, p). \end{aligned} \quad (3.77)$$

Comparing these equations with Eqs. (2.18) and (2.20) one already notices the similarity between the flow of the running coupling in 1-loop order and the flow of the O_\uparrow operator. In the following discussion we work out the details. Using the same approximations as in Sect. 2.1.4 one easily shows

$$\frac{dU_p^\uparrow}{dB} = \frac{g_{\epsilon_p+h/2}^\perp U_{\epsilon_p+h}^\perp}{2B} \left(\frac{e^{-B(\epsilon_p+h+V/2)^2}}{1+R} + \frac{e^{-B(\epsilon_p+h-V/2)^2}}{1+1/R} \right). \quad (3.78)$$

Neglecting the factor two in the exponential, the latter equation is equivalent to Eq. (2.23), provided $U_p^\uparrow = g_p^\uparrow/2$ and $U_{\epsilon_p+h/2}^\perp = g_p^\perp/2$. Analyzing the flow of the spin-flip component we find

$$\begin{aligned} \frac{dU_{\epsilon_p+h/2}^\perp}{dB} &= \frac{g_p^\perp U_{\epsilon_p-h/2}^\uparrow}{4B} \left(\frac{e^{-B(\epsilon_p-h/2+V/2)^2}}{1+R} + \frac{e^{-B(\epsilon_p-h/2-V/2)^2}}{1+1/R} \right) + \\ &\quad + \frac{g_{\epsilon_p+h/2}^\downarrow U_{\epsilon_p+h/2}^\perp}{4B} \left(\frac{e^{-B(\epsilon_p+h/2+V/2)^2}}{1+R} + \frac{e^{-B(\epsilon_p+h/2-V/2)^2}}{1+1/R} \right). \end{aligned} \quad (3.79)$$

Again neglecting the factor two in the exponential, the latter equation is equivalent to the 1-loop flow equation for g_p^\perp (2.25). The higher order terms in the transformation of the operator are discussed in the following section. It turns out that they have similar effect on the flow as the 2-loop terms in the transformation of the Hamiltonian. The calculation for nonzero temperature is again more difficult, nevertheless we find the same relations between the flow of the operator and the running coupling.

Doing an analogue argumentation for the V -terms we identify

$$\begin{aligned} U_p^\uparrow(B) &= \frac{g_p^\uparrow(B)}{2}, & U_p^\perp(B) &= \frac{g_{\epsilon_p-h/2}^\perp(B)}{2}, \\ V_p^\downarrow(B) &= \frac{g_p^\downarrow(B)}{2}, & V_p^\perp(B) &= \frac{g_{\epsilon_p+h/2}^\perp(B)}{2}. \end{aligned} \quad (3.80)$$

Therefore the O_σ operators completely decays into more complicated objects for $B \rightarrow \infty$. Since the inclusion of higher terms is resource intensive (three momentum indices), it is more economic to evaluate the T-Matrix at the decoherence scale [11], where higher order terms are not yet important:

$$\text{Im}[T_\sigma(\omega)] \approx -\frac{\pi}{16} \left((\hat{g}_\omega^\sigma)^2 + 2(\hat{g}_{\omega+\sigma\hat{h}/2}^\perp)^2 \left(1 + \sigma 2\langle S^z \rangle (2\hat{n}_f(\omega + \sigma\hat{h}) - 1) \right) \right). \quad (3.81)$$

Here the hat denotes functions at the decoherence scale. Though the further flow leads to a decay of O_σ , the spectral function remains unchanged for $B > \Gamma_{\parallel/\perp}^{-2}$, where $\Gamma_{\parallel/\perp}$ is the dominant decoherence scale.

We replace the expectation value of S^z at the decoherence scale by the magnetization of the system since the S^z operator decays noticeably only for $B \gg \Gamma_{\parallel/\perp}^{-2}$. As suggested by Rosch *et al.* [11] we use Fermi functions broadened by the decoherence scale Γ_\perp to describe the distribution function for the f -operators at the decoherence scale $\hat{n}_f(\omega)$. In equilibrium at small temperature $T \ll |h|$ the distribution function is then given by $\hat{n}_f(\omega) = f_\Gamma(\omega)$, where $f_\Gamma(\omega) = 1/2 - \arctan(\omega/\Gamma_\perp)/\pi$. At high temperature $T \gg |h|$ the spin expectation value $\langle S^z \rangle$ vanishes. Then the distribution function only enters in subleading order. Note that the imaginary part of the T-Matrix in general depends only weakly on the details of the broadening scheme. In non-equilibrium the step functions at both chemical potentials have to be broadened yielding $\hat{n}_f(\omega) = f_\Gamma(\omega + V/2)/(1 + R) + f_\Gamma(\omega - V/2)/(1 + 1/R)$ for the distribution function.

The additional factor of 1/4 in comparison with the result obtained by Rosch *et al.* [11] is due to a different definition of J . For symmetric coupling ($R = 1$) and therefore also in equilibrium the spin-up and the spin-down component are related by $\text{Im}[T_\uparrow(\omega)] = \text{Im}[T_\downarrow(-\omega)]$.

3.4.2.2 Higher Orders

In the following we discuss the flow equations for the spin up component only, the argumentation for the spin down component is analogue. We use the ansatz

$$\begin{aligned} O_\uparrow(B) &= \sum_r U_r^\perp f_{r\downarrow} S^- + \sum_r U_r^\uparrow f_{r\uparrow} S^z + \\ &+ \sum_{p,q,r} U_\uparrow^-(p, q, r) : f_{p\uparrow}^\dagger f_{q\uparrow} f_{r\downarrow} : S^- + \\ &+ \sum_{p,q,r} U_\downarrow^-(p, q, r) : f_{p\downarrow}^\dagger f_{q\downarrow} f_{r\downarrow} : S^- + \\ &+ \sum_{p,q,r} U_\downarrow^z(p, q, r) : f_{q\downarrow}^\dagger f_{p\uparrow} f_{r\downarrow} : S^z + \\ &+ \sum_r V_\uparrow(r) f_{r\uparrow} + \\ &+ \sum_{p,q,r} W_\uparrow(p, q, r) (: f_{p\uparrow}^\dagger f_{q\downarrow} f_{r\uparrow} : S^- + : f_{q\downarrow}^\dagger f_{p\uparrow} f_{r\uparrow} : S^+) . \end{aligned} \quad (3.82)$$

The commutators are given in Appendix C.6, we only take terms into account that couple back in the flow of $U^{\perp/\uparrow}$. The flow equations for the new couplings are given by

$$\frac{dU_{\uparrow}^{-}(r, s, p)}{dB} = -\frac{1}{2}(\epsilon_r - \epsilon_s)J^{\uparrow}(r, s)U_p^{\perp}, \quad (3.83)$$

$$\frac{dU_{\downarrow}^{-}(r, s, p)}{dB} = \frac{1}{2}(\epsilon_r - \epsilon_s)J^{\downarrow}(r, s)U_p^{\perp}, \quad (3.84)$$

$$\frac{dW_{\uparrow}(r, s, p)}{dB} = \frac{1}{2}(\epsilon_r - \epsilon_s + h)J_{\perp}(r, s)U_p^{\uparrow}, \quad (3.85)$$

$$\begin{aligned} \frac{dV_{\uparrow}(k)}{dB} &= -\frac{1}{8}\sum_r(\epsilon_r - \epsilon_k)J^{\uparrow}(r, k)U_r^{\uparrow} \\ &\approx -\frac{1}{8}g^{\uparrow}(k)U_k^{\uparrow}\sum_r(\epsilon_r - \epsilon_k)e^{-B(\epsilon_r - \epsilon_k)^2} \\ &\approx 0, \end{aligned} \quad (3.86)$$

$$\frac{dU_{\downarrow}^z(r, s, p)}{dB} = -(\epsilon_r - \epsilon_s + h)J_{\perp}(r, s)U_p^{\perp}. \quad (3.87)$$

The flow equations for O_{\uparrow} in cubic order are given by

$$\begin{aligned} \frac{dU_p^{\uparrow}}{dB} &= \frac{1}{2}\sum_r(1 - 2n_f(r))(\epsilon_r - \epsilon_p - h)J_{\perp}(p, r)U_r^{\perp} - \\ &\quad -\frac{1}{2}\sum_r(\epsilon_r - \epsilon_p)J^{\uparrow}(r, p)V_{\uparrow}(r) - \\ &\quad -\sum_{r,s}(n_f(r) + n_f(s) - 2n_f(r)n_f(s))(\epsilon_r - \epsilon_s + h)J_{\perp}(r, s)W_{\uparrow}(r, s, p) + \\ &\quad +\frac{1}{2}\sum_{r,s}(n_f(r) + n_f(s) - 2n_f(r)n_f(s))(\epsilon_r - \epsilon_s + h)J_{\perp}(r, s)W_{\uparrow}(p, s, r) + \\ &\quad +\frac{1}{2}\sum_{r,s}(n_f(r) + n_f(s) - 2n_f(r)n_f(s))(\epsilon_r - \epsilon_s + h)J_{\perp}(r, s)U_{\uparrow}^{-}(r, p, s), \end{aligned} \quad (3.88)$$

$$\begin{aligned}
\frac{dU_p^\perp}{dB} &= \frac{1}{4} \sum_r (1 - 2n_f(r)) (\epsilon_r - \epsilon_p + h) J_\perp(r, p) U_r^\dagger + \\
&+ \frac{1}{4} \sum_r (1 - 2n_f(r)) (\epsilon_r - \epsilon_p) J^\downarrow(r, p) U_r^\perp + \\
&+ \frac{1}{4} \sum_{r,s} (n_f(r) + n_f(s) - 2n_f(r)n_f(s)) (\epsilon_r - \epsilon_s) J^\uparrow(r, s) W_\uparrow(s, p, r) + \\
&+ \frac{1}{4} \sum_{r,s} (n_f(r) + n_f(s) - 2n_f(r)n_f(s)) (\epsilon_r - \epsilon_s + h) J_\perp(r, s) U_\downarrow^z(r, s, p) - \\
&- \frac{1}{2} \sum_r (\epsilon_r - \epsilon_p + h) J_\perp(r, p) V_\uparrow(r) - \\
&- \frac{1}{4} \sum_{r,s} (n_f(r) + n_f(s) - 2n_f(r)n_f(s)) (\epsilon_r - \epsilon_s) J^\uparrow(r, s) U_\uparrow^-(s, r, p) + \\
&+ \frac{1}{4} \sum_{r,s} (n_f(r) + n_f(s) - 2n_f(r)n_f(s)) (\epsilon_r - \epsilon_s) J^\downarrow(r, s) \times \\
&\times (U_\downarrow^-(s, r, p) - U_\downarrow^-(s, p, r)) .
\end{aligned} \tag{3.89}$$

Though an analytical analysis of the latter equations is possible in principal we skip this step since it will very likely exceed even the scaling analysis for the Hamiltonian flow in Chap. 2. Nevertheless upon analytical integration of the flow equations we find terms with similar structure as the 2-loop terms in the flow of the Hamiltonian. By numerical integration one easily shows that Eq. (3.80), which relates the flow of the running coupling to the flow of the O_σ -operators, also holds for large B .

3.4.3 Results

The imaginary part of the T-Matrix and the spectral function are related by $A_\sigma(\omega) = -\text{Im}[T_\sigma(\omega + i\delta)]/\pi$. Fig. 3.3 shows spectral functions for several strengths of the magnetic field. They are strongly peaked at $\omega \sim h$. Rosch *et al.* [11] in detail studied their structure by analyzing the spectral function normalized to 1 as function of ω/h . Since we included the shift of the magnetic field we study them as a function of ω/h^* . The latter shift of the magnetic field originates from an additional field in the dot induced by the conduction band electrons corresponding to a Knight shift. In agreement with the results derived by Rosch *et al.* [11] we find that the width of the left flank is approximately proportional to the decoherence rate (2.89), leading to a sharpening of the left flank for increasing h , while the width of the right flank increases for increasing h .

The imaginary part of the T-Matrix at zero frequency is related to the magnetization via the Friedel sum rule [77–79]. Inserting the leading term of the asymptotic Bethe Ansatz result [79] one finds $\text{Im}[\hat{T}_\sigma(0)] = -\sin^2(\pi/(4 \ln(h/T_K)))/\pi$. The inset of Fig. 3.3 shows a comparison between the Bethe Ansatz and the flow equation result. Again we find excellent agreement for high magnetic fields and deviations for fields smaller than $10 T_K$.

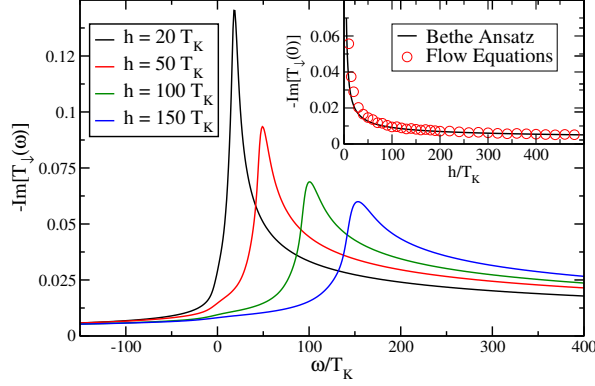


Figure 3.3: Imaginary part of spin-down T-Matrix as function of the magnetic field ($D = 10^3 T_K$). The inset shows a comparison with the asymptotic Bethe Ansatz result for $\omega = 0$.

As found by Logan and Dickens [12, 13] and Rosch *et al.* [11] the spectral function decays proportional to $1/(\ln(\omega/T_K))^2$ for high frequencies. Previous Bethe Ansatz calculations [17] found that the maximum of the spin-down spectral function is at $h^* \approx h(1 - 1/(2 \ln(h/T_K)))$, which is consistent with the shift of the magnetic field (2.84) in the scaling limit $D/T_K \rightarrow \infty$. However, our numerical results are not accurate enough to study the exact position of the maximum.

3.5 Temperature vs. Voltage Bias

In Sect. 2.2.5.2 we derived a simple (effective) scaling equation for the flow of the running coupling at nonzero temperature and $V = h = 0$ ($B \gg T^{-2}$):

$$\frac{dg}{dB} = -\frac{\sqrt{2\pi}}{4} \frac{g^3}{\sqrt{B}} T. \quad (3.90)$$

In the correspondent regime for nonzero voltage bias ($T = h = 0$, $B \gg V^{-2}$) we found the flow equation

$$\frac{dg}{dB} = -\frac{\sqrt{2\pi}}{4} \frac{g^3}{\sqrt{B}} \frac{V}{(1+R)(1+1/R)}. \quad (3.91)$$

The scaling equation are remarkably similar, it is therefore convenient to introduce an effective temperature

$$T_{\text{eff}} = \begin{cases} \frac{V}{(1+R)(1+1/R)} & , \text{ for } V > 0, T = 0 \\ T & , \text{ for } T > 0, V = 0 \end{cases}. \quad (3.92)$$

Since Eqs. (3.90) and (3.91) differ only by the effective temperature one would naively assume that also the physical properties of the impurity (dot) level can be described using this effective temperature. From an objective point of view one would not expect that the

two-level systems actually “sees” the mechanism for noise production, instead one would expect that knowing only the “amount of noise” is enough to describe the systems physical properties. In the following subsections we study this assumption in detail.

The outline of this section is as follows. In Sect. 3.5.1 we discuss the spin-spin correlation function as function of voltage bias, temperature and magnetic field. The T-Matrix is discussed in Sect. 3.5.2. The magnetization and the static spin susceptibility are discussed in Sects. 3.5.3 and 3.5.4.

3.5.1 Spin-Spin Correlation Function

3.5.1.1 Zero Magnetic Field

Typical curves for the spin-spin correlation function and the imaginary part of the dynamical spin susceptibility at zero magnetic field are shown in Fig. 3.4 for nonzero temperature (equilibrium) and in Fig. 3.5 for nonzero voltage bias (non-equilibrium). The spin-spin correlation function is a symmetric function of ω with a zero frequency peak of width $\Gamma = \Gamma_{\perp} = \Gamma_{\parallel}$. Since most of the spectral weight of the spin-spin correlation function lies within an energy interval of $\mathcal{O}(\Gamma)$ our previous interpretation of Γ as the spin relaxation or decoherence rate is confirmed. The sum rule

$$\frac{\pi}{2} = \int_{-\infty}^{\infty} d\omega C^z(\omega) \quad (3.93)$$

is not fulfilled exactly since we neglect higher order terms in the transformation of S^z , see Sect. 3.3.1. The error typically is of order one percent. The imaginary part of the dynamical spin susceptibility is an antisymmetric function of ω and has its maximum at $\chi''(\omega \approx \Gamma_{\text{rel}})$. At zero magnetic field the spin-spin correlation and response function are equivalent for x, y, z -direction. An approximate analytical solution of (3.34) yields [41]:

$$C^z(\omega) \sim \begin{cases} \frac{1}{\Gamma_{\text{rel}}} & \text{for } |\omega| \lesssim \Gamma \\ \frac{\Gamma_{\text{rel}}}{\omega^2} & \text{for } \Gamma \lesssim |\omega| \lesssim T_{\text{eff}} \\ \frac{g^2(\Lambda_{\text{feq}}=|\omega|)}{|\omega|} & \text{for } T_{\text{eff}} \lesssim |\omega| \end{cases} \quad (3.94)$$

$$\chi''(\omega) \sim \begin{cases} \frac{g^2(\Lambda_{\text{feq}}=T,V)}{\Gamma_{\text{rel}}^2} \omega & \text{for } |\omega| \lesssim \Gamma \\ \frac{g^2(\Lambda_{\text{feq}}=|\omega|)}{\omega} & \text{for } \Gamma \lesssim |\omega| . \end{cases} \quad (3.95)$$

Note that $\Lambda_{\text{feq}} = B^{-1/2}$. In Figs. 3.6 and 3.7 we show the dependency of the spin-spin correlation function and the imaginary part of the dynamical spin susceptibility on the asymmetry parameter R . In agreement with Eqs. (3.94) and (3.95) mainly the low frequency properties are affected. The effective temperature and therefore also the decoherence rate

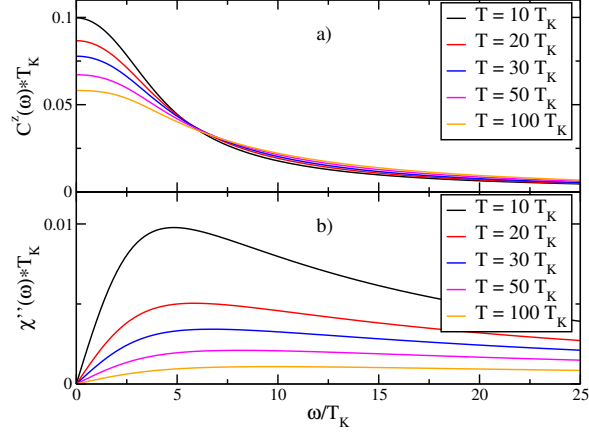


Figure 3.4: Universal curves for a) the spin-spin correlation function $C^z(\omega)$ and b) the imaginary part of the dynamical spin susceptibility $\chi''(\omega)$ at nonzero temperature and zero magnetic field.

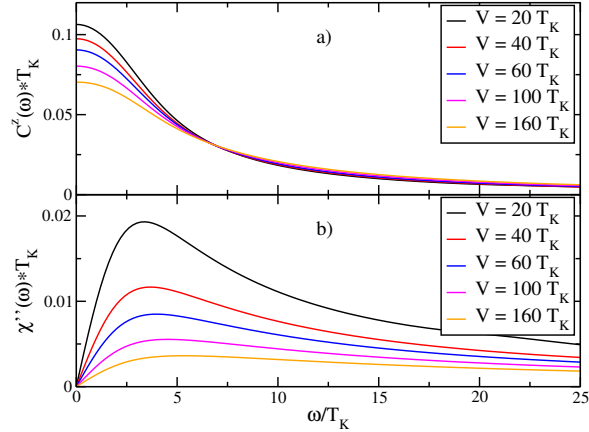


Figure 3.5: Universal curves for a) the spin-spin correlation function $C^z(\omega)$ and b) the imaginary part of the dynamical spin susceptibility $\chi''(\omega)$ in non-equilibrium for symmetric coupling $R = 1$ and zero magnetic field.

is reduced if the asymmetry parameter R is increased yielding increasing maxima of the curves for increasing asymmetry parameter. See Appendix A.2.1 for additional information on the numerical evaluation.

3.5.1.2 Nonzero Magnetic Field

In the previous section we showed that the spin-spin correlation function at zero magnetic field (V or $T \gg T_K$) shows a zero frequency peak whose width is given by the decoherence scale. In Fig. 3.8 we show the decay of the latter structure due to an applied magnetic

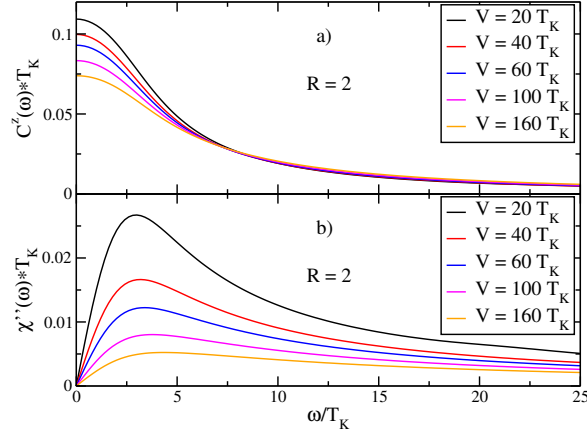


Figure 3.6: Universal curves for a) the spin-spin correlation function $C^z(\omega)$ and b) the imaginary part of the dynamical spin susceptibility $\chi''(\omega)$ in non-equilibrium for asymmetric coupling $R = 2$ and zero magnetic field.

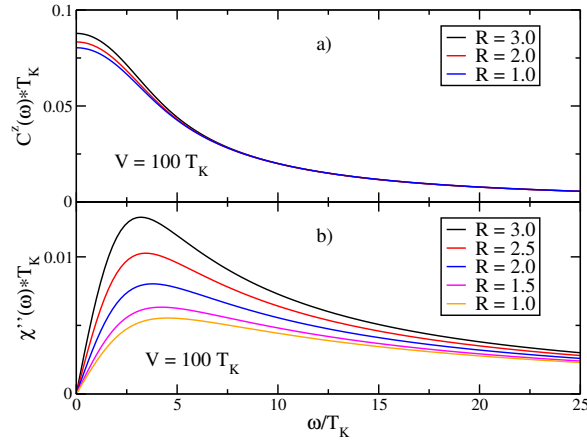


Figure 3.7: Universal curves for a) the spin-spin correlation function $C^z(\omega)$ and b) the imaginary part of the dynamical spin susceptibility $\chi''(\omega)$ in non-equilibrium for asymmetric coupling of the leads and zero magnetic field. The voltage bias is fixed at $V = 100T_K$.

field. Again the zero frequency δ -peak in Eq. (3.58) is not plotted. The sum rule

$$\frac{\pi}{2} = \int_{-\infty}^{\infty} d\omega C^z(\omega) = \tilde{M}^2 \frac{\pi}{2} + \int_{-\infty}^{\infty} d\omega C_{\gamma}^z(\omega) \quad (3.96)$$

is not fulfilled exactly since we neglect higher order terms in the transformation of S^z . The error typically is of order one percent. Here $C_{\gamma}^z(\omega)$ denotes the $\tilde{\gamma}_{pq}$ terms in Eq. (3.58).

For increasing magnetic field also the magnetization \tilde{M} increases. Since the sum rule is approximately fulfilled and $C_{\gamma}^z(\omega)$ is a non-negative function, an increase of \tilde{M} must lead to a decrease of $C_{\gamma}^z(\omega)$, leading to a decay of the correlation function for $\omega \neq 0$.

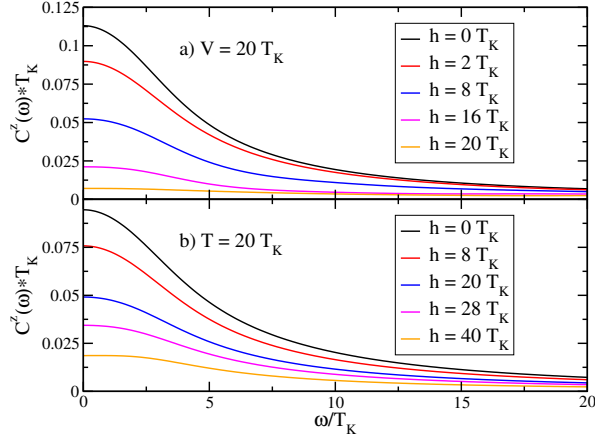


Figure 3.8: Decaying zero frequency structure of correlation function with increasing magnetic field, a) $V = 20T_K$, b) $T = 20T_K$.

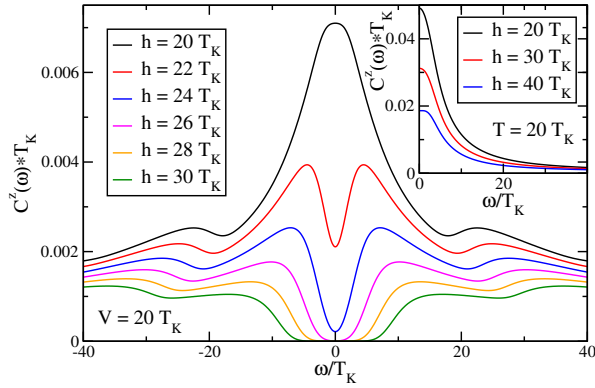


Figure 3.9: Typical buildup of the zero frequency peak in the non-equilibrium correlation function for $V \sim h$. For decreasing h the peaks at $\omega \approx h - V$ join to build up the zero frequency peak. In the regime $h \leq V$ we find a small structure at $\omega \approx h$. The inset shows typical equilibrium correlation functions for nonzero temperatures $T \sim h$. Here all structures except the zero frequency peak are smeared out.

At first glance the decay of the zero frequency structures looks similar for both the equilibrium and the non-equilibrium case. Only the relative decay of the maximum as function of V/h and T/h seems to be different. On closer inspection we find additional structures at $|\omega| \sim |h|$ for $V > |h|$. The relative height of these structures increases with the magnetic field, see Fig. 3.9. For nonzero temperature these structures are smeared out. They are only visible for $T \ll |h|$. For high frequencies we find the usual $C^z(\omega) \sim |\omega|^{-1}/(\ln(|\omega|/T_K))^2$ behavior.

In Fig. 3.10 a) we show the splitting of the h_0 structure in the correlation function due to an applied small voltage bias. The two new features are located at $|\omega| \sim |V \pm h|$. For small temperature we find a broadening of the structure (subfig. b)). See Appendix A.2.1

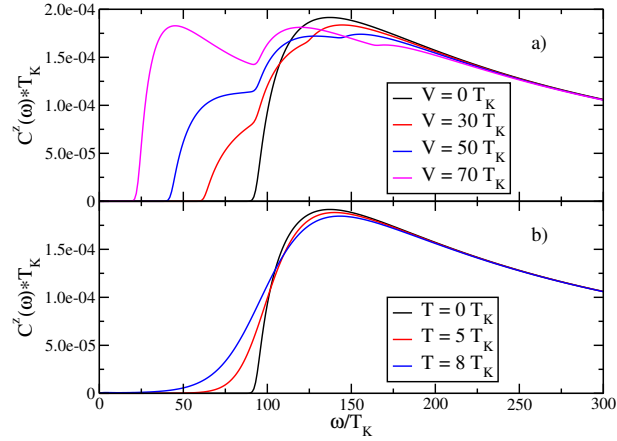


Figure 3.10: a) Splitting of the structure in the correlation function ($h = 100T_K$) due to a small voltage bias. b) Small temperatures lead to broadening.

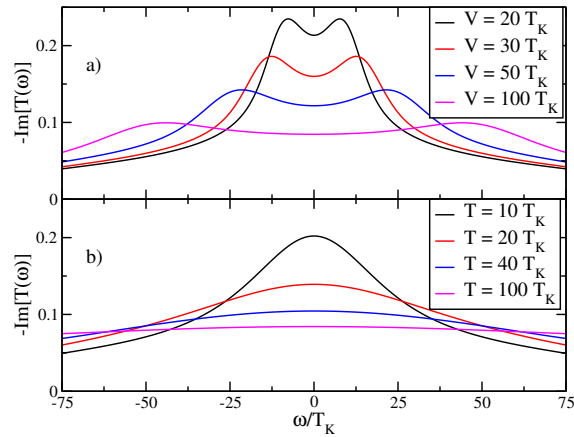


Figure 3.11: Sum of spectral functions for both spin components at zero magnetic field for various values of a) voltage bias and b) temperature.

for additional information on the numerical evaluation.

3.5.2 T-Matrix

In Fig. 3.11 we plotted the spectral function (sum of both spin components) as function of voltage bias and temperature at zero magnetic field calculated from Eq. (3.81). The nonzero voltage bias curve shows a double peak at $\omega \sim \pm V/2$, at nonzero temperature we find broad zero frequency structures in consistence with the results obtained in Refs. [9, 45]. Applying a small magnetic field leads to a shift of these structures by the magnetic field strength and an asymmetric deformation of these structures. Typical curves are shown in Fig. 3.12. As already discussed in Sect. 3.4 the spectral function of the Kondo model in a magnetic field shows a pronounced peak at $\omega \sim \mp h$ (spin-up / spin-down component).

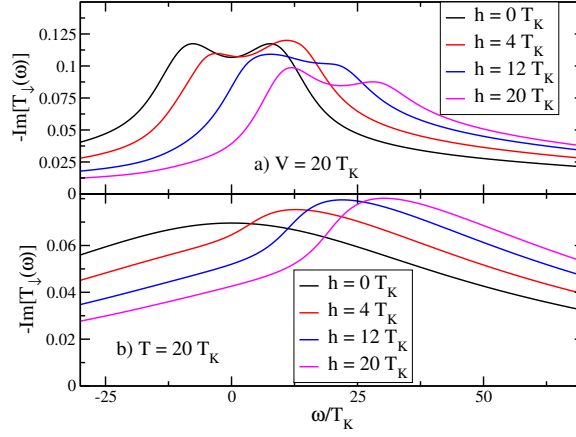


Figure 3.12: An applied magnetic field shifts the central structure of the spectral function, a) $V = 20T_K$, b) $T = 20T_K$.

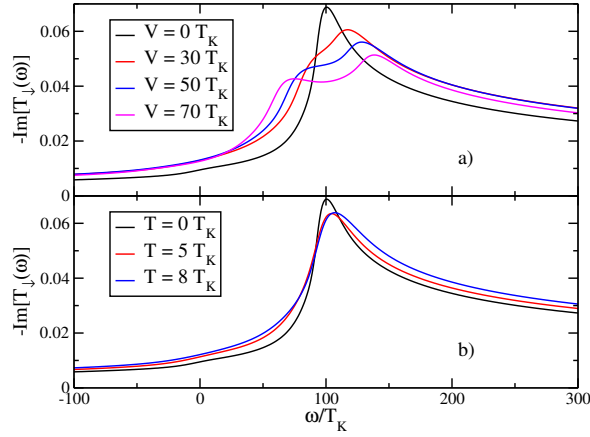


Figure 3.13: a) Splitting of the structure in the spectral function at h due to a small voltage bias. b) Again a small temperature leads to broadening of the latter structure.

In Fig. 3.13 a) we show the splitting of this peak into two at $\omega \sim h \pm V/2$ due to a small voltage bias. Again applying a small temperature leads to a broadening of the structure (subfig. b)).

Again the structures at high frequencies cannot be easily accessed using numerical methods like NRG, the results derived in Ref. [11] were not generalized to nonzero temperatures. Also the perturbative renormalization group and non-equilibrium perturbation theory results for the T-Matrix [11, 45] have not yet been generalized to magnetic field plus voltage bias or temperature.

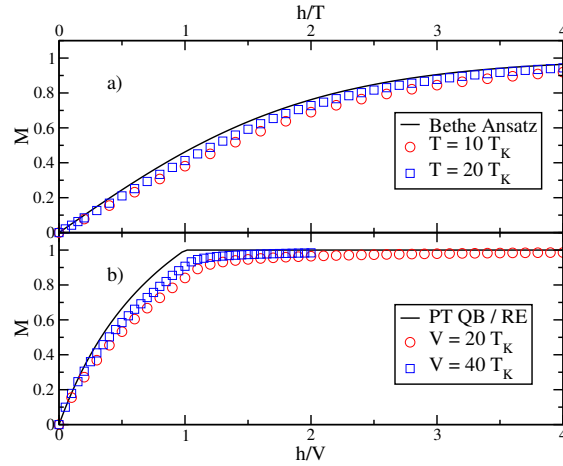


Figure 3.14: Comparison of calculated magnetization with previous zeroth order results a) for fixed temperature and b) for fixed voltage bias at $D = 100T_K$. For increasing temperature or voltage bias the curves are getting closer to the Bethe Ansatz respectively the non-equilibrium perturbation theory (quantum Boltzmann and rate equation) result.

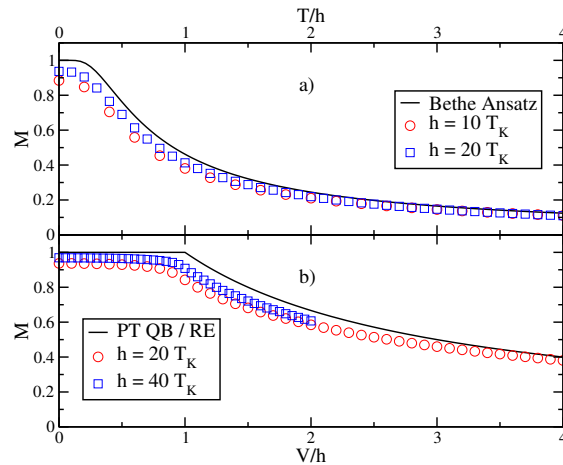


Figure 3.15: Crossover from the equilibrium zero temperature magnetization to a) the high temperature and b) the high voltage result at $D = 100T_K$.

3.5.3 Magnetization

The magnetization could in principal be extracted from the spin-spin correlation function via the sum rule (3.96). Due to the perturbative nature of our approach the sum rule is violated and we were only able to extract qualitative results.

Much better results can be obtained by analyzing the flow of $M(B)$. Due to the slow decay of the spin operator one has to integrate the flow equations up to large values of the flow parameter $B \gg h^{-2}$. Though this is trivial at $V = T = 0$ (as shown in Sect. 3.3.2) it becomes a nontrivial task if one is interested in the magnetization at small magnetic fields

$|h| \ll V, T$.

At high magnetic field $|h| \gg V, T$ we find convergence in the flow of $M(B) + \text{sgn}(h)h^z(B)$ for $B \gg (|h| - V)^{-2}$ in non-equilibrium and $B \gg h^{-2}$ in equilibrium at nonzero temperature as in the (numerical) equilibrium zero temperature calculation in Sect. 3.3.2. This behavior is explained by the sumrule for the spin-spin correlation function (3.96). As shown in Fig. 3.10 the spin-spin correlation function in non-equilibrium has no spectral weight at frequencies $0 < |\omega| \lesssim ||h| - V|$. Therefore at such small energy scales the spin operator (or actually h^z) cannot give any more spectral weight to the γ_{pq} terms, instead the full remaining spectral weight is moved into the number $M(B)$. Note that the zero frequency peak is proportional to M^2 . At nonzero temperature the structure in the spin-spin correlation is broadened and again there is no spectral weight in the correlation function for $0 < |\omega| \lesssim |h|$ (the exact values can be read of from Fig. 3.10).

As already mentioned above the situation is quite different for small magnetic fields $|h| \ll V, T$. Here most of the spectral weight of the spin-spin correlation function lies in the frequency range $0 < |\omega| \leq D$ yielding only very small spectral weight for the zero frequency delta peak. Due to the perturbative nature of the flow equation transformation the sum rule for the spin-spin correlation function (3.96) is violated, typically the error is of order one percent (as already stated above).

If we assume a very small magnetic field ($|h| \rightarrow 0$), then the correlation function should ideally fulfill

$$\frac{2}{\pi} \int_{-\infty}^{\infty} d\omega C_{\gamma}^z(\omega) = 1. \quad (3.97)$$

However, if this sumrule is violated by one percent the integral would e.g. give 0.99 instead of one. The remaining weight would then be accounted to the magnetization by $M^2 = 0.01$ or $M = 0.1$ respectively, which is of course nonsense. Note that the situation is even worse if the sum rule gives one percent too much. If the magnetic field strength is much smaller than the voltage bias or the temperature one therefore cannot use the spectral weight in the spin-spin correlation function to calculate the magnetization. Additionally one cannot expect a convergence of the $M(B) + \text{sgn}(h)h^z(B)$ trick since even at very large B (very small ω) spectral weight is moved from h^z to the γ_{pq} -operators. Instead one has to integrate the flow equations until the spin operator (h^z) has fully decayed, see Appendix A.2.2 for additional information on the numerical evaluation.

In equilibrium the exact magnetization is accessible by solving the Bethe Ansatz equations [75, 80, 81]. Assuming $h > 0$ the asymptotic results relevant for this thesis are given by the zero temperature magnetization $M(h, T = 0) = 1 - 1/(2 \ln(h/T_K))$ for $h \gg T_K$ and the high temperature magnetization $M(h, T) = \tanh(h/(2T))$ for $T \gg T_K$ and $T \gg h$. The high temperature result is the magnetization of a free spin.

Previous non-equilibrium perturbation theory calculations in the limit $V \gg T_K$ or $|h| \gg T_K$ by Parcollet and Hooley [53] and Paaske *et al.* [46] found

$$M_{\text{pt}}(h, V) = \frac{4h}{2|h| + |h + V| + |h - V|} \quad (3.98)$$

for the magnetization. Here the important logarithmic corrections at zero voltage bias are missing since $M_{\text{pt}}(h, V) = \text{sgn}(h)$ for $V < |h|$. Though logarithmic corrections enter the calculation [46] in $\mathcal{O}(J^3)$, they do not change the result if the Hamiltonian is derived from an underlying Anderson impurity model. Therefore $M_{\text{pt}}(h, V)$ has to be interpreted as asymptotic high voltage bias result ($V \rightarrow \infty$).

In Sect. 3.3.2 we already derived the equilibrium zero temperature magnetization within the flow equation framework. Figs. 3.14 and 3.15 show the smooth crossover from the equilibrium zero temperature result to both the asymptotic high temperature result and the asymptotic high voltage bias result.

As in the equilibrium zero temperature calculation the magnetization in Figs. 3.14 and 3.15 depend strongly on the relation D/T_K . We were not able to derive the finite bandwidth corrections beyond Eq. (3.51). We again want to point out that for small magnetic field strengths $|h| \ll V, T$ the magnetization cannot be easily accessed since one has to integrate the flow equations up to very large values of the flow parameter $B \gg h^{-2}$ to find a convergence in the flow of $M(B)$. Therefore a derivation of the static spin susceptibility (see the following section) from the magnetization beyond zeroth order is futile.

3.5.4 Static Spin Susceptibility

The static spin susceptibility is defined as the derivative of the magnetization:

$$\chi_0 = \left. \frac{d\langle S^z \rangle}{dh} \right|_{h=0}. \quad (3.99)$$

It can be alternatively derived from the imaginary part of the response function via a Kramers-Kronig relation:

$$\chi_0 = \frac{1}{\pi} \int_{-\infty}^{\infty} d\omega \frac{\chi''(\omega)}{\omega}. \quad (3.100)$$

As already mentioned in the previous section the static spin susceptibility cannot be derived directly from the magnetization beyond zeroth order. The leading logarithmic corrections are accessible within the flow equation framework using the approach via the Kramers-Kronig relation (3.100) as we show in the following.

The equilibrium high temperature ($T \gg T_K$) static spin susceptibility is given by the asymptotic Bethe Ansatz result [75, 80]:

$$\chi_0(T) = \frac{1}{4T} \left(1 - \frac{1}{\ln(T/T_K)} - \frac{\ln(\ln(T/T_K))}{2(\ln(T/T_K))^2} + \mathcal{O}((\ln(T/T_K))^{-2}) \right). \quad (3.101)$$

The static spin susceptibility in non-equilibrium has been previously calculated in Ref. [53] using a rate equation approach. The zeroth order result ($V \rightarrow \infty$) is given by

$$\chi_0(V) = \frac{(1+R)(1+1/R)}{4V} = \frac{1}{4T_{\text{eff}}}. \quad (3.102)$$

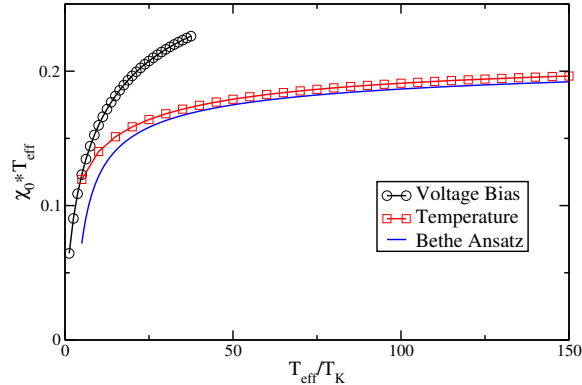


Figure 3.16: Static spin susceptibility at nonzero voltage bias and nonzero temperature (equilibrium). The equilibrium curve agrees well with the asymptotic Bethe Ansatz result for $T \gg T_K$.

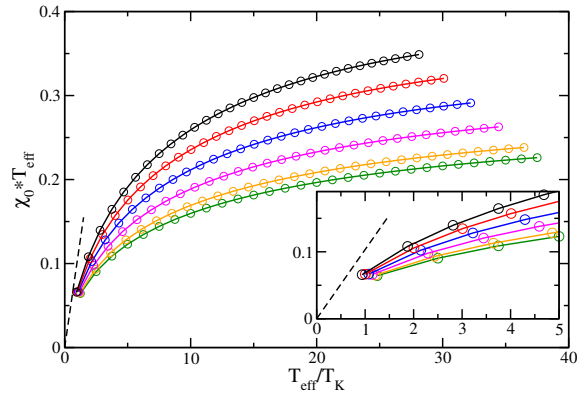


Figure 3.17: Static spin susceptibility χ_0 at nonzero voltage bias for various asymmetry parameters R , the asymmetry parameter increases from bottom to top: $R = 1.0, 1.4, 1.8, 2.2, 2.6, 3.0$. The dashed line is the exact result in the limit of strong asymmetry ($R \rightarrow \infty$ or $R \rightarrow 0$). A zoom on the small voltage bias region is shown in the inset.

Obviously this result is equivalent to the (zeroth order) equilibrium Bethe Ansatz result (3.101), only the temperature T has to be replaced by the effective temperature T_{eff} . Since the logarithmic corrections arise from the Kondo correlations² it is of general interest to derive these corrections also in non-equilibrium. Naively one would expect the non-equilibrium corrections to be similar to the equilibrium ones, as first guess one would simply replace the temperature T in Eq. (3.101) by the effective temperature T_{eff} .

In Fig. 3.16 we plotted the flow equation result for the static spin susceptibility in both equilibrium and non-equilibrium. The nonzero temperature curve agrees very well with the asymptotic Bethe Ansatz result for $T \gg T_K$. In non-equilibrium the corrections from

²The static spin susceptibility of a free spin is (in equilibrium) given by $1/(4T)$.

the zeroth order result (3.102) are clearly not compatible with the logarithmic corrections in equilibrium. Instead we find some genuine non-equilibrium physics.

Fig. 3.17 shows the non-equilibrium static spin susceptibility for various values of the asymmetry parameter R , the deviations from the equilibrium result increase with increasing asymmetry parameter. The convergence of the curves at small voltage bias is interpreted as follows: the equilibrium zero temperature static spin susceptibility is given by

$$\chi_0(T = 0, V = 0) = \frac{W}{4T_K}, \quad (3.103)$$

where $W = 0.413$ is the Wilson ratio. For strong asymmetry the current through the dot vanishes and one arrives at the result from Eq. (3.103) yielding

$$\chi_0(V)T_{\text{eff}} \stackrel{R \rightarrow \infty}{=} \frac{W}{4} \frac{T_{\text{eff}}}{T_K}. \quad (3.104)$$

Though the perturbative truncation of the flow becomes uncontrolled for $R \rightarrow \infty$ we still find indications for this behavior. See Appendix A.2.3 for additional information on the numerical evaluation.

3.6 Summary

In quantum mechanics many relevant physical quantities are evaluated by taking the expectation value of an operator with respect to some reference state like the groundstate. For example, the ground state magnetization is given by $M = 2\langle 0|S^z|0\rangle$, where $|0\rangle$ denotes the ground state. At first glance evaluating expectation values seems to be fairly simple within the flow equation framework, one just has to transform the operators into the diagonal basis of the Hamiltonian. Unfortunately the transformation of an operator is highly nontrivial³ unless the flow equation transformation can be expanded in powers of the running coupling or the operator is trivial (commutes with the transformation). A general operator decays into infinite many higher order terms and once again one has to find a suitable truncation scheme as for the transformation of the Hamiltonian.

In this chapter we studied the spin-spin correlation function, the imaginary part of the corresponding response function, the magnetization, the static spin susceptibility and the T-Matrix as functions of dc-voltage bias, temperature and magnetic field strength (where suitable).

The transformation of the impurity (dot) spin operator turned out to be fairly simple, already a calculation in lowest order is sufficient to derive both the static and the dynamic properties of the spin operator. In equilibrium we reproduced the celebrated asymptotic Bethe Ansatz results for the magnetization and the static spin susceptibility in leading logarithmic order. In non-equilibrium the magnetization and the static spin susceptibility were so far calculated in zeroth order only. As in equilibrium we worked out both functions

³“There ain’t no such thing as a free lunch” [82].

including the leading logarithmic corrections. Note that for the static quantities the Kondo physics is hidden in the logarithmic corrections to the leading zeroth order term.

Upon analyzing the flow equations in Chap. 2 we noticed a surprising accordance in the flow of the running coupling at zero magnetic field, the decoherence rates are equivalent for both nonzero temperature and nonzero dc-voltage bias, the voltage bias V can be replaced by an effective temperature:

$$T_{\text{eff}} = \frac{V}{(1+R)(1+1/R)}, \quad (3.105)$$

where R is the asymmetry parameter. This connection is the key motivation to ask an important question: Are the physical properties of the impurity (dot) spin purely governed by the “amount” of noise or does also the noise producing mechanism play an important role? The static spin susceptibility is the natural choice for answering this question since the exact equilibrium result is known from Bethe Ansatz. We found an astonishingly strong disagreement between the non-equilibrium flow equation result and the result expected from the equilibrium Bethe Ansatz result. The impurity (dot) spin responds differently to different mechanisms for noise production.

In equilibrium the spin-spin correlation function and the corresponding response function are well understood in all parameter regimes, also in the context of the spin boson model. We extended the calculation of these dynamical quantities to non-equilibrium.

The direct evaluation of the T-Matrix within the flow equation framework is impossible since too many higher order terms would have to be included both in the numerical and in the analytical scaling analysis. Nevertheless, we could relate the transformation of the T-Matrix-operators to the flow of the running coupling in transformation of the Hamiltonian. Thereby the T-Matrix became accessible within our approach. We reproduced previously known results from perturbative RG and non-equilibrium perturbation theory and extended the previously known results to the full parameter regime accessible within our approach.

Chapter 4

Thermal Non-Equilibrium

Another realization of a non-equilibrium Kondo dot is the coupling of the dot to two leads at different temperature [39], see Fig. 4.1 for an illustration. In the original Kondo problem, where one studies a magnetic impurity in a nonmagnetic metal in thermal equilibrium,¹ at high temperature ($T \gg T_K$) the logarithmic divergence is cut off by decoherence effects induced by thermal noise. If the dot is coupled to two (or more) heat baths at different temperature one additionally finds decoherence effects due to the transport of thermal energy through the dot. Due to the inflationary use of the word non-equilibrium in the previous chapters we call this new non-equilibrium situation thermal non-equilibrium. The corresponding Hamiltonian (two heat baths) is given by

$$H = \sum_{p,\alpha,\sigma} \epsilon_p c_{p\alpha\sigma}^\dagger c_{p\alpha\sigma} - h S^z \quad (4.1)$$
$$+ \sum_{p,q,\alpha,\beta} \frac{J_{\alpha\beta}}{2} \left(\left(c_{p\alpha\uparrow}^\dagger c_{q\beta\uparrow} - c_{p\alpha\downarrow}^\dagger c_{q\beta\downarrow} \right) S^z + \left(c_{p\alpha\uparrow}^\dagger c_{q\beta\downarrow} S^- + \text{h.c.} \right) \right) ,$$

which is equivalent to the dc-voltage bias Hamiltonian (1.7) with $\mu_{l/r} = 0$. The temperature of the leads is given by T_r for the right one and T_l for the left one. Again we assume that the Hamiltonian is derived from an underlying Anderson impurity model ($J_{lr}^2 = J_{ll} J_{rr}$) to introduce the f - and g -operators, see Eq. (1.8).

The calculation from Chap. 2 is easily recycled. For simplicity we restrict the following discussion to the special case of zero magnetic field ($h = 0$) and symmetric coupling of the leads ($R = 1$). Note that all numerical results previously presented in this thesis² are easily calculated also in thermal non-equilibrium, also for nonzero magnetic field and asymmetric coupling of the leads. In the following discussion we focus on the static spin susceptibility. It is convenient to assume $T_l \geq T_r$ (we previously assumed symmetric coupling!!). The

¹Coupled to a single heat bath.

²Spin-spin correlation function, imaginary part of response function, T-Matrix, magnetization and static spin susceptibility.

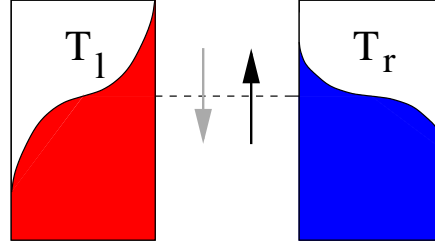


Figure 4.1: Schematic picture of a quantum dot coupled to two leads at different temperature. $T_{l/r}$ labels the temperature of the left and right lead.

distribution function for the f -operators is given by

$$\begin{aligned} n_f(p) &= \langle f_{p\alpha}^\dagger f_{p\alpha} \rangle = \frac{1}{2}(n_l(\epsilon_p) + n_r(\epsilon_p)) \\ &= \frac{1}{2} \left(\frac{1}{1 + \exp(\epsilon_p/T_l)} + \frac{1}{1 + \exp(\epsilon_p/T_r)} \right). \end{aligned} \quad (4.2)$$

As we show in the following the Hamiltonian is diagonalized in a controlled expansion if $T_l \gg T_K$.

4.1 Flow Equation Analysis

4.1.1 Basic Relations

To derive a simple scaling picture we use the so-called IR-parametrization:

$$J(p, q)(B) = g(B)e^{-B(\epsilon_{p'} - \epsilon_p)^2}, \quad g(B) \stackrel{\text{def}}{=} J(0, 0)(B), \quad (4.3)$$

which we already introduced in Sect. 2.1.4. The flow equation (2.50) for the running coupling $J^{\uparrow/\downarrow}(p, q) = J_\perp(p, q) = J(p, q)$ is easily simplified to

$$\begin{aligned} \frac{dg}{dB} &= g^2 \sum_q (1 - 2n_f(q)) \epsilon_q e^{-2B\epsilon_q^2} \\ &\quad - \sum_{q', q} (n_f(q') + n_f(q) - 2n_f(q')n_f(q)) (\epsilon_{q'} - \epsilon_q)^2 e^{-2B(\epsilon_{q'} - \epsilon_q)^2} g \int_0^B d\tilde{B} g^2(\tilde{B}). \end{aligned} \quad (4.4)$$

This equation is the starting point for the following analytical calculation.

4.1.2 1-loop Scaling Analysis

In the following we briefly repeat the scaling analysis in 1-loop order, see Sect. 2.1.4 for more details. For $B \ll T_l^{-2}$ Eq. (4.4) is easily reduced to the usual zero temperature

scaling equation:

$$\frac{dg}{dB} = \frac{g^2}{2B} . \quad (4.5)$$

For $B \gg T_l^{-2}$ it is convenient to rewrite the 1-loop part of the flow equation (4.4) to

$$\frac{dg}{dB} = \frac{g^2}{2} \sum_q (1 - 2n_L(q)) + (1 - 2n_R(q)) \varepsilon_q e^{-2B\varepsilon_q^2} . \quad (4.6)$$

Again recycling the arguments from Sect. 2.1.4 we find

$$\frac{dg}{dB} = \frac{g^2}{4B} \left(1 + \frac{\sqrt{2\pi}}{8} \frac{1}{T_l \sqrt{B}} \right) \quad (4.7)$$

for $B \gg T_l^{-2}$ at $T_r = 0$ (or equivalently $T_l^{-2} \ll B \ll T_r^{-2}$ if $T_r > 0$). If the right lead is at nonzero temperature ($T_r > 0$) we find for $B \gg T_r^{-2}$:

$$\frac{dg}{dB} = \frac{g^2 \sqrt{2\pi}}{B \cdot 32} \left(\frac{1}{T_l \sqrt{B}} + \frac{1}{T_r \sqrt{B}} \right) . \quad (4.8)$$

If $T_r \gg T_K$ the flow of the running coupling is cut off for $B \gg T_r^{-2}$ (note that $T_l \geq T_r$) similar to the previous discussion in thermal equilibrium (Sect. 2.1.4). Otherwise we find the usual strong coupling flow (modulo a factor of $1/2$). As we show in the following section the logarithmic divergence is cut off by the 2-loop terms if $T_l \gg T_K$. In the following discussion we skip the case differentiation for $T_r = 0$ and $T_r > 0$, by *large enough* B we refer to the appropriate limits $B \gg T_l^{-2}$ for $T_r = 0$ and $B \gg T_r^{-2}$ for $T_r > 0$.

4.1.3 2-loop Scaling Analysis

In the equilibrium calculation ($T_l = T_r = T$) in Sect. 2.1.4 we already showed that the 2-loop term dominates over the 1-loop term for $B \gg T^{-2}$:

$$\begin{aligned} \frac{dg}{dB} &= \frac{\sqrt{2\pi}}{4B} \left(\frac{1}{4} g^2 \frac{1}{T \sqrt{B}} - g^3 T \sqrt{B} \right) \\ &\stackrel{T\sqrt{B} \gg 1}{\approx} -g^3 \frac{\sqrt{2\pi}}{4\sqrt{B}} T , \end{aligned} \quad (4.9)$$

yielding a power law decay of the running coupling $g(B) \sim B^{-1/4}$. This argument is easily generalized to the 1-loop term in Eq. (4.7), where the flow in 1-loop order is not cut off by the temperature. If the temperature is smaller than the Kondo temperature the running coupling becomes of $\mathcal{O}(1)$ during the flow and the perturbative truncation of the flow equations is then uncontrolled.

In the following discussion we study the 2-loop term in Eq. (4.4) only. Again we replace $n_f(\epsilon)$ by the Fermi functions for left and right lead:

$$\begin{aligned} 4(n_f(\epsilon) + n_f(\tilde{\epsilon}) - 2n_f(\epsilon)n_f(\tilde{\epsilon})) &= \\ &= \sum_{\alpha=l,r} (n_\alpha(\epsilon) + n_\alpha(\tilde{\epsilon}) - 2n_\alpha(\epsilon)n_\alpha(\tilde{\epsilon})) + (n_l(\epsilon) + n_r(\tilde{\epsilon}) - 2n_l(\epsilon)n_r(\tilde{\epsilon})) + (l \leftrightarrow r) . \end{aligned} \quad (4.10)$$

Using $f(x) \exp(-2B(x-c)^2) \approx f(c) \exp(-2B(x-c)^2)$ for large enough B the summation over the momentum indices in the 2-loop term of Eq. (4.4) leads to ($\rho = 1$ sets the energy scale):

$$\begin{aligned} F_{\alpha\beta} &\stackrel{\text{def}}{=} \int_{-\infty}^{\infty} d\epsilon \int_{-\infty}^{\infty} d\tilde{\epsilon} (n_\alpha(\epsilon) + n_\beta(\tilde{\epsilon}) - 2n_\alpha(\epsilon)n_\beta(\tilde{\epsilon})) (\epsilon - \tilde{\epsilon})^2 e^{-2B(\epsilon - \tilde{\epsilon})^2} \\ &\approx \int_{-\infty}^{\infty} d\epsilon (n_\alpha(\epsilon) + n_\beta(\epsilon) - 2n_\alpha(\epsilon)n_\beta(\epsilon)) \int_{-\infty}^{\infty} d\tilde{\epsilon} \tilde{\epsilon}^2 e^{-2B\tilde{\epsilon}^2} . \end{aligned} \quad (4.11)$$

The latter approximation is easily checked using numerical integration, note that the double integral is solved exactly for $T_\alpha = T_\beta = 0$. In the previous equilibrium calculation (Sect. 2.2.5.2) we already found

$$\begin{aligned} F_{ll} &= \frac{\sqrt{2\pi}}{4} T_l B^{-3/2} , \quad B \gg T_l^{-2} \\ F_{rr} &= \frac{1}{4} \begin{cases} B^{-2} & , T_r = 0 \\ \sqrt{2\pi} T_r B^{-3/2} & , T_r > 0 \text{ and } B \gg T_r^{-2} \end{cases} \\ F_{lr} &= \frac{\sqrt{2\pi}}{4} T_l B^{-3/2} , \quad T_r = T_l \text{ and } B \gg T_l^{-2} . \end{aligned} \quad (4.12)$$

Note that $F_{lr} = F_{rl}$. Using

$$\lim_{T_r \rightarrow 0} \frac{e^{\epsilon/T_l} + e^{\epsilon/T_r}}{(1 + e^{\epsilon/T_l})(1 + e^{\epsilon/T_r})} = \frac{1}{1 + e^{|\epsilon|/T_l}} \quad (4.13)$$

we find for $T_r = 0$ and $B \gg T_l^{-2}$:

$$F_{lr} = \frac{\sqrt{2\pi}}{4} \ln(2) T_l B^{-3/2} . \quad (4.14)$$

By numerical integration one easily shows that $F_{lr} \sim B^{-3/2}$ also holds for $0 < T_r < T_l$ at large enough B as we show in the following section. The flow of the running coupling at large enough B is then given by (we already neglected the 1-loop term)

$$\frac{dg}{dB} = -g^3 \frac{\sqrt{2\pi}}{4\sqrt{B}} \frac{T_l + T_r + 2T_{lr}}{4} , \quad (4.15)$$

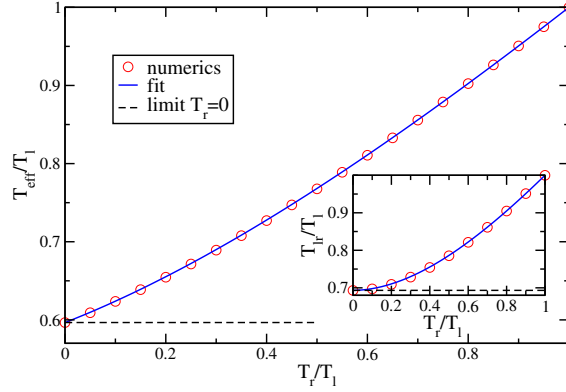


Figure 4.2: Universal curve for the effective temperature in thermal non-equilibrium (4.17). The inset shows the universal curve for T_{lr} defined in Eq. (4.16).

where we defined the new temperature scale

$$T_{lr} = B^{3/2} \frac{4}{\sqrt{2\pi}} F_{lr} \quad (4.16)$$

and neglected the irrelevant B^{-2} term for $T_r = 0$. In comparison with Eq. (4.9) we define an effective temperature

$$T_{\text{eff}} = \frac{1}{4} (T_l + T_r + 2T_{lr}) . \quad (4.17)$$

By analytical integration we already found the most interesting special cases:

$$T_{lr} = \begin{cases} \ln(2)T_l & , T_r = 0 \\ T_l & , T_r = T_l \end{cases} , \quad (4.18)$$

numerical results for general values of T_r are discussed in the following section.

4.2 Numerical Results

4.2.1 Effective Temperature

The double integral (4.11) is easily integrated numerically, as already mentioned above we always find $F_{lr} \sim B^{-3/2}$ for large enough B . In Fig. 4.2 we plotted the resulting effective temperature (4.17) for $0 \leq T_r \leq T_l$. The inset shows the corresponding curve for T_{lr} , which is extremely well fitted by

$$T_{lr} = \ln(2) (T_l^c + T_r^c)^{1/c} , \quad c = -\frac{\ln(2)}{\ln(\ln(2))} . \quad (4.19)$$

The error is only about one percent. Within this error range also a hyperbola ($c = 2$) is sufficient, but the latter fails to reproduce the exact result $T_{\text{eff}} = T_l$ for $T_r = T_l$. Summing

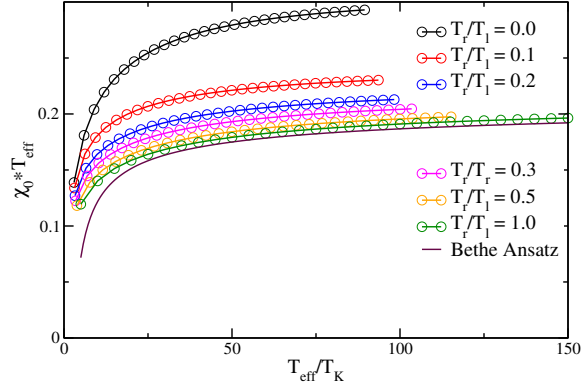


Figure 4.3: Static spin susceptibility in thermal non-equilibrium, the curves for $T_r/T_l \gtrsim 0.6$ lie within the error bars of the equilibrium curve ($T_r = T_l$).

up, by numerical integration we find that the effective temperature is in very high accuracy given by

$$T_{\text{eff}} = \frac{1}{4} \left(T_l + T_r + 2 \ln(2) (T_l^c + T_r^c)^{1/c} \right). \quad (4.20)$$

4.2.2 Static Spin Susceptibility

The asymptotic equilibrium ($T_r = T_l = T$, $T \gg T_K$) Bethe Ansatz result for the static spin susceptibility is given by

$$\chi_0(T) = \frac{1}{4T} \left(1 - \frac{1}{\ln(T/T_K)} - \frac{\ln(\ln(T/T_K))}{2(\ln(T/T_K))^2} + \mathcal{O}((\ln(T/T_K))^{-2}) \right). \quad (4.21)$$

As shown in Sect. 3.5.4 the equilibrium flow equation result is in good agreement with the Bethe Ansatz one for $T \gg T_K$. In Fig. 4.3 we plotted the static spin susceptibility as function of T_{eff}/T_K for various values of T_r/T_l . Again we ask the question on the logarithmic corrections in non-equilibrium. Are they again different from the equilibrium result?

In contrast to the results for a dc-biased Kondo dot in Sect. 3.5.4 the description of the static spin susceptibility by the effective temperature works extremely well for $T_r/T_l \gtrsim 0.6$. For smaller ratios we find strong deviations from the equilibrium formula (4.21) similar to the dc-voltage bias result.

This result is interpreted as follows. We get contributions from both equilibrium and non-equilibrium decoherence sources, namely the thermal noise and the shot noise of the thermocurrent through the dot (if $T_r < T_l$). For $T_r \sim T_l$ the system is nearly in thermal equilibrium and we find the usual equilibrium physics. The situation is clearly different for $T_r \ll T_l$. Here interlead scattering processes dominate the flow of the Hamiltonian at large enough B since $T_{l_r} > T_l, T_r$ and we again find genuine non-equilibrium physics.

Previous theoretical studies of a Kondo dot in thermal non-equilibrium focused on the thermopower and the thermocurrent [83–88]. See Appendix A.2.3 for additional information on the numerical evaluation.

4.3 Summary

In the original Kondo problem the impurity spin is in thermal equilibrium with the surrounding metallic host. A Kondo dot is attached to multiple leads which are easily prepared at different temperature. Here the dot spin is in a non-equilibrium situation since it is coupled to two (or more) heat baths at different temperature. We call this situation thermal non-equilibrium.

Due to the general setup of the flow equations in Chap. 2 there was no need to re-derive the scaling equations for this new situation, only the scaling analysis had to be repeated. Again we found similarities between the decoherence rate in equilibrium and in non-equilibrium expressed by the effective temperature:

$$T_{\text{eff}} = \frac{1}{4} \left(T_l + T_r + 2 \ln(2) (T_l^c + T_r^c)^{1/c} \right), \quad c = -\frac{\ln(2)}{\ln(\ln(2))}, \quad (4.22)$$

where $T_{l/r}$ is the temperature of the left and right lead. At small temperature differences we surprisingly found that the static spin susceptibility is extremely well described by the equilibrium Bethe Ansatz result, only the temperature T had to be replaced by the effective temperature T_{eff} . For large temperature difference we again found genuine non-equilibrium physics. This result is interpreted as follows: in thermal non-equilibrium there are two decoherence sources, the thermal noise and the shot noise from the thermocurrent through the dot. Depending on which of these two noise sources dominates one either finds equilibrium or non-equilibrium physics.

Chapter 5

Conclusion

In this thesis we developed a perturbative scaling picture for the Kondo model in a magnetic field for both equilibrium and non-equilibrium situations using the flow equation approach. We diagonalized the Hamiltonian in the weak coupling regime $\max(V, |h|, T) \gg T_K$ where the logarithmic divergence of the running coupling typical for the Kondo problem is cut off by decoherence effects or by the Zeeman splitting of the dot levels due to an applied magnetic field (or by combinations of the latter). The decoherence is induced either by the thermal noise or by the shot noise of the current through the dot. By the diagonalization of the Hamiltonian both the static and the dynamic properties of the system became accessible. In detail we worked out the magnetization, the static spin susceptibility, the T-matrix, the spin-spin correlation function, and the spin response function as functions of voltage bias, temperature, and magnetic field. We reproduced previously known results from Bethe Ansatz, perturbative renormalization group, and non-equilibrium perturbation theory and extended them to full parameter regime accessible within our approach.

The famous asymptotic Bethe Ansatz result for the equilibrium magnetization of the impurity spin at high magnetic field strengths is given by $M = 1 - 1/(2 \ln(h/T_K)) + \dots$. Here the Kondo physics does not appear in leading order, instead it is hidden in the sub-leading logarithmic corrections. We rederived the previous equilibrium Bethe Ansatz result in leading logarithmic order and consistently worked out the transition to the asymptotic high temperature result and to the asymptotic high voltage bias result. Both asymptotic results are zeroth order only. Our approach provides the first perturbative scaling calculation that reproduces the magnetization including the leading logarithmic corrections in the Kondo model. In equilibrium at nonzero temperature the magnetization is accessible in arbitrary precision by numerically solving the Bethe Ansatz equations. For the non-equilibrium magnetization only the zeroth order high voltage result has previously been accessible from non-equilibrium perturbation theory calculations.

The situation is similar for the static spin susceptibility. The equilibrium high temperature result is again accessible from Bethe Ansatz calculations and for the non-equilibrium result only the zeroth order high voltage result is known from non-equilibrium perturbation theory. Again we focused on the leading logarithmic corrections. In equilibrium we

reproduced the asymptotic Bethe Ansatz result at high temperature. These results can be reproduced when we introduce an effective temperature $T_{\text{eff}} = V/((1+R)(1+1/R))$ in non-equilibrium, where R is the asymmetry parameter. In non-equilibrium the structure of the logarithmic corrections is unknown and we therefore studied the static spin susceptibility as function of the effective temperature and compared it to the equilibrium result. Not unexpected, the logarithmic correction clearly differ from the equilibrium result.

We also studied the static spin susceptibility in “thermal non-equilibrium”, where the Kondo dot is connected to two leads at different temperature. We again studied the static spin susceptibility as function of an effective temperature $T_{\text{eff}} = (T_l + T_r + 2T_{lr})/4$, where $T_{l/r}$ is the temperature of the left and right lead and T_{lr} is the effective temperature corresponding to the noise by the thermocurrent through the dot. For small temperature difference, where the system nearly is in equilibrium, we found an agreement of the logarithmic corrections in thermal non-equilibrium and in equilibrium: only the temperature had to be replaced by the effective temperature. At large temperature difference, where transport processes dominate the system’s properties, we again found genuine non-equilibrium physics.

In the Kondo model the concept of an effective temperature turned out to be practical in thermal non-equilibrium at small temperature difference, which is a close to equilibrium situation. In far out of equilibrium situations this concept breaks down as we have shown for large temperature difference. We obtained a similar result for a dc-biased Kondo dot at high voltage bias ($V \gg T_K$). Though in leading order a dc-voltage bias or a large temperature difference can be described by an effective temperature, the subleading logarithmic corrections clearly differ.

In the equilibrium Kondo model the T-matrix is a well studied object, since the closely related spectral function can be measured in experiments. We reproduced previous perturbative RG results for the spectral function in high magnetic fields at zero temperature and additionally worked out the spectral function as function of temperature and magnetic field. In non-equilibrium the spectral function has been previously calculated for zero magnetic field using non-equilibrium perturbation theory. We again reproduced the previously known result and worked out the spectral function as function of voltage bias and magnetic field.

The spin dynamics is described by the spin-spin correlation function and the corresponding response function. In equilibrium both functions are well known in all parameter regimes, also in the context of the spin boson model. We extended the previously known results to non-equilibrium situations. We used the response function to work out the static spin susceptibility from a Kramers-Kronig relation.

Summing up, the flow equation approach provides a handy tool kit for studying the physical properties of the Kondo model in both equilibrium and non-equilibrium situations.

Appendix A

Numerics Trivia

A.1 Solution of the Flow Equations

The flow equations were solved using the Runge-Kutta algorithm from Ref. [89]. In this implementation the stepper function is optimized for general problems and therefore rather conservative. By optimistic finetuning one easily reduces the number of intermediate integration steps. Note that the number of intermediate steps is directly proportional to the runtime. For the solution of the flow equations in diagonal parametrization we used the following discretization:

- $0 \leq B < 1/(4D^2)$ (small B): step size $1/(16D^2)$
- $1/(4D^2) \leq B < 10^3$: next step size is 1.5 times the size of the previous step
- $10^3 \leq B$: next step size is twice the size of the previous step
- general: step size should not overshoot $0.5B$ for large B .

For $D \sim 0.5$ and reasonable accuracy (relative error: 10^{-5} , absolute error: 10^{-20}) typically no intermediate steps are needed. Note that we still used the original stepper function as backup. On current workstations system sizes of $\mathcal{O}(10^3)$ are accessible, note that the runtime scales with the number of states cube.

The typical runtime for the solution of the momentum independent running coupling appearing in the scaling analysis sections of Chap. 2 is of order seconds and there is no need for runtime optimizations. The full systems of flow equations turns out to be quite stiff (solution changes on many different scales). Therefore the step size cannot be easily adjusted and finetuning of the stepper function usually does not lead to a significant reduction of intermediate steps. However, the dimension of this system of differential equations scales with number of states to the four, so one typically runs out of ram before cpu time becomes relevant.

A.2 Additional Approximations

A.2.1 Correlation and Response Function

For zero magnetic field the spin-spin correlation function is zero at $\omega = 0$ since $\gamma_{pp}(B) \equiv 0$ (follows directly from Eq. (3.34)). Since the correlation function at zero magnetic field is continuous by definition,¹ one finds a small frequency region around $\omega = 0$ where the correlation functions does not show the expected behavior but instead decays to zero. The width of this region depends on the discretization of the conduction band electron states, for our parameter sets it is typically less than one T_K . It is easily removed by broadening the curves.

At nonzero magnetic field the discretization of the conduction band plays another important role, since here $h(B = \infty)$ enters the momentum indices of $\tilde{\gamma}$ in two different ways: $\epsilon_p, e_p + \omega + \tilde{h}$ and $\epsilon_p, e_p - \omega + \tilde{h}$. Here ω can no longer be chosen as multiples of the energy difference of two neighboring conduction band states (\pm the magnetic field) since one would at most hit one of the two contributions. Therefore a suitable interpolation or broadening is needed.

In our detailed study of the spin-spin correlation function and the imaginary part of the response function we naturally find combinations of both problems. To reduce additional errors by broadening and (or) interpolation we therefore broadened all curves using a normal distribution with variance $1.5T_K$.

A.2.2 Magnetization

At high magnetic field $|h| \gg V, T$ we find a convergence of $M + h^z \text{sgn}(h)$ for $B \gg h^{-2}$. The magnetization is then determined as the latter expression.

For small magnetic field ($|h| \lesssim V, T$) the $M + h^z \text{sgn}(h)$ trick cannot be used (see discussion in Sect. 3.5.3) and one has to wait for a convergence in the flow of M . At very small magnetic field $|h| \ll V, T$ the spin operator (h^z) decays to zero before the flow of $M(B)$ converged. As discussed in Sect. 3.3.1 the spin operator does not decay nicely to zero but instead oscillates around zero with decreasing amplitude. In the oscillating regime one can no longer guarantee the stability of the perturbative expansion since the leading term in the flow equation for γ is proportional to h^z and is therefore also oscillating. Here we determined the magnetization of the system as $M(B_{\text{osci}})$, where B_{osci} is the value of the flow parameter at which $h^z < 10^{-4}$ for the first time.

Summing up: if we did not find a convergence of either $M + h^z \text{sgn}(h)$ or M before the system enters the oscillating regime we have chosen the magnetization as $M(B_{\text{osci}})$, where B_{osci} is the flow parameter at which h^z becomes smaller than 10^{-4} (for the first time).

¹See your favorite textbook on ordinary differential equations.

A.2.3 Static Spin Susceptibility

The imaginary part of the response function is bandwidth dependent and therefore also the static spin susceptibility depends on the bandwidth if it is calculated via a Kramers-Kronig relation. Since there is no way to calculate or even estimate the corresponding error directly, we have to use a rather creative approach via the properties of the spin-spin correlation function. For high frequencies $\omega \gg \Gamma$ the spin-spin correlation function and the imaginary part of the response function are equal, see Eqs. (3.94) and (3.95). This property is used to extrapolate the static spin susceptibility to infinite bandwidth.

First we extrapolate the spin-spin correlation function to infinite bandwidth using the analytic formula from Eq. (3.94). To eliminate effects at the band edges the extrapolation should start at $\omega \sim 0.75D$. We then rescale the spin-spin correlation function such that its sumrule is fulfilled. As final steps we attach the rescaled extrapolation to the imaginary part of the response function which is of course rescaled with the same factor. We then used the extrapolated imaginary part of the response function as input for the Kramers-Kronig relation.

Since there exists no sumrule for the imaginary part of the response function we had to take the indirect route over the spin-spin correlation function.

Appendix B

Math

B.1 Momentum Summation, 2-loop

In this section we calculate the integral

$$\int_{-\infty}^{\infty} d\epsilon_r \int_{-\infty}^{\infty} d\epsilon_s (n_f(\epsilon_r) + n_f(\epsilon_s) - 2n(\epsilon_r)n(\epsilon_s))(\epsilon_r - \epsilon_s + h)^2 e^{-2B(\epsilon_r - \epsilon_s + h)^2} . \quad (\text{B.1})$$

We start with the simple case $T = 0$, $V \geq 0$:

$$\begin{aligned} \int_a^b dx (x - y + h)^2 e^{-2B(x-y+h)^2} &= \frac{1}{2B\sqrt{2B}} \int_{\sqrt{2B}(a-y+h)}^{\sqrt{2B}(b-y+h)} dz z^2 e^{-z^2} = \\ &= \frac{1}{4B} \left((a - y + h)e^{-2B(a-y+h)^2} - (b - y + h)e^{-2B(b-y+h)^2} \right) + \\ &+ \frac{\sqrt{\pi}}{8B\sqrt{2B}} \left(\text{erf}(\sqrt{2B}(b - y + h)) - \text{erf}(\sqrt{2B}(a - y + h)) \right) , \end{aligned} \quad (\text{B.2})$$

$$\begin{aligned} \int_a^b dx \int_c^d dy (x - y + h)^2 e^{-2B(x-y+h)^2} &= \frac{1}{16B^2} \times \\ &\times \left(2e^{-2B(a+h-d)^2} - 2e^{-2B(a+h-c)^2} - 2e^{-2B(b+h-d)^2} + 2e^{-2B(b+h-c)^2} + \right. \\ &+ \sqrt{2\pi B}(a+h-d)\text{erf}(\sqrt{2B}(a+h-d)) - \sqrt{2\pi B}(a+h-c)\text{erf}(\sqrt{2B}(a+h-c)) - \\ &\left. - \sqrt{2\pi B}(b+h-d)\text{erf}(\sqrt{2B}(b+h-d)) + \sqrt{2\pi B}(b+h-c)\text{erf}(\sqrt{2B}(b+h-c)) \right) . \end{aligned} \quad (\text{B.3})$$

After some accounting one arrives at

$$\begin{aligned}
& \lim_{D \rightarrow \infty} \int_{-D}^D d\epsilon_r \int_{-D}^D d\epsilon_s (n_f(\epsilon_r) + n_f(\epsilon_s) - 2n_f(\epsilon_r)n_f(\epsilon_s))(\epsilon_r - \epsilon_s + h)^2 e^{-2B(\epsilon_r - \epsilon_s + h)^2} = \\
& = \lim_{D \rightarrow \infty} \left(\frac{1}{1 + 1/R} \left(\int_{-D}^{V/2} d\epsilon_r \int_{-D}^D d\epsilon_s + \int_{-D}^D d\epsilon_r \int_{-D}^{V/2} d\epsilon_s \right) + \right. \\
& \quad \left. + \frac{1}{1 + R} \left(\int_{-D}^{-V/2} d\epsilon_r \int_{-D}^D d\epsilon_s + \int_{-D}^D d\epsilon_r \int_{-D}^{-V/2} d\epsilon_s \right) - \right. \\
& \quad \left. - \frac{2}{(1 + R)^2} \int_{-D}^{-V/2} d\epsilon_r \int_{-D}^{-V/2} d\epsilon_s - \frac{2}{(1 + 1/R)^2} \int_{-D}^{V/2} d\epsilon_r \int_{-D}^{V/2} d\epsilon_s - \right. \\
& \quad \left. - \frac{2}{(1 + R)(1 + 1/R)} \left(\int_{-D}^{V/2} d\epsilon_r \int_{-D}^{-V/2} d\epsilon_s + \int_{-D}^{-V/2} d\epsilon_r \int_{-D}^{V/2} d\epsilon_s \right) \right) \times \\
& \quad \times (\epsilon_r - \epsilon_s + h)^2 e^{-2B(\epsilon_r - \epsilon_s + h)^2} \\
& = \frac{1}{8B^2} \frac{1}{(1 + R)(1 + 1/R)} \left(2(R + 1/R)e^{-2Bh^2} + 2e^{-2B(V+h)^2} + \right. \\
& \quad \left. + 2e^{-2B(V-h)^2} + \sqrt{2\pi B} \operatorname{erf}(\sqrt{2B}h)(R + 1/R) + \right. \\
& \quad \left. + \sqrt{2\pi B}(V + h)\operatorname{erf}(\sqrt{2B}(V + h)) + \sqrt{2\pi B}(V - h)\operatorname{erf}(\sqrt{2B}(V - h)) \right) . \quad (\text{B.4})
\end{aligned}$$

In equilibrium at $T > 0$ we use the approximation

$$\begin{aligned}
& \lim_{D \rightarrow \infty} \int_{-D}^D d\epsilon_r \int_{-D}^D d\epsilon_s (n_f(\epsilon_r) + n_f(\epsilon_s) - 2n_f(\epsilon_r)n_f(\epsilon_s))(\epsilon_r - \epsilon_s + h)^2 e^{-2B(\epsilon_r - \epsilon_s + h)^2} \approx \\
& \approx \int_{-\infty}^{\infty} d\epsilon_r (n_f(\epsilon_r) + n_f(\epsilon_r + h) - 2n_f(\epsilon_r)n_f(\epsilon_r + h)) \times \\
& \quad \times \int_{-\infty}^{\infty} d\epsilon_s (\epsilon_r - \epsilon_s + h)^2 e^{-2B(\epsilon_r - \epsilon_s + h)^2} \\
& = \frac{\sqrt{2\pi}}{8B^{3/2}} h \coth \left(\frac{h}{2T} \right) . \quad (\text{B.5})
\end{aligned}$$

B.2 Rewriting the 2-loop Scaling Equations

In this section we rewrite the 2-loop scaling equations (2.94) using a brute force approach. Note that the success of this approach cannot be seen before Eq. (B.13). The scaling equations are of the form

$$\frac{1}{g_{\perp}} \frac{dg_{\perp}}{dB} = -\frac{g_{\parallel}^2}{2\sqrt{B}} c_1 - \frac{g_{\perp}^2}{2\sqrt{B}} c_2 \quad (\text{B.6})$$

$$\frac{1}{g_{\parallel}} \frac{dg_{\parallel}}{dB} = -\frac{g_{\perp}^2}{\sqrt{B}} c_2. \quad (\text{B.7})$$

Rewriting Eq. (B.7) to an integral equation yields

$$g_{\parallel} = g_{\parallel}^* \exp \left[-\int_{B_0}^B d\tilde{B} \frac{g_{\perp}^2(\tilde{B})}{\sqrt{\tilde{B}}} c_2 \right]. \quad (\text{B.8})$$

The integral equation for Eq. (B.6) is given by

$$g_{\perp} = g_{\perp}^* \sqrt{\frac{g_{\parallel}}{g_{\parallel}^*}} \exp \left[-\int_{B_0}^B d\tilde{B} \frac{g_{\parallel}^2(\tilde{B})}{2\sqrt{\tilde{B}}} c_1 \right], \quad (\text{B.9})$$

where we used Eq. (B.8). By inserting Eq. (B.9) in Eq. (B.7) we derived an equation containing g_{\parallel} only:

$$\frac{dg_{\parallel}}{dB} = -\frac{(g_{\perp}^*)^2 c_2}{g_{\parallel}^* \sqrt{B}} g_{\parallel}^2 \exp \left[-\int_{B_0}^B d\tilde{B} \frac{g_{\parallel}^2(\tilde{B})}{\sqrt{\tilde{B}}} c_1 \right]. \quad (\text{B.10})$$

Using a simple mathematical trick we rewrite the latter equation to an expression with a full derivative on both sides:

$$\begin{aligned} \frac{dg_{\parallel}}{dB} &= \frac{(g_{\perp}^*)^2 c_2}{g_{\parallel}^* c_1} \left(-\frac{g_{\parallel}^2}{\sqrt{B}} c_1 \right) \exp \left[-\int_{B_0}^B d\tilde{B} \frac{g_{\parallel}^2(\tilde{B})}{\sqrt{\tilde{B}}} c_1 \right] \\ &= \frac{(g_{\perp}^*)^2 c_2}{g_{\parallel}^* c_1} \frac{d}{dB} \exp \left[-\int_{B_0}^B d\tilde{B} \frac{g_{\parallel}^2(\tilde{B})}{\sqrt{\tilde{B}}} c_1 \right]. \end{aligned} \quad (\text{B.11})$$

Integration of Eq. (B.11) yields

$$g_{\parallel} - g_{\parallel}^* = \frac{(g_{\perp}^*)^2 c_2}{g_{\parallel}^* c_1} \left(\exp \left[-\int_{B_0}^B d\tilde{B} \frac{g_{\parallel}^2(\tilde{B})}{\sqrt{\tilde{B}}} c_1 \right] - 1 \right). \quad (\text{B.12})$$

As final steps we remove the integral from the exponential by taking the logarithm and differentiating by B :

$$\begin{aligned}
\exp \left[- \int_{B_0}^B d\tilde{B} \frac{g_{\parallel}^2(\tilde{B})}{\sqrt{\tilde{B}}} c_1 \right] &= \frac{g_{\parallel}^* c_1}{(g_{\perp}^*)^2 c_2} (g_{\parallel} - g_{\parallel}^*) + 1 \\
- \int_{B_0}^B d\tilde{B} \frac{g_{\parallel}^2(\tilde{B})}{\sqrt{\tilde{B}}} c_1 &= \ln \left(\frac{g_{\parallel}^* c_1}{(g_{\perp}^*)^2 c_2} (g_{\parallel} - g_{\parallel}^*) + 1 \right) \\
- \frac{g_{\parallel}^2 c_1}{\sqrt{B}} &= \frac{1}{g_{\parallel} - g_{\parallel}^* + \frac{(g_{\perp}^*)^2 c_2}{g_{\parallel}^* c_1}} \frac{d}{dB} g_{\parallel} .
\end{aligned} \tag{B.13}$$

Rearranging the terms in Eq. (B.13) leads to

$$\frac{dg_{\parallel}}{dB} = - \frac{g_{\parallel}^3}{\sqrt{B}} c_1 - \frac{g_{\parallel}^2}{\sqrt{B}} \left(\frac{(g_{\perp}^*)^2}{g_{\parallel}^*} c_2 - g_{\parallel}^* c_1 \right) . \tag{B.14}$$

With Eq. (B.7) immediately follows

$$g_{\perp} = \sqrt{g_{\parallel}^2 \frac{c_1}{c_2} + g_{\parallel} \left(\frac{(g_{\perp}^*)^2}{g_{\parallel}^*} - g_{\parallel}^* \frac{c_1}{c_2} \right)} . \tag{B.15}$$

Appendix C

Commutators

C.1 Hamiltonian, 1-loop

$$\begin{aligned}
[\eta_0^\perp, H_\perp] &= -\frac{1}{2} \sum_{p,q,r,s} \left((\epsilon_p - \epsilon_q + h) J_\perp(p, q) J_\perp(r, s) + \right. \\
&\quad \left. + (\epsilon_r - \epsilon_s + h) J_\perp(r, s) J_\perp(p, q) \right) : f_{s\downarrow}^\dagger f_{r\uparrow} f_{p\uparrow}^\dagger f_{q\downarrow} : S^z - \\
&\quad - \frac{1}{2} \sum_{p,q} (n_f(p) + n_f(q) - 2n_f(p)n_f(q)) (\epsilon_p - \epsilon_q + h) (J_\perp(p, q))^2 S^z - \\
&\quad - \frac{1}{2} \sum_{p,q} (n_f(p) - n_f(q)) h J_\perp(p, q) J_\perp(q, p) - \\
&\quad - \frac{1}{4} \sum_{p,q,r} (1 - 2n_f(r)) (2\epsilon_r - \epsilon_p - \epsilon_q + 2h) J_\perp(r, q) J_\perp(r, p) : f_{p\downarrow}^\dagger f_{q\downarrow} : S^z + \\
&\quad + \frac{1}{4} \sum_{p,q,r} (1 - 2n_f(r)) (2\epsilon_r - \epsilon_p - \epsilon_q - 2h) J_\perp(p, r) J_\perp(q, r) : f_{p\uparrow}^\dagger f_{q\uparrow} : S^z - \\
&\quad - \frac{1}{8} \sum_{p,q,r} (2\epsilon_r - \epsilon_p - \epsilon_q + 2h) J_\perp(r, q) J_\perp(r, p) : f_{p\downarrow}^\dagger f_{q\downarrow} : - \\
&\quad - \frac{1}{8} \sum_{p,q,r} (2\epsilon_r - \epsilon_p - \epsilon_q - 2h) J_\perp(q, r) J_\perp(p, r) : f_{p\downarrow}^\dagger f_{q\downarrow} : \tag{C.1}
\end{aligned}$$

$$\begin{aligned}
[\eta_0, H_0] &= -\frac{1}{2} \sum_{p,q} (\epsilon_p - \epsilon_q)^2 \left(J^\uparrow(p, q) : f_{p\uparrow}^\dagger f_{q\uparrow} : - J^\downarrow(p, q) : f_{p\downarrow}^\dagger f_{q\downarrow} : \right) S^z - \\
&\quad - \frac{1}{2} \sum_{p,q} (\epsilon_p - \epsilon_q + h)^2 J_\perp(p, q) \left(: f_{p\uparrow}^\dagger f_{q\downarrow} : S^{-+} + : f_{q\downarrow}^\dagger f_{p\uparrow} : S^{+} \right) \tag{C.2}
\end{aligned}$$

$$\begin{aligned}
[\eta_0^\parallel, H_\parallel] &= \frac{1}{16} \sum_{p,q} (n_f(p) - n_f(q)) (\epsilon_p - \epsilon_q) \left((J^\uparrow(p, q))^2 + J^\downarrow(p, q)^2 \right) + \\
&+ \frac{1}{16} \sum_{p,q,r} (\epsilon_p + \epsilon_q - 2\epsilon_r) J^\uparrow(p, r) J^\uparrow(r, q) : f_{p\uparrow}^\dagger f_{q\uparrow} : + \\
&+ \frac{1}{16} \sum_{p,q,r} (\epsilon_p + \epsilon_q - 2\epsilon_r) J^\downarrow(p, r) J^\uparrow(r, q) : f_{p\downarrow}^\dagger f_{q\downarrow} : \quad (C.3)
\end{aligned}$$

$$\begin{aligned}
[\eta_0^\perp, H_\parallel] &= \frac{1}{4} \sum_{p,q,r,s} (\epsilon_p - \epsilon_q + h) J_\perp(p, q) \times \\
&\times \left(J^\uparrow(r, s) (: f_{p\uparrow}^\dagger f_{q\downarrow} f_{r\uparrow}^\dagger f_{s\uparrow} : S^- + : f_{q\downarrow}^\dagger f_{p\uparrow} f_{r\uparrow}^\dagger f_{s\uparrow} : S^+) - \right. \\
&- J^\downarrow(p, q) (: f_{p\uparrow}^\dagger f_{q\downarrow} f_{r\downarrow}^\dagger f_{s\downarrow} : S^- + : f_{q\downarrow}^\dagger f_{p\uparrow} f_{r\downarrow}^\dagger f_{s\downarrow} : S^+) \left. \right) + \\
&+ \frac{1}{8} \sum_{p,q,r} (1 - 2n_f(r)) \left((\epsilon_r - \epsilon_q + h) J_\perp(r, q) J^\uparrow(p, r) - \right. \\
&- (\epsilon_p - \epsilon_r + h) J_\perp(p, r) J^\downarrow(q, r) \left. \right) \left(: f_{p\uparrow}^\dagger f_{q\downarrow} : S^- + : f_{q\downarrow}^\dagger f_{p\uparrow} : S^+ \right) \quad (C.4)
\end{aligned}$$

$$\begin{aligned}
[\eta_0^\parallel, H_\perp] &= \frac{1}{4} \sum_{p,q,r,s} (\epsilon_p - \epsilon_q) J_\perp(r, s) \times \\
&\times \left(J^\uparrow(p, q) (- : f_{p\uparrow}^\dagger f_{q\uparrow} f_{r\uparrow}^\dagger f_{s\downarrow} : S^- + : f_{p\uparrow}^\dagger f_{q\uparrow} f_{s\downarrow}^\dagger f_{r\uparrow} : S^+) - \right. \\
&- J^\downarrow(p, q) (- : f_{p\downarrow}^\dagger f_{q\downarrow} f_{r\downarrow}^\dagger f_{s\downarrow} : S^- + : f_{p\downarrow}^\dagger f_{q\downarrow} f_{s\downarrow}^\dagger f_{r\uparrow} : S^+) \left. \right) + \\
&+ \frac{1}{8} \sum_{p,q,r} (1 - 2n_f(r)) \left((\epsilon_r - \epsilon_p) J^\uparrow(p, r) J_\perp(r, q) + \right. \\
&+ (\epsilon_r - \epsilon_q) J^\downarrow(r, q) J_\perp(p, r) \left. \right) \left(: f_{p\uparrow}^\dagger f_{q\downarrow} : S^- + : f_{q\downarrow}^\dagger f_{p\uparrow} : S^+ \right) \quad (C.5)
\end{aligned}$$

C.2 Hamiltonian, 2-loop

$$\begin{aligned}
[\eta_K^\uparrow, H_0] &= - \sum_{p,q,r,s} (\epsilon_p - \epsilon_q + \epsilon_r - \epsilon_s + h)^2 K^\uparrow(p, q, r, s) \times \\
&\times \left(: f_{p\uparrow}^\dagger f_{q\downarrow} f_{r\uparrow}^\dagger f_{s\uparrow} : S^- - : f_{q\downarrow}^\dagger f_{p\uparrow} f_{s\uparrow}^\dagger f_{r\uparrow} : S^+ \right) \quad (C.6)
\end{aligned}$$

$$[\eta_K^\downarrow, H_0] = - \sum_{p,q,r,s} (\epsilon_p - \epsilon_q + \epsilon_r - \epsilon_s + h)^2 K^\downarrow(p, q, r, s) \times \\ \times (: f_{p\uparrow}^\dagger f_{q\downarrow} f_{r\downarrow}^\dagger f_{s\downarrow} : S^- - : f_{q\downarrow}^\dagger f_{p\uparrow} f_{s\downarrow}^\dagger f_{r\downarrow} : S^+) \quad (\text{C.7})$$

$$[\eta_K^\perp, H_0] = - \sum_{p,q,r,s} (\epsilon_p - \epsilon_q + \epsilon_r - \epsilon_s)^2 K_\perp(p, q, r, s) : f_{p\uparrow}^\dagger f_{q\downarrow} f_{r\downarrow}^\dagger f_{s\uparrow} : S^z \quad (\text{C.8})$$

$$[\eta_K^\uparrow, H_\parallel] = \frac{1}{4} \sum_{p,q,r,s} (n_f(r) + n_f(s) - 2n_f(r)n_f(s)) (\epsilon_p - \epsilon_q + \epsilon_r - \epsilon_s + h) \times \\ \times (K^\uparrow(p, q, r, s) - K^\uparrow(r, q, p, s)) J^\uparrow(s, r) (: f_{p\uparrow}^\dagger f_{q\downarrow} : S^- + : f_{q\downarrow}^\dagger f_{p\uparrow} : S^+) \quad (\text{C.9})$$

$$[\eta_K^\downarrow, H_\parallel] = -\frac{1}{4} \sum_{p,q,r,s} (n_f(r) + n_f(s) - 2n_f(r)n_f(s)) (\epsilon_p - \epsilon_q + \epsilon_r - \epsilon_s + h) \times \\ \times (K^\downarrow(p, q, r, s) - K^\downarrow(p, s, r, q)) J^\downarrow(s, r) (: f_{p\uparrow}^\dagger f_{q\downarrow} : S^- + : f_{q\downarrow}^\dagger f_{p\uparrow} : S^+) \quad (\text{C.10})$$

$$[\eta_K^\perp, H_\parallel] = 0 \text{ (no spin operator)} \quad (\text{C.11})$$

$$[\eta_K^\uparrow, H_\perp] = -\frac{1}{2} \sum_{p,q,r,s} (n_f(r) + n_f(s) - 2n_f(r)n_f(s)) \times \\ \times \left((\epsilon_p - \epsilon_q + \epsilon_r - \epsilon_s + h) (K^\uparrow(r, s, p, q) - K^\uparrow(p, s, r, q)) - \right. \\ \left. - (\epsilon_p - \epsilon_q - \epsilon_r + \epsilon_s - h) (K^\uparrow(r, s, q, p) - K^\uparrow(q, s, r, p)) \right) \times \\ \times J_\perp(r, s) : f_{p\uparrow}^\dagger f_{q\uparrow} : S^z \quad (\text{C.12})$$

$$[\eta_K^\downarrow, H_\perp] = -\frac{1}{2} \sum_{p,q,r,s} (n_f(r) + n_f(s) - 2n_f(r)n_f(s)) \times \\ \times \left((\epsilon_p - \epsilon_q + \epsilon_r - \epsilon_s + h) (K^\downarrow(r, s, p, q) - K^\downarrow(r, q, p, s)) - \right. \\ \left. - (\epsilon_p - \epsilon_q - \epsilon_r + \epsilon_s - h) (K^\downarrow(r, s, q, p) - K^\downarrow(r, p, q, s)) \right) \times \\ \times J_\perp(r, s) : f_{p\downarrow}^\dagger f_{q\downarrow} : S^z \quad (\text{C.13})$$

$$[\eta_K^\perp, H_\perp] = -\frac{1}{4} \sum_{p,q,r,s} (n_f(r) + n_f(s) - 2n_f(r)n_f(s)) (\epsilon_p - \epsilon_q + \epsilon_r - \epsilon_s) \times \\ \times K_\perp(p, q, r, s) J_\perp(s, r) (: f_{p\uparrow}^\dagger f_{q\downarrow} : S^- + : f_{q\downarrow}^\dagger f_{p\uparrow} : S^+) \quad (\text{C.14})$$

$$\begin{aligned}
[\eta_0, H_K^\uparrow] &= \frac{1}{4} \sum_{p,q,r,s} (n_f(r) + n_f(s) - 2n_f(r)n_f(s))(\epsilon_r - \epsilon_s) J^\uparrow(s, r) \times \\
&\times (K^\uparrow(p, q, r, s) - K^\uparrow(r, q, p, s)) (: f_{p\uparrow}^\dagger f_{q\downarrow} : S^- + : f_{q\downarrow}^\dagger f_{p\uparrow} : S^+) - \\
&- \frac{1}{2} \sum_{p,q,r,s} (n_f(r) + n_f(s) - 2n_f(r)n_f(s))(\epsilon_r - \epsilon_s + h) J_\perp(r, s) \times \\
&\times (K^\uparrow(r, s, p, q) - K^\uparrow(p, s, r, q) + K^\uparrow(r, s, q, p) - K^\uparrow(q, s, r, p)) \times \\
&\times : f_{p\uparrow}^\dagger f_{q\uparrow} : S^z \tag{C.15}
\end{aligned}$$

$$\begin{aligned}
[\eta_0, H_K^\downarrow] &= -\frac{1}{4} \sum_{p,q,r,s} (n_f(r) + n_f(s) - 2n_f(r)n_f(s))(\epsilon_r - \epsilon_s) J^\downarrow(s, r) \times \\
&\times (K^\downarrow(p, q, r, s) - K^\downarrow(p, s, r, q)) (: f_{p\uparrow}^\dagger f_{q\downarrow} : S^- + : f_{q\downarrow}^\dagger f_{p\uparrow} : S^+) - \\
&\frac{1}{2} \sum_{p,q,r,s} (n_f(r) + n_f(s) - 2n_f(r)n_f(s))(\epsilon_r - \epsilon_s + h) J_\perp(r, s) \times \\
&\times (K^\downarrow(r, s, q, p) - K^\downarrow(r, p, q, s) - K^\downarrow(r, q, p, s) + K^\downarrow(r, s, p, q)) \times \\
&\times : f_{p\downarrow}^\dagger f_{q\downarrow} : S^z \tag{C.16}
\end{aligned}$$

$$\begin{aligned}
[\eta_0, H_K^\perp] &= \frac{1}{4} \sum_{p,q,r,s} (n_f(r) + n_f(s) - 2n_f(r)n_f(s))(\epsilon_s - \epsilon_r + h) J_\perp(s, r) \times \\
&\times K_\perp(p, q, r, s) (: f_{p\uparrow}^\dagger f_{q\downarrow} : S^- + : f_{q\downarrow}^\dagger f_{p\uparrow} : S^+) \tag{C.17}
\end{aligned}$$

C.3 Trafo S^z

$$[\eta_0, h^z S^z] = \frac{h^z}{2} \sum_{p,q} (\epsilon_p - \epsilon_q + h) J_\perp(p, q) (: f_{p\uparrow}^\dagger f_{q\downarrow} : S^- + : f_{q\downarrow}^\dagger f_{p\uparrow} : S^+) \tag{C.18}$$

$$[\eta_0, \frac{M}{2}] = 0 \tag{C.19}$$

$$\begin{aligned}
[\eta_0^\perp, S^\perp] &= \frac{1}{2} \sum_{p,q} (n_f(p) - n_f(q))(\epsilon_p - \epsilon_q + h) J_\perp(p, q) \gamma_{pq} - \\
&- \sum_{p,q} (n_f(p) + n_f(q) - 2n_f(p)n_f(q))(\epsilon_p - \epsilon_q + h) J_\perp(p, q) \gamma_{pq} S^z \tag{C.20}
\end{aligned}$$

$$\begin{aligned}
[\eta_0^\parallel, S^\perp] &= \frac{1}{4} \sum_{p,q,r} (1 - 2n_f(r))((\epsilon_r - \epsilon_p) J^\uparrow(p, r) \gamma_{rq} + (\epsilon_r - \epsilon_q) J^\downarrow(r, q) \gamma_{pr}) \times \\
&\times (: f_{p\uparrow}^\dagger f_{q\downarrow} : S^- + : f_{q\downarrow}^\dagger f_{p\uparrow} : S^+) \tag{C.21}
\end{aligned}$$

C.4 Trafo S^x

$$\begin{aligned}
[\eta_0, h^x S^x] &= i \frac{h^x}{2} \sum_{p,q} (\epsilon_p - \epsilon_q) (J^\dagger(p, q) : f_{p\uparrow}^\dagger f_{q\uparrow} : - J^\downarrow(p, q) : f_{p\downarrow}^\dagger f_{q\downarrow} :) S^y - \\
&\quad - \frac{h^x}{2} \sum_{p,q} (\epsilon_p - \epsilon_q + h) J_\perp(p, q) (: f_{p\uparrow}^\dagger f_{q\downarrow} : + : f_{q\downarrow}^\dagger f_{p\uparrow} :) S^z \quad (C.22)
\end{aligned}$$

$$[\eta_0^\parallel, S_\uparrow^x] = \frac{1}{4} \sum_{p,q} (n_f(p) + n_f(q) - 2n_f(p)n_f(q)) (\epsilon_p - \epsilon_q) J^\dagger(p, q) \mu^\uparrow(q, p) S^x \quad (C.23)$$

$$[\eta_0^\parallel, S_\downarrow^x] = -\frac{1}{4} \sum_{p,q} (n_f(p) + n_f(q) - 2n_f(p)n_f(q)) (\epsilon_p - \epsilon_q) J^\downarrow(p, q) \mu^\downarrow(q, p) S^x \quad (C.24)$$

$$[\eta_0^\parallel, S_z^x] = \text{no spin operator} \quad (C.25)$$

$$\begin{aligned}
[\eta_0^\perp, S_\uparrow^x] &= -\frac{1}{4} \sum_{p,q,r} (1 - 2n_f(r)) (\epsilon_r - \epsilon_q + h) J_\perp(r, q) \mu^\uparrow(p, r) : f_{p\uparrow}^\dagger f_{q\downarrow} : S^z + \\
&\quad + \frac{1}{4} \sum_{p,q,r} (1 - 2n_f(r)) (\epsilon_r - \epsilon_q + h) J_\perp(r, q) \mu^\uparrow(r, p) : f_{q\downarrow}^\dagger f_{p\uparrow} : S^z \quad (C.26)
\end{aligned}$$

$$\begin{aligned}
[\eta_0^\perp, S_\downarrow^x] &= -\frac{1}{4} \sum_{p,q,r} (1 - 2n_f(r)) (\epsilon_p - \epsilon_r + h) J_\perp(p, r) \mu^\downarrow(r, q) : f_{p\uparrow}^\dagger f_{q\downarrow} : S^z + \\
&\quad + \frac{1}{4} \sum_{p,q,r} (1 - 2n_f(r)) (\epsilon_p - \epsilon_r + h) J_\perp(p, r) \mu^\downarrow(q, r) : f_{q\downarrow}^\dagger f_{p\uparrow} : S^z \quad (C.27)
\end{aligned}$$

$$\begin{aligned}
[\eta_0^\perp, S_z^x] &= \frac{1}{2} \sum_{p,q} (n_f(p) + n_f(q) - 2n_f(p)n_f(q)) (\epsilon_p - \epsilon_q + h) J_\perp(p, q) \mu^z(p, q) S^x - \\
&\quad - \frac{i}{4} \sum_{p,q,r} (1 - 2n_f(r)) (\epsilon_p - \epsilon_r + h) J_\perp(p, r) \mu^z(q, r) : f_{p\uparrow}^\dagger f_{q\uparrow} : S^y + \\
&\quad + \frac{i}{4} \sum_{p,q,r} (1 - 2n_f(r)) (\epsilon_q - \epsilon_r + h) J_\perp(q, r) \mu^z(p, r) : f_{p\uparrow}^\dagger f_{q\uparrow} : S^y - \\
&\quad - \frac{i}{4} \sum_{p,q,r} (1 - 2n_f(r)) (\epsilon_r - \epsilon_q + h) J_\perp(r, q) \mu^z(r, p) : f_{p\downarrow}^\dagger f_{q\downarrow} : S^y + \\
&\quad + \frac{i}{4} \sum_{p,q,r} (1 - 2n_f(r)) (\epsilon_r - \epsilon_p + h) J_\perp(r, p) \mu^z(r, q) : f_{p\downarrow}^\dagger f_{q\downarrow} : S^y \quad (C.28)
\end{aligned}$$

C.5 T-Matrix, Lowest Order

$$\begin{aligned}
[\eta_0^\parallel, O_\uparrow^\perp] &= -\frac{1}{2} \sum_{k,p,q} (\epsilon_p - \epsilon_q) J^\uparrow(p, q) U_k^\perp : f_{p\uparrow}^\dagger f_{q\uparrow} f_{k\downarrow} : S^- + \\
&\quad + \frac{1}{2} \sum_{k,p,q} (\epsilon_p - \epsilon_q) J^\downarrow(p, q) U_k^\perp : f_{p\downarrow}^\dagger f_{q\downarrow} f_{k\downarrow} : S^- + \\
&\quad + \frac{1}{4} \sum_{k,q} (\epsilon_k - \epsilon_q) J^\downarrow(k, q) U_k^\perp (1 - 2n_f(k)) : f_{q\downarrow} : S^- \quad (C.29)
\end{aligned}$$

$$\begin{aligned}
[\eta_0^\perp, O_\uparrow^\perp] &= - \sum_{k,p,q} (\epsilon_p - \epsilon_q + h) J_\perp(p, q) U_k^\perp : f_{q\downarrow}^\dagger f_{p\uparrow} f_{k\downarrow} : S^z - \\
&\quad - \frac{1}{2} \sum_{k,p} (1 - 2n_f(k)) (\epsilon_p - \epsilon_k + h) J_\perp(p, k) U_k^\perp : f_{p\uparrow} : S^z + \\
&\quad + \frac{1}{4} \sum_{k,p} (\epsilon_p - \epsilon_k + h) J_\perp(p, k) U_k^\perp : f_{p\uparrow} : \quad (C.30)
\end{aligned}$$

$$[\eta_0^\parallel, O_\uparrow^\parallel] = -\frac{1}{8} \sum_{k,q} (\epsilon_k - \epsilon_q) J^\uparrow(k, q) U_k^\uparrow : f_{q\uparrow} : \quad (C.31)$$

$$\begin{aligned}
[\eta_0^\perp, O_\uparrow^\parallel] &= \frac{1}{2} \sum_{k,p,q} (\epsilon_p - \epsilon_q + h) J_\perp(p, q) U_k^\uparrow \times \\
&\quad \times (: f_{p\uparrow}^\dagger f_{q\downarrow} f_{k\uparrow} : S^- + : f_{q\downarrow}^\dagger f_{p\uparrow} f_{k\uparrow} : S^+) + \\
&\quad + \frac{1}{4} \sum_{k,q} (1 - 2n_f(k)) (\epsilon_k - \epsilon_q + h) J_\perp(k, q) U_k^\uparrow : f_{q\downarrow} : S^- \quad (C.32)
\end{aligned}$$

$$\begin{aligned}
[\eta_0^\parallel, O_\uparrow^\perp] &= \frac{1}{4} \sum_{k,q} (1 - 2n_f(k)) (\epsilon_k - \epsilon_q) J^\uparrow(k, q) V_k^\perp : f_{q\uparrow} : S^+ + \quad (C.33) \\
&\quad + \frac{1}{2} \sum_{k,p,q} (\epsilon_p - \epsilon_q) V_k^\perp (J^\uparrow(p, q) : f_{p\uparrow}^\dagger f_{q\uparrow} f_{k\uparrow} : - J^\downarrow(p, q) : f_{p\downarrow}^\dagger f_{q\downarrow} f_{k\uparrow} :) S^+
\end{aligned}$$

$$\begin{aligned}
[\eta_0^\perp, O_\downarrow^\perp] &= -\frac{1}{2} \sum_{k,q} (1 - 2n_f(k)) (\epsilon_k - \epsilon_q + h) J_\perp(k, q) V_k^\perp : f_{q\downarrow} : S^z - \\
&\quad - \sum_{k,p,q} (\epsilon_p - \epsilon_q + h) J_\perp(p, q) V_k^\perp : f_{p\uparrow}^\dagger f_{q\downarrow} f_{k\uparrow} : S^z - \\
&\quad - \frac{1}{4} \sum_{k,q} (\epsilon_k - \epsilon_q + h) J_\perp(k, q) V_k^\perp : f_{q\downarrow} : \quad (C.34)
\end{aligned}$$

$$[\eta_0^\parallel, O_\downarrow^\parallel] = -\frac{1}{8} \sum_{k,q} (\epsilon_k - \epsilon_q) J^\perp(k, q) V_k^\perp : f_{q\downarrow} : \quad (\text{C.35})$$

$$\begin{aligned} [\eta_0^\perp, O_\downarrow^\parallel] &= -\frac{1}{4} \sum_{k,p} (1 - 2n_f(k)) (\epsilon_p - \epsilon_k + h) J_\perp(p, k) V_k^\perp : f_{p\uparrow} : S^+ - \\ &\quad -\frac{1}{4} \sum_{k,p,q} (\epsilon_p - \epsilon_q + h) J_\perp(p, q) V_k^\perp (: f_{p\uparrow}^\dagger f_{q\downarrow} f_{k\downarrow} : S^- + : f_{q\downarrow}^\dagger f_{p\uparrow} f_{k\downarrow} : S^+) \end{aligned} \quad (\text{C.36})$$

C.6 T-Matrix, Higher Order Terms

$$[\eta_0^\parallel, O_\uparrow^{U^-}] = -\frac{1}{4} \sum_{p,q,r} (n_f(p) + n_f(q) - 2n_f(p)n_f(q)) (\epsilon_p - \epsilon_q) J^\uparrow(p, q) U_\uparrow^-(q, p, r) f_{r\downarrow} S^- \quad (\text{C.37})$$

$$[\eta_0^\perp, O_\uparrow^{U^-}] = \frac{1}{2} \sum_{p,q,r} (n_f(p) + n_f(q) - 2n_f(p)n_f(q)) (\epsilon_p - \epsilon_q + h) J_\perp(p, q) U_\uparrow^-(p, r, q) f_{r\uparrow} S^z \quad (\text{C.38})$$

$$\begin{aligned} [\eta_0^\parallel, O_\uparrow^{U^-}] &= \frac{1}{4} \sum_{p,q,r} (n_f(p) + n_f(q) - 2n_f(p)n_f(q)) (\epsilon_p - \epsilon_q) \times \\ &\quad \times J^\perp(p, q) (U_\downarrow^-(q, p, r) - U_\downarrow^-(q, r, p)) f_{r\downarrow} S^- \end{aligned} \quad (\text{C.39})$$

$$[\eta_0^\parallel, O_\uparrow^{V^\uparrow}] = -\frac{1}{2} \sum_{p,q} (\epsilon_p - \epsilon_q) J^\uparrow(p, q) V_\uparrow(p) f_{q\uparrow} S^z \quad (\text{C.40})$$

$$[\eta_0^\parallel, O_\uparrow^{W^\uparrow}] = \frac{1}{4} \sum_{p,q,r} (n_f(p) + n_f(q) - 2n_f(p)n_f(q)) (\epsilon_p - \epsilon_q) J^\uparrow(p, q) W_\uparrow(q, r, p) f_{r\downarrow} S^- \quad (\text{C.41})$$

$$[\eta_0^\perp, O_\uparrow^{U^z}] = \frac{1}{4} \sum_{p,q,r} (n_f(p) + n_f(q) - 2n_f(p)n_f(q)) (\epsilon_p - \epsilon_q + h) J_\perp(p, q) U_\downarrow^z(p, q, r) f_{r\downarrow} S^- \quad (\text{C.42})$$

$$[\eta_0^\perp, O_\uparrow^{V^\uparrow}] = -\frac{1}{2} \sum_{p,q} (\epsilon_p - \epsilon_q + h) J_\perp(p, q) V_\uparrow(p) f_{q\downarrow} S^- \quad (\text{C.43})$$

$$\begin{aligned} [\eta_0^\perp, O_\uparrow^{W^\uparrow}] &= -\sum_{p,q,r} (n_f(p) + n_f(q) - 2n_f(p)n_f(q)) (\epsilon_p - \epsilon_q + h) \times \\ &\quad \times J_\perp(p, q) W_\uparrow(p, q, r) f_{r\uparrow} S^z + \\ &\quad + \frac{1}{2} \sum_{p,q,r} (n_f(p) + n_f(q) - 2n_f(p)n_f(q)) (\epsilon_p - \epsilon_q + h) \times \\ &\quad \times J_\perp(p, q) W_\uparrow(r, q, p) f_{r\uparrow} S^z \end{aligned} \quad (\text{C.44})$$

List of Figures

1.1	Minimum in the resistance of two gold wires (Au_1 and Au_2) at low temperature [2]. The resistance $R(T)$ is plotted in units of R_0 as function of the temperature T , where R_0 denotes the resistance at 273 K. The Au_1 - and the Au_2 -wire were made from the same source material. The Au_2 -wire has been additionally deformed to estimate effects by mechanical deformations of the wire on the residual resistance, the experimental setup is discussed in Ref. [1]. Note that the aim of the experiments [1–4] was to extract the so-called ideal resistance, the resistance due to scattering by thermal lattice vibrations.	6
1.2	Scanning electron microscope image of a quantum dot [18]. The middle electrode on the left controls the energy of the dot relative to the conduction band electrons, the other three control the tunnel barriers between the dot and the leads. The contacts for source and drain at the top and bottom are not shown.	7
1.3	In conventional scaling approaches states at high energies are successively integrated out. The scaling parameter Λ describes the progress: while states at energies larger than Λ are already integrated out, states at smaller energies are still retained in the Hamiltonian.	8
1.4	Using infinitesimal unitary transformations a Hamiltonian is brought into a banddiagonal form. The remaining effective bandwidth $\Delta\epsilon$ and the flow parameter B are related via $\Delta\epsilon = B^{-1/2}$. \tilde{D} is a shorthand notation for $D(B)$	9
1.5	Subfig. a) Schematic energy diagram of a quantum dot in the Coulomb blockade regime at zero magnetic field. The lower level at energy ϵ_d is occupied by a single electron (either spin-up or spin-down), the Coulomb repulsion for an additional electron in the upper level is given by U , and V denotes the voltage bias. Subfig. b) In equilibrium the dot's density of states shows a narrow resonance at the Fermi energies of the leads. The lower bump corresponds to the broadened level at ϵ_d . Subfig. c) In non-equilibrium the resonance is split in peaks at the upper and the lower chemical potential.	11

1.6	So-called Coulomb oscillations in the conductance G for the temperature range $15mK$ (thick black) to $800mK$ (thick red) at a magnetic field strength of 0.4 Tesla [23]. The gate voltage V_{gl} is used to alter the occupation of the quantum dot, in the valleys the total number of electrons in the dot is odd, at the peaks the electron number is even. Upon cooling the conductance in the middle valley (and also in the right one) is increased up to the maximal value $G = 2e^2/h$, the so-called unitary limit. Here e is the electronic charge and h is Planck's constant. The left inset shows the same setup as in Fig. 1.5 a), $\Gamma_{L,R}$ is the level broadening Δ (see Sect. 1.1.2) of the dot level by the hybridization with the left and the right lead, the chemical potential is given by $\mu_{L,R} = \pm V/2$, and finally $\epsilon_0 = \epsilon_d$. The inset on the right shows the logarithmic dependence of the center valley's height on the temperature.	12
1.7	Schematic picture of a quantum dot in the Kondo regime coupled to two leads at the chemical potentials $\mu_{l,r} = \pm V/2$. The dot levels are split by an applied magnetic field. Note that in the Kondo model the dot level position ϵ_d enters only indirectly via the coupling J , see Eqs. (1.3) and (1.4). For a sketch it is convenient to set $\epsilon_d = 0$.	13
1.8	Sketch of the Keldysh contour C in the complex time plane (for $t \rightarrow \infty$): the time evolution starts at $t = 0$ and ends at $t = -i\beta$.	20
1.9	If the RG-bandwidth Λ becomes smaller than the voltage bias, energy diagonal scattering processes between the two leads are impossible. In the flow equations picture these are still included in the Hamiltonian.	21
1.10	Tunneling in an asymmetric double well potential: Two levels with energy splitting ϵ are connected by the tunneling rate Δ .	25
1.11	Flow of $\epsilon(B)$ and $\Delta(B)$ for the initial values $\epsilon_0 = \Delta_0 = 1$.	28
1.12	Normal-ordering is similar to the reduction of diagrams. While Subfig. a) is reducible to simpler objects (by cutting the straight line) Subfig. b) is irreducible.	31
2.1	Flow of $J^\perp(p, q)$ at $h = 0.25$ ($V = T = 0$) for $B = 10, 100, 500$ from top to bottom. Red points: full system, green points: diagonal parametrization (see text).	53
2.2	Phase portrait for the 1-loop scaling equations of the anisotropic Kondo model. There exist two important regimes, the (white) strong coupling regime where the running coupling flows to infinity and the weak coupling regime where g_\perp flows to zero. In the literature the parameter regime $g_\parallel > 0$ is typically called antiferromagnetic (AFM) regime, $g_\parallel < 0$ is the ferromagnetic (FM) regime.	61
2.3	Comparison 2-loop scaling equations of the anisotropic Kondo model in a magnetic field with the standard 1-loop scaling equations in zero magnetic field. Note that the 2-loop phase portrait is not universal, the colored curves were calculated for $h = 0.05$ and $B_0 = D^{-2} = 1$.	63

2.4	Comparison 2-loop scaling equations of the non-equilibrium anisotropic Kondo model with the standard 1-loop scaling equations. The colored curves were calculated for $V = 0.05$, $R = 1$ and $B_0 = D^{-2} = 1$	64
2.5	Comparison 2-loop scaling equations of the anisotropic Kondo model at $T > 0$ with the standard 1-loop scaling equations. The colored curves were calculated for $T = 0.05$ and $B_0 = D^{-2} = 1$	65
3.1	Comparison magnetization from Eq. (3.51) with numerical results for $D = 10^3 T_K$. The inset shows the bandwidth dependence of the magnetization at $h = 100 T_K$	77
3.2	S^z correlation function for various magnetic fields ($V=T=0$). The inset shows the power law behavior of the peak height as function of the magnetic field.	80
3.3	Imaginary part of spin-down T-Matrix as function of the magnetic field ($D = 10^3 T_K$). The inset shows a comparison with the asymptotic Bethe Ansatz result for $\omega = 0$	88
3.4	Universal curves for a) the spin-spin correlation function $C^z(\omega)$ and b) the imaginary part of the dynamical spin susceptibility $\chi''(\omega)$ at nonzero temperature and zero magnetic field.	90
3.5	Universal curves for a) the spin-spin correlation function $C^z(\omega)$ and b) the imaginary part of the dynamical spin susceptibility $\chi''(\omega)$ in non-equilibrium for symmetric coupling $R = 1$ and zero magnetic field.	90
3.6	Universal curves for a) the spin-spin correlation function $C^z(\omega)$ and b) the imaginary part of the dynamical spin susceptibility $\chi''(\omega)$ in non-equilibrium for asymmetric coupling $R = 2$ and zero magnetic field.	91
3.7	Universal curves for a) the spin-spin correlation function $C^z(\omega)$ and b) the imaginary part of the dynamical spin susceptibility $\chi''(\omega)$ in non-equilibrium for asymmetric coupling of the leads and zero magnetic field. The voltage bias is fixed at $V = 100 T_K$	91
3.8	Decaying zero frequency structure of correlation function with increasing magnetic field, a) $V = 20 T_K$, b) $T = 20 T_K$	92
3.9	Typical buildup of the zero frequency peak in the non-equilibrium correlation function for $V \sim h$. For decreasing h the peaks at $\omega \approx h - V$ join to build up the zero frequency peak. In the regime $h \leq V$ we find a small structure at $\omega \approx h$. The inset shows typical equilibrium correlation functions for nonzero temperatures $T \sim h$. Here all structures except the zero frequency peak are smeared out.	92
3.10	a) Splitting of the structure in the correlation function ($h = 100 T_K$) due to a small voltage bias. b) Small temperatures lead to broadening.	93
3.11	Sum of spectral functions for both spin components at zero magnetic field for various values of a) voltage bias and b) temperature.	93
3.12	An applied magnetic field shifts the central structure of the spectral function, a) $V = 20 T_K$, b) $T = 20 T_K$	94

3.13	a) Splitting of the structure in the spectral function at h due to a small voltage bias. b) Again a small temperature leads to broadening of the latter structure.	94
3.14	Comparison of calculated magnetization with previous zeroth order results a) for fixed temperature and b) for fixed voltage bias at $D = 100T_K$. For increasing temperature or voltage bias the curves are getting closer to the Bethe Ansatz respectively the non-equilibrium perturbation theory (quantum Boltzmann and rate equation) result.	95
3.15	Crossover from the equilibrium zero temperature magnetization to a) the high temperature and b) the high voltage result at $D = 100T_K$	95
3.16	Static spin susceptibility at nonzero voltage bias and nonzero temperature (equilibrium). The equilibrium curve agrees well with the asymptotic Bethe Ansatz result for $T \gg T_K$	98
3.17	Static spin susceptibility χ_0 at nonzero voltage bias for various asymmetry parameters R , the asymmetry parameter increases from bottom to top: $R = 1.0, 1.4, 1.8, 2.2, 2.6, 3.0$. The dashed line is the exact result in the limit of strong asymmetry ($R \rightarrow \infty$ or $R \rightarrow 0$). A zoom on the small voltage bias region is shown in the inset.	98
4.1	Schematic picture of a quantum dot coupled to two leads at different temperature. $T_{l/r}$ labels the temperature of the left and right lead.	102
4.2	Universal curve for the effective temperature in thermal non-equilibrium (4.17). The inset shows the universal curve for T_{lr} defined in Eq. (4.16). . .	105
4.3	Static spin susceptibility in thermal non-equilibrium, the curves for $T_r/T_l \gtrsim 0.6$ lie within the error bars of the equilibrium curve ($T_r = T_l$).	106

Bibliography

- [1] W.J. de Haas and J. de Boer. The electrical resistance of platinum at low temperatures. *Physica*, 1(7-12):609 – 616, 1934.
DOI: [http://dx.doi.org/10.1016/S0031-8914\(34\)80247-9](http://dx.doi.org/10.1016/S0031-8914(34)80247-9) .
- [2] W.J. de Haas, J. de Boer, and G.J. van den Berg. The electrical resistance of gold, copper and lead at low temperatures. *Physica*, 1(7-12):1115 – 1124, 1934.
DOI: [http://dx.doi.org/10.1016/S0031-8914\(34\)80310-2](http://dx.doi.org/10.1016/S0031-8914(34)80310-2) .
- [3] W.J. de Haas, J. de Boer, and G.J. van den Berg. The electrical resistance of cadmium, thallium and tin at low temperatures. *Physica*, 2(1-12):453 – 459, 1935.
DOI: [http://dx.doi.org/10.1016/S0031-8914\(35\)90114-8](http://dx.doi.org/10.1016/S0031-8914(35)90114-8) .
- [4] W.J. de Haas and G.J. van den Berg. The electrical resistance of gold and silver at low temperatures. *Physica*, 3(6):440 – 449, 1936.
DOI: [http://dx.doi.org/10.1016/S0031-8914\(36\)80009-3](http://dx.doi.org/10.1016/S0031-8914(36)80009-3) .
- [5] A. C. Hewson. *The Kondo Problem to Heavy Fermions*. Cambridge Uni. Press, 1997.
ISBN: 0521599474.
- [6] Kenneth G. Wilson. The renormalization group: Critical phenomena and the kondo problem. *Rev. Mod. Phys.*, 47(4):773–840, Oct 1975.
DOI: <http://dx.doi.org/10.1103/RevModPhys.47.773> .
- [7] N. Andrei, K. Furuya, and J. H. Lowenstein. Solution of the kondo problem. *Rev. Mod. Phys.*, 55(2):331–402, Apr 1983.
DOI: <http://dx.doi.org/10.1103/RevModPhys.55.331> .
- [8] A. M. Tsvelick and P. B. Wiegmann. Exact results in the theory of magnetic alloys. *Adv. Phys.*, 32:453–713, 1983.
DOI: <http://dx.doi.org/10.1080/00018738300101581> .
- [9] T. A. Costi. Kondo effect in a magnetic field and the magnetoresistivity of kondo alloys. *Phys. Rev. Lett.*, 85(7):1504–1507, Aug 2000.
DOI: <http://dx.doi.org/10.1103/PhysRevLett.85.1504> .

- [10] Ralf Bulla, Theo A. Costi, and Thomas Pruschke. Numerical renormalization group method for quantum impurity systems. *Rev. Mod. Phys.*, 80:395, 2008.
DOI: <http://dx.doi.org/10.1103/RevModPhys.80.395> .
- [11] A. Rosch, T. A. Costi, J. Paaske, and P. Wölfle. Spectral function of the kondo model in high magnetic fields. *Phys. Rev. B*, 68(1):014430, Jul 2003.
DOI: <http://dx.doi.org/10.1103/PhysRevB.68.014430> .
- [12] D. E. Logan and N. L. Dickens. Magnetic properties of the anderson model: A local moment approach. *Europhys. Lett.*, 54(2):227–233, Apr 2001.
DOI: <http://dx.doi.org/10.1209/epl/i2001-00299-3> .
- [13] N. L. Dickens and D. E. Logan. On the scaling spectrum of the anderson impurity model. *J. Phys.: Cond. Matt.*, 13(20):4505–4517, 2001.
DOI: <http://dx.doi.org/10.1088/0953-8984/13/20/311> .
- [14] T. A. Costi and C. Kieffer. Equilibrium dynamics of the dissipative two-state system. *Phys. Rev. Lett.*, 76(10):1683–1686, Mar 1996.
DOI: <http://dx.doi.org/10.1103/PhysRevLett.76.1683> .
- [15] Maura Sasseti and Ulrich Weiss. Correlation functions for dissipative two-state systems: Effects of the initial preparation. *Phys. Rev. A*, 41(10):5383–5393, May 1990.
DOI: <http://dx.doi.org/10.1103/PhysRevA.41.5383> .
- [16] W. Hofstetter and S. Kehrein. Flow equation analysis of the anisotropic kondo model. *Phys. Rev. B*, 63(14):140402, Mar 2001.
DOI: <http://dx.doi.org/10.1103/PhysRevB.63.140402> .
- [17] Joel E. Moore and Xiao-Gang Wen. Anomalous magnetic splitting of the kondo resonance. *Phys. Rev. Lett.*, 85(8):1722–1725, Aug 2000.
DOI: <http://dx.doi.org/10.1103/PhysRevLett.85.1722> .
- [18] D. Goldhaber-Gordon, Hadas Shtrikman, D. Mahalu, David Abusch-Magder, U. Meirav, and M. A. Kastner. Kondo effect in a single-electron transistor. *Nature*, 391:156–159, 1998.
DOI: <http://dx.doi.org/10.1038/34373> .
- [19] Sara M. Cronenwett, Tjerk H. Oosterkamp, and Leo P. Kouwenhoven. A Tunable Kondo Effect in Quantum Dots. *Science*, 281(5376):540–544, 1998.
DOI: <http://dx.doi.org/10.1126/science.281.5376.540> .
- [20] J. Schmid, J. Weis, K. Eberl, and K. v. Klitzing. A quantum dot in the limit of strong coupling to reservoirs. *Physica B: Cond. Matt.*, 256-258:182–185, 1998.
DOI: [http://dx.doi.org/10.1016/S0921-4526\(98\)00533-X](http://dx.doi.org/10.1016/S0921-4526(98)00533-X) .

- [21] L. Glazman and M. Raikh. Resonant kondo transparency of a barrier with quasilocal impurity states. *JETP Lett.*, 47:452, 1988.
URL: http://www.jetpletters.ac.ru/ps/1095/article_16538.shtml .
- [22] Tai Kai Ng and Patrick A. Lee. On-site coulomb repulsion and resonant tunneling. *Phys. Rev. Lett.*, 61(15):1768–1771, Oct 1988.
DOI: <http://dx.doi.org/10.1103/PhysRevLett.61.1768> .
- [23] W. G. van der Wiel, S. De Franceschi, T. Fujisawa, J. M. Elzerman, S. Tarucha, and L. P. Kouwenhoven. The Kondo Effect in the Unitary Limit. *Science*, 289(5487):2105–2108, 2000.
DOI: <http://dx.doi.org/10.1126/science.289.5487.2105> .
- [24] Frithjof B. Anders. Steady-state currents through nanodevices: A scattering-states numerical renormalization-group approach to open quantum systems. *Phys. Rev. Lett.*, 101(6):066804, 2008.
DOI: <http://dx.doi.org/10.1103/PhysRevLett.101.066804> .
- [25] E. Boulat, H. Saleur, and P. Schmitteckert. Twofold advance in the theoretical understanding of far-from-equilibrium properties of interacting nanostructures. *Phys. Rev. Lett.*, 101(14):140601, 2008.
DOI: <http://dx.doi.org/10.1103/PhysRevLett.101.140601> .
- [26] Pankaj Mehta and Natan Andrei. Nonequilibrium transport in quantum impurity models: The bethe ansatz for open systems. *Phys. Rev. Lett.*, 96(21):216802, 2006.
DOI: <http://dx.doi.org/10.1103/PhysRevLett.96.216802> .
- [27] Pankaj Mehta, Sung po Chao, and Natan Andrei. Erratum: Nonequilibrium transport in quantum impurity models (bethe-ansatz for open systems) [26]. 2007. arXiv:cond-mat/0703426
URL: <http://arxiv.org/abs/cond-mat/0703426> .
- [28] E. Abrahams, P. W. Anderson, D. C. Licciardello, and T. V. Ramakrishnan. Scaling theory of localization: Absence of quantum diffusion in two dimensions. *Phys. Rev. Lett.*, 42(10):673–676, Mar 1979.
DOI: <http://dx.doi.org/10.1103/PhysRevLett.42.673> .
- [29] J. R. Schrieffer and P. A. Wolff. Relation between the anderson and kondo hamiltonians. *Phys. Rev.*, 149(2):491–492, Sep 1966.
DOI: <http://dx.doi.org/10.1103/PhysRev.149.491> .
- [30] Tadao Kasuya. A theory of metallic ferro- and antiferromagnetism on zener’s model. *Prog. Theor. Phys.*, 16(1):45, 1956.
DOI: <http://dx.doi.org/10.1143/PTP.16.45> .

- [31] C. Zener. Interaction between the d shells in the transition metals. *Phys. Rev.*, 81(3):440–444, Feb 1951.
DOI: <http://dx.doi.org/10.1103/PhysRev.81.440> .
- [32] Stefan K. Kehrein and Andreas Mielke. Theory of the anderson impurity model: The schrieffer-wolff transformation reexamined. *Annals of Physics*, 252(1):1 – 32, 1996.
DOI: <http://dx.doi.org/10.1006/aphy.1996.0123> .
- [33] J. Kondo. Resistance minimum in dilute magnetic alloys. *Prog. Theor. Phys.*, 32:37, 1964.
DOI: <http://dx.doi.org/10.1143/PTP.32.37> .
- [34] P. Fritsch. Flow equation solution of the kondo model with nontrivial density of states, 2004. Diplomarbeit (master thesis) at Universität Augsburg.
URL: http://www.physik.uni-augsburg.de/theo3/Theses/fritsch_dipl.pdf .
- [35] P W Anderson. A poor man’s derivation of scaling laws for the kondo problem. *J. of Phys. C*, 3(12):2436–2441, 1970.
DOI: <http://dx.doi.org/10.1088/0022-3719/3/12/008> .
- [36] A. Rosch, J. Kroha, and P. Wölfle. Kondo effect in quantum dots at high voltage: Universality and scaling. *Phys. Rev. Lett.*, 87(15):156802, Sep 2001.
DOI: <http://dx.doi.org/10.1103/PhysRevLett.87.156802> .
- [37] A. Rosch, J. Paaske, J. Kroha, and P. Wölfle. Nonequilibrium transport through a kondo dot in a magnetic field: Perturbation theory and poor man’s scaling. *Phys. Rev. Lett.*, 90(7):076804, Feb 2003.
DOI: <http://dx.doi.org/10.1103/PhysRevLett.90.076804> .
- [38] A. Rosch, J. Paaske, J. Kroha, and P. Wölfle. The kondo effect in non-equilibrium quantum dots: Perturbative renormalization group. *J. Phys. Soc. Jpn.*, 74:118–126, 2005.
DOI: <http://dx.doi.org/10.1143/JPSJ.74.118> .
- [39] R. Scheibner, H. Buhmann, D. Reuter, M. N. Kiselev, and L. W. Molenkamp. Thermopower of a kondo spin-correlated quantum dot. *Phys. Rev. Lett.*, 95(17):176602, Oct 2005.
DOI: <http://dx.doi.org/10.1103/PhysRevLett.95.176602> .
- [40] S. Kehrein. Scaling and decoherence in the nonequilibrium kondo model. *Phys. Rev. Lett.*, 95(5):056602, 2005.
DOI: <http://dx.doi.org/10.1103/PhysRevLett.95.056602> .
- [41] S. Kehrein. *The Flow Equation Approach to Many Particle Systems*. Springer, Berlin, 2006.
DOI: <http://dx.doi.org/10.1007/3-540-34068-8> .

- [42] A. Kaminski, Yu. V. Nazarov, and L. I. Glazman. Suppression of the kondo effect in a quantum dot by external irradiation. *Phys. Rev. Lett.*, 83(2):384–387, Jul 1999.
DOI: <http://dx.doi.org/10.1103/PhysRevLett.83.384> .
- [43] A. Kaminski, Yu. V. Nazarov, and L. I. Glazman. Universality of the kondo effect in a quantum dot out of equilibrium. *Phys. Rev. B*, 62(12):8154–8170, Sep 2000.
DOI: <http://dx.doi.org/10.1103/PhysRevB.62.8154> .
- [44] P. Coleman, C. Hooley, and O. Parcollet. Is the quantum dot at large bias a weak-coupling problem? *Phys. Rev. Lett.*, 86(18):4088–4091, Apr 2001.
DOI: <http://dx.doi.org/10.1103/PhysRevLett.86.4088> .
- [45] J. Paaske, A. Rosch, J. Kroha, and P. Wölfle. Nonequilibrium transport through a kondo dot: Decoherence effects. *Phys. Rev. B*, 70(15):155301, Oct 2004.
DOI: <http://dx.doi.org/10.1103/PhysRevB.70.155301> .
- [46] J. Paaske, A. Rosch, and P. Wölfle. Nonequilibrium transport through a kondo dot in a magnetic field: Perturbation theory. *Phys. Rev. B*, 69(15):155330, 2004.
DOI: <http://dx.doi.org/10.1103/PhysRevB.69.155330> .
- [47] Herbert Schoeller. An introduction to real-time renormalization group. *Lect. Notes Phys.*, 544:137, 2000.
DOI: http://dx.doi.org/10.1007/3-540-46438-7_7 .
- [48] Severin G. Jakobs, Volker Meden, and Herbert Schoeller. Nonequilibrium functional renormalization group for interacting quantum systems. *Phys. Rev. Lett.*, 99(15):150603, 2007.
DOI: <http://dx.doi.org/10.1103/PhysRevLett.99.150603> .
- [49] Herbert Schoeller and Frank Reininghaus. Real-time renormalization group in frequency space: A 2-loop analysis of the nonequilibrium anisotropic kondo model at finite magnetic field. 2009. arxiv:0902.1446
URL: <http://arxiv.org/abs/0902.1446> .
- [50] Herbert Schoeller. A perturbative nonequilibrium renormalization group method for dissipative quantum mechanics: Real-time rg in frequency space (rtrg-fs). 2009. arxiv:0902.1449
URL: <http://arxiv.org/abs/0902.1449> .
- [51] Aditi Mitra and A. J. Millis. Coulomb gas on the keldysh contour: Anderson-yuval-hamann representation of the nonequilibrium two-level system. *Phys. Rev. B*, 76(8):085342, 2007.
DOI: <http://dx.doi.org/10.1103/PhysRevB.76.085342> .
- [52] Dvira Segal, David R. Reichman, and Andrew J. Millis. Nonequilibrium quantum dissipation in spin-fermion systems. *Phys. Rev. B*, 76(19):195316, 2007.
DOI: <http://dx.doi.org/10.1103/PhysRevB.76.195316> .

- [53] O. Parcollet and C. Hooley. Perturbative expansion of the magnetization in the out-of-equilibrium kondo model. *Phys. Rev. B*, 66(8):085315, Aug 2002.
DOI: <http://dx.doi.org/10.1103/PhysRevB.66.085315> .
- [54] S. De Franceschi, R. Hanson, W. G. van der Wiel, J. M. Elzerman, J. J. Wijkema, T. Fujisawa, S. Tarucha, and L. P. Kouwenhoven. Out-of-equilibrium kondo effect in a mesoscopic device. *Phys. Rev. Lett.*, 89(15):156801, Sep 2002.
DOI: <http://dx.doi.org/10.1103/PhysRevLett.89.156801> .
- [55] W. Mao, P. Coleman, C. Hooley, and D. Langreth. Spin dynamics from majorana fermions. *Phys. Rev. Lett.*, 91(20):207203, Nov 2003.
DOI: <http://dx.doi.org/10.1103/PhysRevLett.91.207203> .
- [56] U. Walter, E. Holland-Moritz, and Z. Fisk. Kondo resonance in the neutron spectra of intermediate-valent *yba13*. *Phys. Rev. B*, 43(1):320–325, Jan 1991.
DOI: <http://dx.doi.org/10.1103/PhysRevB.43.320> .
- [57] W Marshall and R D Lowde. Magnetic correlations and neutron scattering. *Rep. Prog. Phys.*, 31(2):705–775, 1968.
DOI: <http://dx.doi.org/10.1088/0034-4885/31/2/305> .
- [58] Elihu Abrahams and Peter Wölfle. Electron spin resonance in kondo systems. *Phys. Rev. B*, 78(10):104423, 2008.
DOI: <http://dx.doi.org/10.1103/PhysRevB.78.104423> .
- [59] J. Sichelschmidt, V. A. Ivanshin, J. Ferstl, C. Geibel, and F. Steglich. Low temperature electron spin resonance of the kondo ion in a heavy fermion metal: *ybrh2si2*. *Phys. Rev. Lett.*, 91(15):156401, Oct 2003.
DOI: <http://dx.doi.org/10.1103/PhysRevLett.91.156401> .
- [60] C. Krellner, T. Förster, H. Jeevan, C. Geibel, and J. Sichelschmidt. Relevance of ferromagnetic correlations for the electron spin resonance in kondo lattice systems. *Phys. Rev. Lett.*, 100(6):066401, 2008.
DOI: <http://dx.doi.org/10.1103/PhysRevLett.100.066401> .
- [61] Paul Manneville. *Dissipative Structures and Weak Turbulence*. Academic Press Inc., 1990.
ISBN: 0124692605.
- [62] M. Greiner, O. Mandel, T. W. Hänsch, and I. Bloch. Collapse and revival of the matter wave field of a bose-einstein condensate. *Nature*, 419:51, 2002.
DOI: <http://dx.doi.org/10.1038/nature00968> .
- [63] T. Kinoshita, T. Wenger, and D. Weiss. A quantum newton’s cradle. *Nature*, 440:900, 2006.
DOI: <http://dx.doi.org/10.1038/nature04693> .

- [64] R. van Leeuwen, N.E. Dahlen, G. Stefanucci, C.-O. Almbladh, and U. von Barth. Introduction to the keldysh formalism. *Lect. Notes Phys.*, 706:33, 2006.
DOI: http://dx.doi.org/10.1007/3-540-35426-3_3 .
- [65] J. Rammer and H. Smith. Quantum field-theoretical methods in transport theory of metals. *Rev. Mod. Phys.*, 58(2):323–359, Apr 1986.
DOI: <http://dx.doi.org/10.1103/RevModPhys.58.323> .
- [66] F. Wegner. Flow-equations for hamiltonians. *Ann. Physik (Leipzig)*, 506(2):77–91, 1994.
DOI: <http://dx.doi.org/10.1002/andp.19945060203> .
- [67] G. C. Wick. The evaluation of the collision matrix. *Phys. Rev.*, 80(2):268–272, Oct 1950.
DOI: <http://dx.doi.org/10.1103/PhysRev.80.268> .
- [68] Jan von Delft and Herbert Schoeller. Bosonization for beginners - refermionization for experts. *Annalen der Physik*, 7:225–305, 1998.
DOI: [http://dx.doi.org/10.1002/\(SICI\)1521-3889\(199811\)7:4<225::AID-ANDP225>3.0.CO;2-L](http://dx.doi.org/10.1002/(SICI)1521-3889(199811)7:4<225::AID-ANDP225>3.0.CO;2-L) .
- [69] Douglas Adams. *The Hitchhiker's Guide to the Galaxy*. Del Rey, 1995.
ISBN: 0345391802.
- [70] A. J. Leggett, S. Chakravarty, A. T. Dorsey, Matthew P. A. Fisher, Anupam Garg, and W. Zwerger. Dynamics of the dissipative two-state system. *Rev. Mod. Phys.*, 59(1):1–85, Jan 1987.
DOI: <http://dx.doi.org/10.1103/RevModPhys.59.1> .
- [71] J. Sólyom and A. Zawadoski. Are the scaling laws for the kondo problem exact? *J. Phys. F*, 4(1):80–90, 1974.
DOI: <http://dx.doi.org/10.1088/0305-4608/4/1/009> .
- [72] K. Vladár and A. Zawadowski. Theory of the interaction between electrons and the two-level system in amorphous metals. ii. second-order scaling equations. *Phys. Rev. B*, 28(3):1582–1595, Aug 1983.
DOI: <http://dx.doi.org/10.1103/PhysRevB.28.1582> .
- [73] A. A. Abrikosov and A. A. Migdal. On the theory of the kondo effect. *J. Low Temp. Phys.*, 3:519–536, 1970.
DOI: <http://dx.doi.org/10.1007/BF00628220> .
- [74] M. Fowler and A. Zawadowski. Scaling and the renormalization group in the kondo effect. *Solid State Comm.*, 9(8):471 – 476, 1971.
DOI: [http://dx.doi.org/10.1016/0038-1098\(71\)90324-3](http://dx.doi.org/10.1016/0038-1098(71)90324-3) .

- [75] N. Andrei and J. H. Lowenstein. Scales and scaling in the kondo model. *Phys. Rev. Lett.*, 46(5):356–360, Feb 1981.
DOI: <http://dx.doi.org/10.1103/PhysRevLett.46.356> .
- [76] Herbert B. Callen and Theodore A. Welton. Irreversibility and generalized noise. *Phys. Rev.*, 83(1):34–40, Jul 1951.
DOI: <http://dx.doi.org/10.1103/PhysRev.83.34> .
- [77] D. C. Langreth. Friedel sum rule for anderson’s model of localized impurity states. *Phys. Rev.*, 150(2):516–518, Oct 1966.
DOI: <http://dx.doi.org/10.1103/PhysRev.150.516> .
- [78] P. Nozières. A fermi-liquid description of the kondo problem at low temperatures. *J. Low Temp. Phys.*, 17:31–42, Oct 1974.
DOI: <http://dx.doi.org/10.1007/BF00654541> .
- [79] N. Andrei. Calculation of the magnetoresistance in the kondo model. *Phys. Lett. A*, 87(6):299–302, 1982.
DOI: [http://dx.doi.org/10.1016/0375-9601\(82\)90702-2](http://dx.doi.org/10.1016/0375-9601(82)90702-2) .
- [80] V. M. Filyov, A. M. Tzvelik, and P. B. Wiegmann. Thermodynamics of the s-d exchange model (kondo problem). *Phys. Lett. A*, 81(2-3):175–178, January 1981.
DOI: [http://dx.doi.org/10.1016/0375-9601\(81\)90055-4](http://dx.doi.org/10.1016/0375-9601(81)90055-4) .
- [81] V. T. Rajan, J. H. Lowenstein, and N. Andrei. Thermodynamics of the kondo model. *Phys. Rev. Lett.*, 49(7):497–500, Aug 1982.
DOI: <http://dx.doi.org/10.1103/PhysRevLett.49.497> .
- [82] Pierre Dos Utt. *TANSTAAFL: a plan for a new economic world order*. Cairo Publications, 1949.
- [83] Björn Kubala, Jürgen König, and Jukka Pekola. Violation of the wiedemann-franz law in a single-electron transistor. *Phys. Rev. Lett.*, 100(6):066801, 2008.
DOI: <http://dx.doi.org/10.1103/PhysRevLett.100.066801> .
- [84] M. Krawiec and K. I. Wysokiński. Thermoelectric phenomena in a quantum dot asymmetrically coupled to external leads. *Phys. Rev. B*, 75(15):155330, 2007.
DOI: <http://dx.doi.org/10.1103/PhysRevB.75.155330> .
- [85] Björn Kubala and Jürgen König. Quantum-fluctuation effects on the thermopower of a single-electron transistor. *Phys. Rev. B*, 73(19):195316, 2006.
DOI: <http://dx.doi.org/10.1103/PhysRevB.73.195316> .
- [86] X. Zianni. Theory of the energy-spectrum dependence of the electronic thermoelectric tunneling coefficients of a quantum dot. *Phys. Rev. B*, 78(16):165327, 2008.
DOI: <http://dx.doi.org/10.1103/PhysRevB.78.165327> .

-
- [87] D. Boese and R. Fazio. Thermoelectric effects in kondo-correlated quantum dots. *Europhys. Lett.*, 56(4):576–582, nov 2001.
DOI: <http://dx.doi.org/10.1209/epl/i2001-00559-8> .
- [88] Bing Dong and X L Lei. Effect of the kondo correlation on the thermopower in a quantum dot. *J. Phys.: Cond. Matt.*, 14(45):11747–11756, 2002.
DOI: <http://dx.doi.org/10.1088/0953-8984/14/45/316> .
- [89] W. H. Press, S. A. Teukolsky, W. T. Vetterling, and B. P. Flannery. *Numerical Recipes (Third Edition)*. Cambridge Uni. Press, 2007.
ISBN: 0521880688, URL: <http://www.nr.com> .
- [90] The Four Marx Brothers. *Horse Feathers*. Paramount Pictures, 1932.

List of Publications

The results presented in this thesis were published in:

- Non-Equilibrium Scaling Analysis of the Kondo Model with Voltage Bias
P. Fritsch and S. Kehrein
Accepted for publication by Annals of Physics (2009); arXiv:0811.0759
DOI: <http://dx.doi.org/10.1016/j.aop.2009.01.004>
- Non-Equilibrium Kondo Model with Voltage Bias in a Magnetic Field
P. Fritsch and S. Kehrein
To be submitted to Phys. Rev. B; arXiv:0903.2865 (2009)
URL: <http://arxiv.org/abs/0903.2865>

Acknowledgments

Jennings: Pretty popular place, huh?

Professor Wagstaff: Yes, a hot dog stand would clean up here. [90]

First and foremost, I would like to thank my adviser Stefan Kehrein for guiding me through this project. It has been a great pleasure to discuss the physical problems with him. His stimulating and critical questions were crucial for gaining a deep insight into physical problems and their solution. I am grateful for the opportunity to attend numerous conferences and for the opportunity to have scientific collaborations with students.

I further thank Alexander Buchner, Markus Heyl, and Michael Möckel for umpteen stimulating discussions on flow equations, non-equilibrium physics, and life in general. Another big thanks goes to my office mates Ioana Serban, Jörn Kupferschmidt, Andreas Holzner, Maximilian Treiber, Alexander Hoffmann, and Korbinian Paul, I had a great time with you.

Thanks to all other group members. It has been a great pleasure to work with you. I especially thank Barbara “that’s not purple” Englert for numerous chats, Theresa Hecht for eating my candies, Wolfgang “Wolle” Münder for entertaining the whole corridor and for giving away muffins on a regular basis, Enrique Solano for many encouraging discussions, Hamed Saberi for organizing the one and only football match, and Alexandre Faribault for bringing some color in our group.

Further thanks goes to all my colleagues at the ASC, particularly to Anna Melbinger and Clemens Gneiting for many chats, and to Monika Kürzinger for feeding the coffee maker. A high caffeine level has been vital to accomplish this thesis.

I am deeply grateful to all my friends for always pushing me in the right direction. Especially, I thank Verena Körting for continuous support throughout my “scientific career”, particularly for proofreading my theses and publications.

Curriculum Vitae

Peter Fritsch
Diplom-Physiker Univ.

Born in Augsburg, Germany

Academic Education

October 2005 - March 2009 Ph.D. studies in Theoretical Condensed Matter Physics
at Ludwig-Maximilians-Universität München

October 1999 - June 2005 Studies in Physics at Universität Augsburg

June 2005 Diploma in Physics at Universität Augsburg

December 2004 Diploma Thesis at Universität Augsburg
*Flow equation solution of the Kondo model with
nontrivial density of states*

October 2001 Vordiplom in Physics at Universität Augsburg

June 1998 Allgemeine Hochschulreife
Rudolf-Diesel-Gymnasium Augsburg